Investigating blue and fin whale populations through passive acoustic monitoring using ocean bottom seismometers

Rose Hilmo

A dissertation
submitted in partial fulfillment of the
requirements for the degree of

Doctor of Philosophy
University of Washington
2024

Reading Committee:
William S. D. Wilcock, Chair
Parker MacCready
Manuel Castellote Morales

Program Authorized to Offer Degree:
School of Oceanography

University of Washington

Abstract

Investigating blue and fin whale populations through passive acoustic monitoring using ocean bottom seismometers

Rose Hilmo

Chair of the Supervisory Committee:
William S. D. Wilcock
School of Oceanography

Many large baleen whale species are endangered due to decades of commercial whaling before its international ban in the 1980s. Monitoring the recovery of their populations is difficult to study with traditional animal survey methods. Visual transect methods using ships and planes cover only small portions of baleen whales' vast migratory ranges that span thousands of kilometers and are incomplete because they only record surfacing whales. GPS tagging studies are invaluable for studying behavior but are limited to small numbers due to cost. Passive acoustic monitoring (PAM), which detects whale presence through recording calls, is a complementary method that is not sight-limited and can provide long-term continuous data on a large spatial scale. Ocean bottom seismometers (OBSs), geophysical instruments used to study earthquakes through recording ground motion, are opportunistic PAM sensors that record large baleen whale calls. There are large amounts of publicly available OBS data, but these datasets have so far been underutilized as tool to study whales. This dissertation develops new methodologies for PAM using OBSs and highlights their utility for characterizing populations and studying behaviors of fin and blue whales. In Chapter 2, I develop, implement, and evaluate a method for ranging to fin whales using multipath reflected arrivals of calls on solitary OBSs deployed in different regions of the abyssal ocean. I demonstrate how to account for various site properties and discuss how the method might be implemented in different environments. In

Chapter 3, I employ the multipath ranging method and point-transect distance sampling methods to estimate fin whale call densities using OBSs deployed in the Marianas region. This chapter demonstrates the utility of single-OBS ranging for estimating populations through PAM. In Chapter 4, I employ a previously developed acoustic localization algorithm to track calling northeast Pacific (NEP) blue whales with a pair of large OBS networks off the Pacific Northwest coast. I characterize the behavior of an understudied subpopulation of NEP blue whales that skip southward migration to investigate how they are using the temperate habitat while they overwinter. Behavioral metrics indicate that overwintering whales likely forage off the coast of Washington and Vancouver Island throughout the fall and early winter.

TABLE OF CONTENTS

Page

ACKNOWLEDGEMENTS

I have never lacked support during my time as a graduate student at the UW School of Oceanography, and many people contributed to my success in various ways. I thank all individuals named here and many more, which, if listed, would expand this section by many pages. Without you I could not have achieved this.

First, I thank my family. Isaac has been a pillar of support during my time as a student and has been the best partner anyone could ask for. I also thank my parents, who have also been critical to my success, always encouraging my inquisitive mentality and supporting me financially through my initial years in higher education.

I also thank my mentors who guided my development as a scholar and teacher. Mikelle Nuwer and Arthur Nowell especially supported me through tough times and helped me grow as an academic and as a person.

I thank my friends and peers, who never failed to encourage me and make me laugh. Specific thanks go to my best friend Kaitlyn who fought through the foggy days of COVID with me as a fellow graduate student, frequently grammar-checked my manuscripts, and helped me revise many talks.

I also thank my committee members. First, Parker MacCready, who has stuck with my committee for the duration of my time as a graduate student even as my research diverged from his field. Additional thanks are due to Manuel Castellote who served as the resident whale expert and ensured I did not err in the biological interpretations of my research. I also thank Deb Kelley, who made time for me as an essential last-minute committee addition, and Peter Dahl, my GSR who also contributed to my committee with his considerable acoustics expertise.

Finally, I thank my advisor, William Wilcock. William provided excellent research mentorship and writing support and adapted smoothly to my remote work needs as a student who lived far from campus. He also wrote some *incredible* letters of recommendation.

I wish all of you all the best.

Dedication

To my family, near and far

Chapter 1: Introduction and Organization of the Dissertation

Despite an international ban on commercial whaling in the 1980s, many large baleen whale populations are still in recovery and are at risk due to anthropogenetic factors such as noise pollution, ship collisions, entanglement, and climate change. However, their recovery is deceptively difficult to study. Baleen whales are too large to study in captivity, and their endangered status motivates the use of non-invasive monitoring methods. Monitoring whale populations using visual observation from ships and planes covers only small portions of baleen whales' vast migratory ranges that span thousands of kilometers, and counts are incomplete because whales spend most of their time under the ocean surface (Kaschner et al., 2012; Roberts et al., 2016; Virgili et al., 2019). Recently, high-resolution satellite imaging has expanded available methods to visually observe whales, but still only detects whales at the surface and is stymied by cloud cover (Guirado et al., 2019). Temporary attachment of GPS tags provides detailed whale location and behavioral information, but only for short durations and studies are limited to small numbers due to cost (Bailey et al., 2009; Irvine et al., 2014; Mate et al., 1999; Oleson et al., 2007a; Szesciorka et al., 2016). Passive acoustic monitoring (PAM) is complementary to other monitoring methods. PAM records whale calls, usually using hydrophones. PAM can provide high spatial coverage, detecting high intensity baleen whale calls from tens of kilometers away, and provide long-term continuous data that are difficult to obtain by other means (Mellinger et al., 2007).

Ocean bottom seismometers (OBSs), geophysical instruments designed to study earthquakes through measuring ground motion, can also record calls from large baleen whales (McDonald et al., 1995). OBS experiments comprise a remarkable global dataset and are increasingly being leveraged for a variety of opportunistic acoustic studies. OBSs have been used

to characterize baleen whale movement in regions through acoustic tracking (Dreo et al., 2017; Dréo et al., 2019; Dunn and Hernandez, 2009; Soule and Wilcock, 2013), measuring long term trends in acoustic behavior (Mcdonald et al., 2009; Weirathmueller et al., 2017a), and estimating call abundances and densities (Harris et al., 2013; Matias and Harris, 2015; Weirathmueller et al., 2017b).

Two far-ranging migratory species that are ideal for study using PAM OBS methods are blue whales (*Balaenoptera musculus*) and fin whales (*Balaenoptera physalus*), both of which produce low frequency calls that are observable on OBSs that sample at 50 Hz at least, which resolve signals at or below the Nyquist frequency of 25 Hz (McDonald et al., 1995). Fin whales are distributed throughout the world's oceans. Fin whale populations declined due to whaling from pre-exploitation estimates of ~400,000 to historic lows of ~15,000 individuals remaining worldwide in 1972 (Mizroch et al., 1984), and became protected as "endangered" under the Endangered Species Act in 1973. Today, NOAA stock assessments place fin whale populations at ~100,000 though they are still listed as endangered. Despite their relatively large current population, their distributions and migrational habits are difficult to constrain because they are infrequently observed by visual transect studies (Archer et al., 2019; Hamilton et al., 2009; Jackson et al., 2004; Mizroch et al., 1984).

Male fin whales produce a stereotypical song (Croll et al., 2002; Watkins, 1981). Notes are downswept over ~1 second and are centered around ~20 Hz, though frequencies and note spacings vary regionally (Delarue and Todd, 2009; Hilmo and Wilcock, 2024; Morano et al., 2012; Rankin et al., 2011, 2018). Acoustic sensors record seasonal presence of fin whale song globally (Miksis-Olds et al., 2019; Shabangu et al., 2019; Dréo et al., 2019; K. Stafford et al., 2009) and the songs are observed to evolve slowly over time (Best et al., 2022; Romagosa et al.,

2024; Weirathmueller et al., 2017a). Dense deployments (<10 km spacing) of OBSs have been used to study fin whales through localizing calls (Dréo et al., 2019b; Soule and Wilcock, 2013), but many arrays are deployed too sparsely for multi-station trilateration. This motivates the development of methods that can range or locate fin calls using single OBSs (Harris et al., 2013; Matias and Harris, 2015; Weirathmueller et al., 2017b) to expand the potential for studying fin whale populations using these datasets.

Like fin whales, blue whales are protected as "endangered" and are also rarely observed by visual transect studies. In contrast to fin whales, there are ~10 acoustically distinct subpopulations of blue whales that have been identified in various ocean basins (Mcdonald et al., 2006; Mcdonald et al., 2009; Thomas et al., 2016). This dissertation focuses on one of the most accessible blue whale populations in the world, the ~1900 individuals that compose North East Pacific (NEP) blue whale subpopulation (Carretta et al., 2023; Monnahan et al., 2015). NEP blue whales are considered to be capital breeders. They are commonly found summering off the coast of Southern California to feed and overwintering in the Eastern Tropical Pacific to breed (Bailey et al., 2009, Irvine et al., 2014). However, smaller groups within the NEP blue whale subpopulation migrate differently, including individuals who skip southward migration and overwinter off of the U.S. West Coast (Burtenshaw et al., 2004; Busquets-Vass et al., 2021; Irvine et al., 2014; Mate et al., 1999).

The male NEP blue whale song is characterized by interspersion of A and B type notes which are both observed on OBSs (McDonald et al., 1995). The A-note is a broadband pulsed call centered at 14 Hz that lasts at for ~20 seconds while the B-note is a louder tonal call that is downswept from 16-14 Hz over ~20 seconds. The frequency of the calls has been slowly decreasing for many decades (Mcdonald et al., 2009; Rice et al., 2022). The powerful B-note can

be localized by OBS arrays through trilateration (Stafford et al., 1999a; Wilcock and Hilmo, 2021), which enables investigations of whale movement behavior through acoustic tracking of calling individuals.

This dissertation seeks to expand the use of OBSs for studying fin and blue whales through PAM. It contributes significantly to fin and blue whale research in three ways. First, it improves the utility of single instruments for studying fin whales by developing and evaluating and accessible method to range to calls. Next, it demonstrates how distance sampling methods can be applied in concert with our ranging method to estimate fin whale call densities. Finally, it characterizes NEP blue whale behavior in a region with few previous observations through application of a recently developed acoustic tracking algorithm to a pair of large OBS networks.

In chapter 2, I expand upon a previously described method for ranging to fin whale calls using a single OBS through measuring the timings of multipath arrivals that reflect from the sea surface and sea floor (Weirathmueller et al., 2017b). I enhance the method by combining consecutive calls to improve the detectability of multipath arrivals. I demonstrate the applicability of multipath ranging to fin and sei whale calls using deep ocean OBSs in multiple regions and discuss how to account for site-specific properties such as subsurface structure, bathymetric relief, and varying song metrics. The contents of this chapter are published in the *Journal of the Acoustical Society of America* under the title "Estimating distances to baleen whales using multipath arrivals recorded by individual seafloor seismometers at full ocean depth" (Hilmo and Wilcock, 2024).

In chapter 3, I further automate the multipath ranging method of Chapter 2 and employ it in concert with point-transect distance sampling to estimate fin whale call densities in the Marianas region. I apply these methods to 7 OBSs deployed between February 2012-January

2013 to estimate monthly call densities during the Winter-Spring song season. This chapter demonstrates the utility of single station ranging and distance sampling methods and discusses their potential for monitoring fin whale populations. This work is being prepared for publication in a peer reviewed journal.

In chapter 4, I implement a previously developed B-call acoustic localization method (Nosal, 2013; Wilcock and Hilmo, 2021) to track overwintering NEP blue whales off the U.S. West Coast with two large OBS networks. I compile an unprecedented dataset of tracks that link whale movement and song metrics during the 2013-2014 Fall-Winter song season. I synthesize previously identified song metrics (Oestreich et al., 2020, 2022) and observations of whale movement to identify distinct migration corridors and foraging grounds for overwintering whales. I also describe spatial, seasonal, and behavioral differences in song patterns, which suggest that different calls and phrase types are used in different behavioral contexts. This study not only expands our understanding of habitat use by NEP blue whales overwintering in temperate waters but showcases the potential of leveraging opportunistic OBS networks to study whales in regions with few other monitoring options. This work is also being prepared for publication in a peer reviewed journal.

Chapters 2-4 exemplify the PAM potential for monitoring blue and fin whale populations using OBS datasets. In Chapter 5, I summarize how this dissertation has progressed the field and suggest potential applications of these methods for future studies.

Chapter 2:

Estimating distances to baleen whales using multipath arrivals recorded by individual seafloor seismometers at full ocean depth

Rose Hilmo[1], William S.D. Wilcock[1]

[1]School of Oceanography, University of Washington, Seattle, WA 98195, USA

2.0 | ABSTRACT

Ocean bottom seismometer networks can record opportunistic data sets of 20-Hz fin whale calls. Because networks are often too sparse for multi-station tracking, single-station methods are needed to estimate call density. We investigated a method to range to singing fin whales at full ocean depths using the spacing of water column multiples. Calls were detected by cross-correlating a spectrogram with a template call. To enhance multipath signals, we considered 20-minute windows and either summed the spectrograms of all calls aligned on the strongest detection before measuring the multipath spacing or measured the spacing directly from the autocorrelation of the cross-correlation time series. We evaluated the methods at 5 sites with contrasting seafloor and subsurface properties, bathymetric relief, and water depths of 4000-6000 m, using fin whale songs at 4 sites and a sei whale song at the fifth. The autocorrelation method works best, and ranges can be obtained to >15 km. Ranging at sedimented sites requires carefully accounting for subsurface reflections. Ranges have considerable uncertainty in regions of bathymetric relief. The method requires that the time between calls is different from that of the multipaths and does not work reliably when more than one whale is singing nearby.

2.1 | INTRODUCTION

Studies of baleen whales rely on effective monitoring to understand their ecology, the recovery of populations from whaling, and the impacts of anthropogenic activity (Mizroch et al., 1984; Monnahan et al., 2015). Techniques for monitoring animal populations include cue detection and physical capture methods. Whaling catch records provide historical physical capture data (Gregr et al., 2000; Rocha et al., 2015). Aerial and shipboard surveys are long-standing approaches to visual cue detection (Roberts et al., 2016; Virgili et al., 2019), and high-resolution satellite imagery can now also be used as a detection tool (Cubaynes and Fretwell, 2022; Guirado et al., 2019). However, monitoring baleen whales using visual cues is complicated because they spend most of their time submerged, and have large migratory ranges (Thomas et al., 2016).

Passive acoustic monitoring is a complementary method that can expand temporal and spatial coverage. Acoustic sensors are not limited by low light conditions, can be deployed continuously for months, and can detect high intensity baleen whale calls from tens of kilometers away. Studies that implement both methods show that acoustic sensors detect more whales than visual observers (McDonald and Moore, 2002; Rankin et al., 2007). Monitoring through call detection is limited to individuals that vocalize and can only observe behaviors associated with calling (Kowarski and Moors-Murphy, 2021; Mellinger et al., 2007; Risch et al., 2014). However, it can provide long-term continuous data that are difficult to obtain by any other means.

Ocean bottom seismometers (OBSs) are deployed all around the globe, and an increasing number of studies are building upon the pioneering work of McDonald et al. (1995) by exploiting them for opportunistic acoustic studies of baleen whales. OBSs measure ground

velocity and sometimes also include a hydrophone. For earthquake and mantle imaging studies, networks of autonomous OBSs are often deployed for a year or more and can span hundreds of kilometers. In a few locations, cabled OBS networks are operating on decadal timescales (Barnes et al., 2013; Kawaguchi et al., 2015; Smith et al., 2018). OBSs typically have sampling rates of 50-200 Hz, which limits their use to species with low frequency calls. Numerous studies have used autonomous (e.g. Dunn and Hernandez, 2009; Harris et al., 2013; Matias and Harris, 2015; Soule and Wilcock, 2013; Wilcock and Hilmo, 2021) and cabled (Iwase, 2015; Oestreich et al., 2020; Weirathmueller et al., 2017a) OBSs to study blue and fin whales, and one study also recorded Bryde's whales (Brodie and Dunn, 2015).

Fin whales are ubiquitous in the oceans. Their most powerful call is a chirp centered around ~20 Hz and sweeps down ~10 Hz in frequency in under 1 second (Watkins et al., 1987). Fin whales produce 20 Hz notes in repetitive bouts which compose their "song". The 20 Hz note is easily identifiable on OBSs (McDonald et al., 1995) even at 50-Hz sampling rates, which makes it an ideal note for passive acoustic monitoring with OBSs. Genetic sub-populations of fin whales exist in various ocean basins, but the visual physiological differences are slight (Archer et al., 2013; Lockyer and Waters, 1986). Characterization of sub-populations can be significantly enhanced by studying differences in the frequency and spacing of "20-Hz" notes in the stereotyped songs (Castellote et al., 2012; Helble et al., 2020; Sirovic et al., 2013) that are produced by males which are related to breeding (Croll et al., 2002; Hatch, 2004).

Estimating fin whale population densities using acoustic data requires 1) a method to localize or determine the range of calls so that call counts can be converted to spatial call densities and 2) knowledge of the calling rate, termed "cue rate", of the calling species (Marques et al., 2013) so that call densities can be converted to animal densities. Cue rate is best

characterized by independent studies that use acoustic tags (Goldbogen et al., 2014), while call densities can be obtained through the use of fixed acoustic sensors. For fin whales, multi-station time difference of arrival (TDOA) localization requires OBSs to be spaced ≤ ~10 km apart (Soule and Wilcock, 2013) which is smaller than the spacing of OBS in many networks. This limitation motivates the development of single OBS methods for fin whale call localization or ranging, which can be used to estimate spatial call densities using similar methods to point-transect distance sampling (Buckland et al., 2001; Harris et al., 2013).

There are two methods suitable for localizing fin whales with single stations both of which are dependent on the short duration of the call relative to the two-way propagation time through the water column. One method localizes fin whale calls using the particle motions determined from three orthogonal channels of an OBS, to calculate the azimuth and apparent incidence angle (Harris et al., 2013; Matias and Harris, 2015). The Zoeppritz equations are then used to determine the true incidence angle based on seafloor seismic properties and thus, estimate the range and bearing to the whale. The method only works out to the critical distance, the range at which the call is critically reflected, and requires a means to identify calls that do not meet this criterion. The critical reflection range is inversely related to the seafloor substrate's P-wave (compression wave) velocity (V_P). For a site at ~4500 m depth off the Portuguese coast with soft sediments with (V_p = 1.8 km/s), ranging is limited to ≤ 5 km. (Harris et al., 2013; Matias and Harris, 2015). At the same depths with a basaltic seafloor (V_P = 2.5 km/s), ranging would be limited to <3 km.

Here, we focus on an alternative method that estimates horizontal range to fin whales on a single OBS or bottom-moored hydrophone using the relative timing of multipaths, arrivals of multiple consecutive echoes of a single chirp that reflect off the seafloor and sea surface, to

estimate the distance to a calling whale (Kuna and Nábělek, 2021; McDonald et al., 1995; Širović et al., 2007; Weirathmueller et al., 2017b). The multipath method does not estimate bearing, but it is advantageous because it can range well past the critical distance. Weirathmueller et al. (2017b) tested multipath fin whale calls ranging at two contrasting sites at ~2500 m depth in the Northeast Pacific. At a site on the Juan de Fuca mid-ocean ridge, highly reflective basaltic seafloor resulted in four or more visible multipaths recorded on an OBS, but complex bathymetry increased uncertainty in ranging. At a flat sedimented site in Cascadia Basin, only one low-amplitude reflected multipath was visible when the whale was nearby because of a low impedance contrast between seafloor sediments and seawater. This arrival was complicated by a basement reflection that traveled through a 300-600 m thick sediment layer and sometimes had a higher amplitude than the seafloor reflection. Although multipath ranging was successful at both OBS test sites, ranging to all whales within 5 km and to some whales up to 20 km, it was unclear how well the approach would work for sedimented sites at full ocean depths where spherical spreading will lead to even lower amplitude multipath arrivals.

In this study, we expand upon the work of Weirathmueller et al. (2017b) by developing techniques to enhance the detection of low-amplitude multipath arrivals. We assess multipath ranging using OBSs at five sites with contrasting seafloor properties at 4000-6000 m depth in the North Pacific and Atlantic oceans. We explore how the seafloor properties, the presence of subseafloor reflectors, and the presence of multiple calling whales influence multipath ranging and identify additional site-specific approaches that improve ranging results.

2.2 | METHODS

A. Analysis

Fin whales call near the sea surface at depths up to a few tens of meters (Stimpert et al., 2015; Watkins et al., 1987). Multipaths arrivals are the downward propagating rays from whale calls that reflect from the seafloor and the sea surface (Fig. 2.1). The direct path travels from the whale to the OBS with no reflections. The first multipath (MP1) is reflected once by the seafloor (or subsurface reflector) and once by the sea surface before arriving at the OBS. The second multipath (MP2) is reflected twice by the seafloor and the sea surface. We note that upward propagating rays from a whale call that reflect from the sea surface interact with downward propagation rays to create a Lloyd's mirror effect (Pereira et al., 2020); given the shallow depths of calls the combined paths can be approximated by a single source at the surface for the purposes to calculating the arrival times of the peak signal. Our method focused on enhancing and detecting the direct, MP1, and MP2 arrivals of fin whale calls, then estimated horizontal whale range by comparing their relative arrival times to those predicted by propagation models.

Acoustic ray paths in the ocean are refracted due to vertical gradients in sound speed, which affects the travel times of multipaths. To account for refraction, we modeled relative arrival times of the direct, MP1, and MP2 waterborne arrivals using BELLHOP ray tracing software (Dushaw and Colosi, 1998; Porter and Bucker, 1987). Arrival time models assumed a flat seafloor, a source depth of 50 meters, and were calculated at 10-meter range intervals out to 20-km distance.

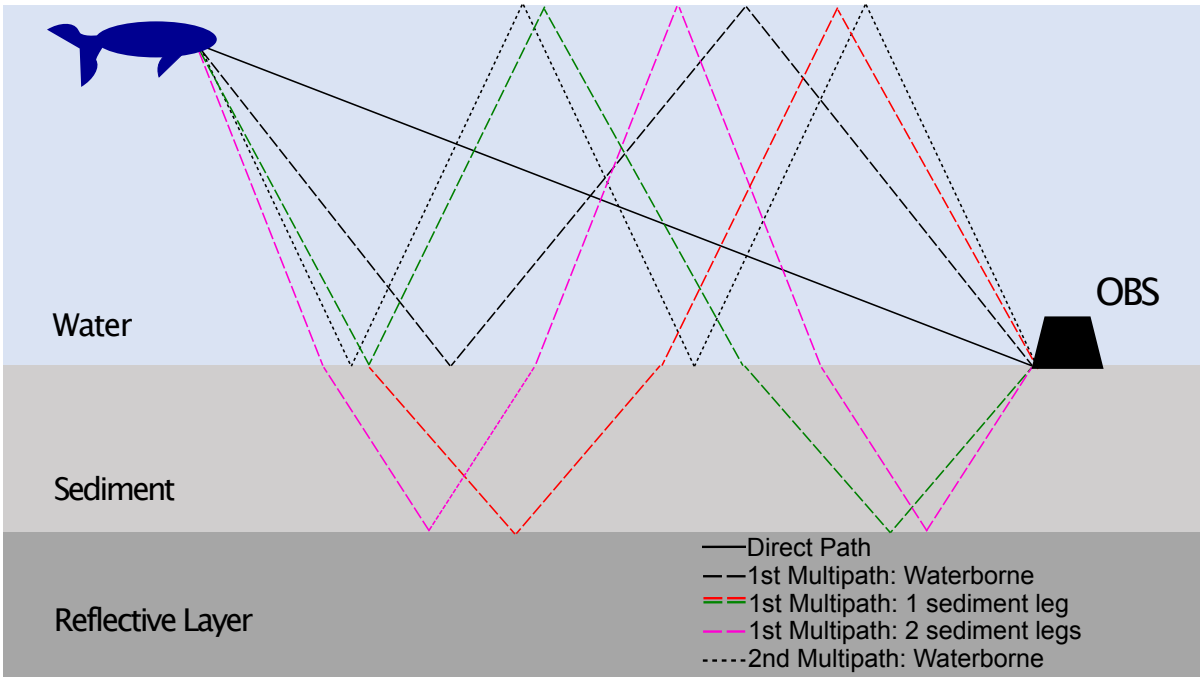

FIG. 2.1. Cartoon illustrating the geometry of ray paths of the direct (solid black), first multipath (black dashed), and second multipath (black dotted) arrivals with a subsurface reflector. Two ray paths are possible for MP1 arrivals with single subsurface reflections (red & green dashed) that arrive at the OBS after the waterborne MP1. A MP1 arrival with two subsurface reflections (magenta dashed) is even later.

We tested multipath ranging at various deep-water OBS sites (Fig. 2.2). At each site, we removed the frequency-dependent instrument response from the vertical seismometer channel using ObsPy, a Python toolbox for seismology (Beyreuther et al., 2010). We built spectrograms using 0.8-s Hanning windows with 95% overlap, then detected 20 Hz fin whale calls using 2-D cross-correlation (Mellinger and Clark, 1997), initially using a generalized template comprising a 1-s call that downsweeps linearly from 25-15 Hz with a bandwidth of 3 Hz. It was designed to detect high amplitude calls (Archer et al., 2020; Weirathmueller et al., 2017a) regardless of regional variations in frequency and duration. We refer to the product of the cross-correlation of the template with the spectrogram as the "detection score" (Mellinger and Clark, 1997). We visually analyzed periods with higher detection scores to identify periods where fin whales called near the OBS. We then selected two calling periods to test multipath ranging at each site based

on the following criteria: 1) strong calls (defined as calls with high detection scores) were present indicating a whale passed closely to the OBS, and 2) the strong calls were part of a song that lasted at least 4 hours.

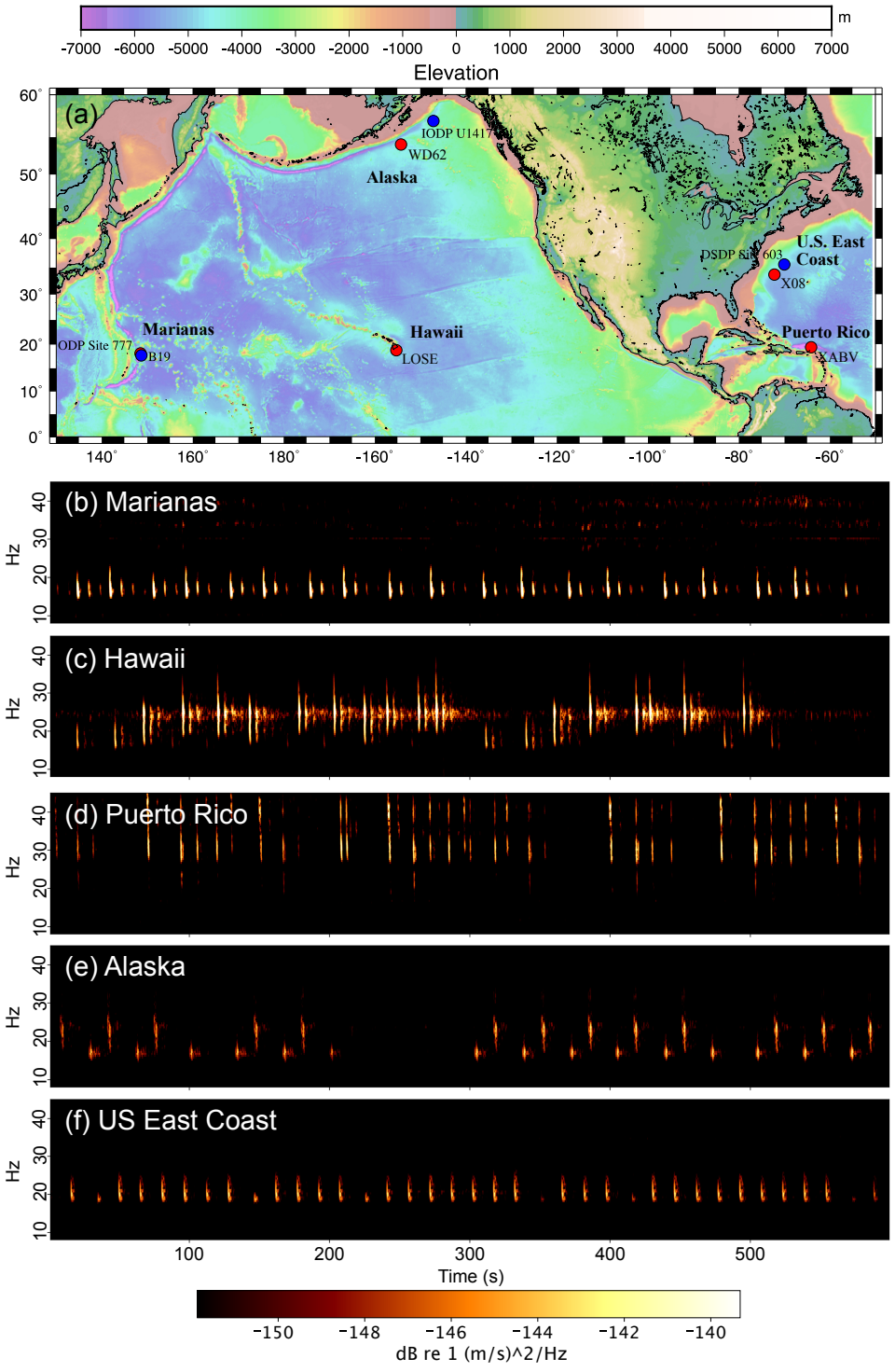

FIG. 2.2. (a) Bathymetric map showing the five deep water OBS sites selected for analysis and the nearby boreholes used to characterize seafloor properties for 3 sites. Ten-minute representative spectrograms of songs used for multipath ranging recorded on OBSs at (b) Marianas, (c) Hawaii, (d) Puerto Rico, (e) Alaska, and (f) US East Coast.

We found fin whale song at each site, except at Puerto Rico where we found sei whale song (Table 2.1). Songs are extended periods of calling composed of stereotypical repetitive notes with regular spacings; in this chapter we define the times between successive notes as inter-pulse intervals (IPIs) though they are often referred to in recent papers as inter-note intervals (INIs). Singlet patterns, dominant at Marianas and US East Coast sites, were composed of single notes and IPIs (Fig. 2.2(b) and (f)). Doublet patterns at the Alaska site were composed of alternating higher and lower frequency calls, with corresponding alternating IPIs (Fig. 2.2(e)). Complex patterns at the Hawaii site have higher frequency notes than stereotypical fin whale song and vary in frequency and IPI (Fig. 2.2(c)). Sei whales produced the complex patterns at Puerto Rico, which are composed of longer, higher frequency notes than fin whales and varying IPIs (Fig. 2.2(d)).

We refined our detection template separately for calls at each site to maximize the detection scores for multipath arrivals (Table 2.1). Multipath arrivals are relatively enriched in the lower frequencies at the end of the downswept call, likely due to attenuation by the seafloor reflection which is proportional to the frequency squared at fin whale frequencies (Holland and Dosso, 2021; Pierce et al., 2005). High frequency attenuation is particularly apparent at weakly reflective sites, where multipaths are the most difficult to detect. Therefore, we tuned site-specific templates to the lower-frequency component of the call.

TABLE 2.1: Call patterns, template parameters, and multipath search parameters at each site. The template frequencies vary at each site, but the bandwidth is constant at 3 Hz.

	Call note patterns	IPI (s)[1]	Template duration (s)	2-D Template downsweep	Time proximity filter (s)[2]	Maximum TWTT (s)[3]	Start of multipath search window (s)[4]	End of multipath search window (s)[5]
Marianas	Singlet	15-25	0.8	20-15 Hz	13	<8	1	9
Hawaii	Complex	15-25	0.8	30-20 Hz	20	<6	1	7
Puerto Rico	Complex	4-25	1.3	40-25 Hz	15	<7	4.5	8
Alaska	Doublet	15-25	0.8	30-20 Hz, 20-15 Hz	13	<7	2	8
US East Coast	Singlet	15	0.8	23-17 Hz	13	<7	2	7.2

[1]The time difference between regularly spaced fin whale calls is defined as the interpulse interval (IPI). [2]The time proximity filter eliminates weaker detections when they are less than a minimum time from a stronger detection. This prevents the detection of more than one arrival for a single call. [3]The maximum two-way travel time (TWTT) from the sea surface to the seafloor is the largest expected arrival time difference between multipath arrivals, which occurs when a whale is directly above the OBS. [4]Start of search window for multipath following the strongest detected arrival. [5]End of search window for multipath following the strongest detected arrival.

To detect waterborne multipath arrivals reliably, we evaluated two methods to increase their signal-to-noise ratio by combining adjacent calls. Weirathmueller et al. (2017b) improved multipath visibility by summing aligned time series of detection scores for calls within 6-minute windows. For our first method, we similarly summed spectrograms of all fin whale calls within a time window after aligning them on the detection. To ensure that we only had one detection per call, we measured the IPIs for song periods at each site and employed a time-proximity filter to eliminate detections that are closer to a stronger detection than the smallest IPI (Table 2.1, Fig. 2.3(a)). We detected direct and multipath call arrivals on the summed spectrogram using spectrogram cross-correlation with the site-specific template (Fig. 2.3(b)). The time difference between the two peaks with the highest detection scores that fell within the multipath search window (Table 2.1) was measured as the multipath spacing, and were used to calculate range (Fig. 2.3(d)). Spacings were expected to be the direct and first multipath (termed MP1-direct) at closer ranges but transition to the first and second multipaths (MP2-MP1) at larger ranges once ray bending caused the second multipath to have a higher amplitude than the direct arrival (Weirathmueller et al., 2017b).

For our second method, we computed the autocorrelation of the detection score series for the full time window (Fig. 2.3(c)). We found the largest peak in the autocorrelation with a lag that corresponded to a feasible spacing of multipaths (Table 2.1). This lag corresponded to the time difference between the two arrivals with the highest detection score. Like the summed spectrogram method, this spacing was expected to be MP1-direct or MP2-MP1, depending on the distance of the whale from the OBS.

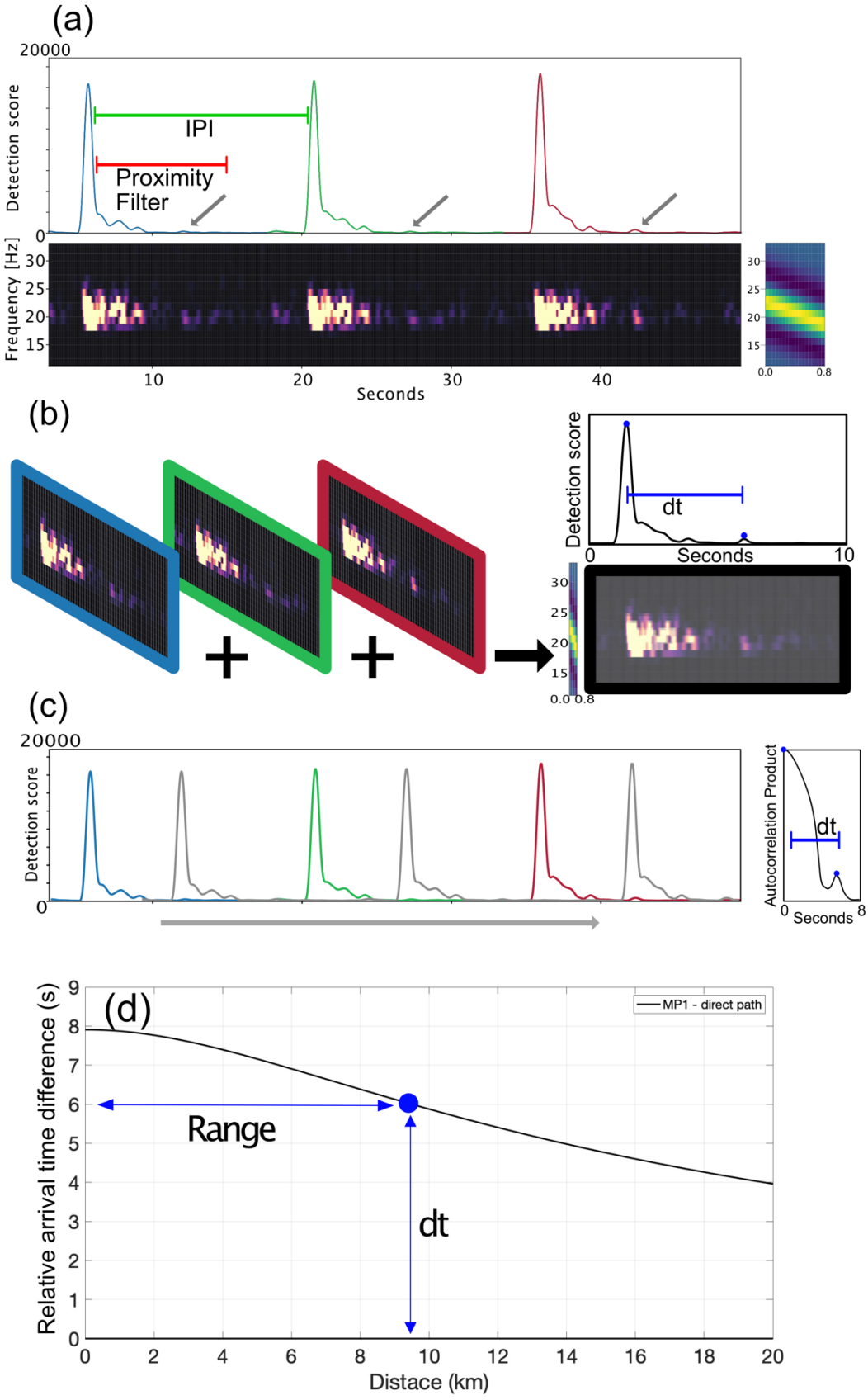
(a)
20000
Detection score
0
IPI
Proximity
Filter
Frequency [Hz]
30
25
20
15
10
20
30
40
Seconds
(b)
Detection score
dt
0
Seconds
10
(c)
20000
Detection score
0
Autocorrelation Product
dt
0
Seconds
8
(d)
MP1 - direct path
Relative arrival time difference (s)
Range
dt
Distace (km)

FIG. 2.3. Schematic diagram illustrating the methods that were used to estimate the time between multipath arrivals. (a) Detection score of three fin whale calls with faint multipath arrivals indicated by gray arrows, calculated via cross-correlation of the spectrogram and call template (template timescale expanded 5-fold for better visualization). The spectrogram highlights how subsurface reflections arrive for several seconds following waterborne arrivals, complicating the detection of ~1s duration direct and multipath signals. The green bar shows the call interpulse interval (IPI) which is the time difference between regularly spaced calls. The red bar shows the time proximity filter, which is long enough to exclude the multipath but is shorter than the IPI. (b) Summed spectrogram method. Sections of the spectrogram are aligned on the call detection (blue, green, red boxes) and summed to create a composite spectrogram (black box). The template is cross-correlated with the sum to create a composite detection score. (c) Detection score autocorrelation method. The detection score time series (individual call arrivals shown in blue, green, and red) is cross correlated with itself (left). This emphasizes the repetitive signal of multipath arrivals which are picked from the autocorrelation product (right). The blue bar (dt) shows relative multipath arrival timing. (d) Example of horizontal range calculation using relative time of combined MP1-direct arrivals.

B. Data

The Incorporated Research Institutions for Seismology Data Management Center database (now part of the Earthscope Consortium Data Services) includes all US autonomous OBS experiments since 2001. To select our test sites, we searched for deployments in at least 4000 m of water that lasted for >6 months and included the fall and winter calling season and for sample rates of ≥100 Hz to record the full frequency range of stereotypical 20 Hz fin whale songs. For the experiments meeting these criteria, we compared the deepest OBSs and selected one in a region with the flattest bathymetry. We then chose five test sites with a range of seafloor properties, namely 1) east of the Marianas trench, 2) southeast of Loihi seamount off the Big Island of Hawaii, 3) south of the Alaska subduction zone in the Gulf of Alaska, 4) northeast of Puerto Rico on the continental rise, and 5) east of the continental margin of the US East Coast off North Carolina (Table 2. 2, Fig. 2.2, Fig. 2.4).

TABLE 2.2. OBS networks and stations used in this study. Network codes are unique identifiers for seismological data assigned by the International Federation of Digital Seismograph Networks.

Region	Experiment Name	Network Code	Station	Dates of Operation	Latitude, °N	Longitude, °E	Depth, m
Marianas	Mantle serpentinization and water cycling through the Mariana Trench and Forearc	XF	B19	02/2012-02/2013	18.1025	148.5211	5949
Hawaii	Loihi Seismicity	9A	LOSE	09/2010-07/2011	18.8349	-155.1618	4410
Puerto Rico	USGS Puerto Rico Trench	ZZ	XABV	05/2015-05/2016	19.3418	-64.1353	5426
Alaska	Alaska Amphibious Community Seismic Experiment (AACSE)	XO	WD62	05/2018-08/2019	53.3619	- 157.3318	4626
US East Coast	Eastern North American Margin (ENAM) Community Seismic Experiment	YO	X08	04/2014-04/2015	32.6931	-72.8164	5271

We obtained winter sound speed profiles from the World Ocean Atlas (Boyer et al., 2018) at the OBS test site. We applied BELLHOP to develop waterborne multipath arrival timing models assuming a flat seafloor at all sites, except for Hawaii where we also considered the effects of an idealized bathymetry of Loihi Seamount. Waterborne multipath arrival models alone were sufficient for ranging at the basaltic Hawaii site and at Puerto Rico where the carbonate seafloor is highly reflective (ten Brink, 2005) so no subsurface reflections are visible.

For thickly sedimented sites with poorly reflective seafloor (Marianas, Alaska, and US East Coast), we also investigated subsurface properties using nearby drilling project boreholes (Fig. 2.2, Table S2.1) and MCS profiles (Bécel et al., 2020; Oakley et al., 2008; Shillington et al., 2015). At Marianas, there was a thin surface sediment layer that was nearly acoustically transparent, overlaying a highly reflective cherty clay/porcellanite layer (Harding et al., 1990). This informed the development of a waterborne arrival model at the Marianas site that considered the top of the cherty clay/porcellanite layer to be the "seafloor" and modeled the OBS as suspended in the water column.

At Alaska and US East Coast sites, MCS studies (Bécel et al., 2020; Shillington et al., 2015) and borehole data (Table S2.1) were used to account for subsurface multipath arrivals. We modeled relative arrival timings of first multipaths that propagate for one or two legs in a sediment layer that overlayed a reflective interface (Fig. 2.1). At the Alaska site, there were no reflective layers besides the basaltic basement, and we modeled subsurface propagation through the relatively thin sediment layer using Snell's law and the simplifying assumption of constant velocities in the water column and the sediment layer. At the US East Coast site where the sediment layer is thick and includes multiple reflectors, we modeled subsurface arrivals with a full-waveform seismic reflectivity algorithm (Kennett, 2009).

We did not consider refracted arrivals to be significant because seismic experiments using airguns (Bécel et al., 2020; Shillington et al., 2015) and fin whale calls as the source (Kuna and Nábělek, 2021) show that unlike subsurface reflections, these have small amplitudes relative to the waterborne arrivals. In addition, the refracted arrivals do not arrive within the feasible multipath window where they have the highest amplitudes at relatively short ranges. During the analysis, we found no evidence of precursors to the direct path arrival with sufficiently high amplitudes to impact the ranging.

Additional bathymetrical/geologic site information and a detailed description of the US East Coast reflectivity model are provided in Appendix 1: Supplementary Materials for Chapter 2.

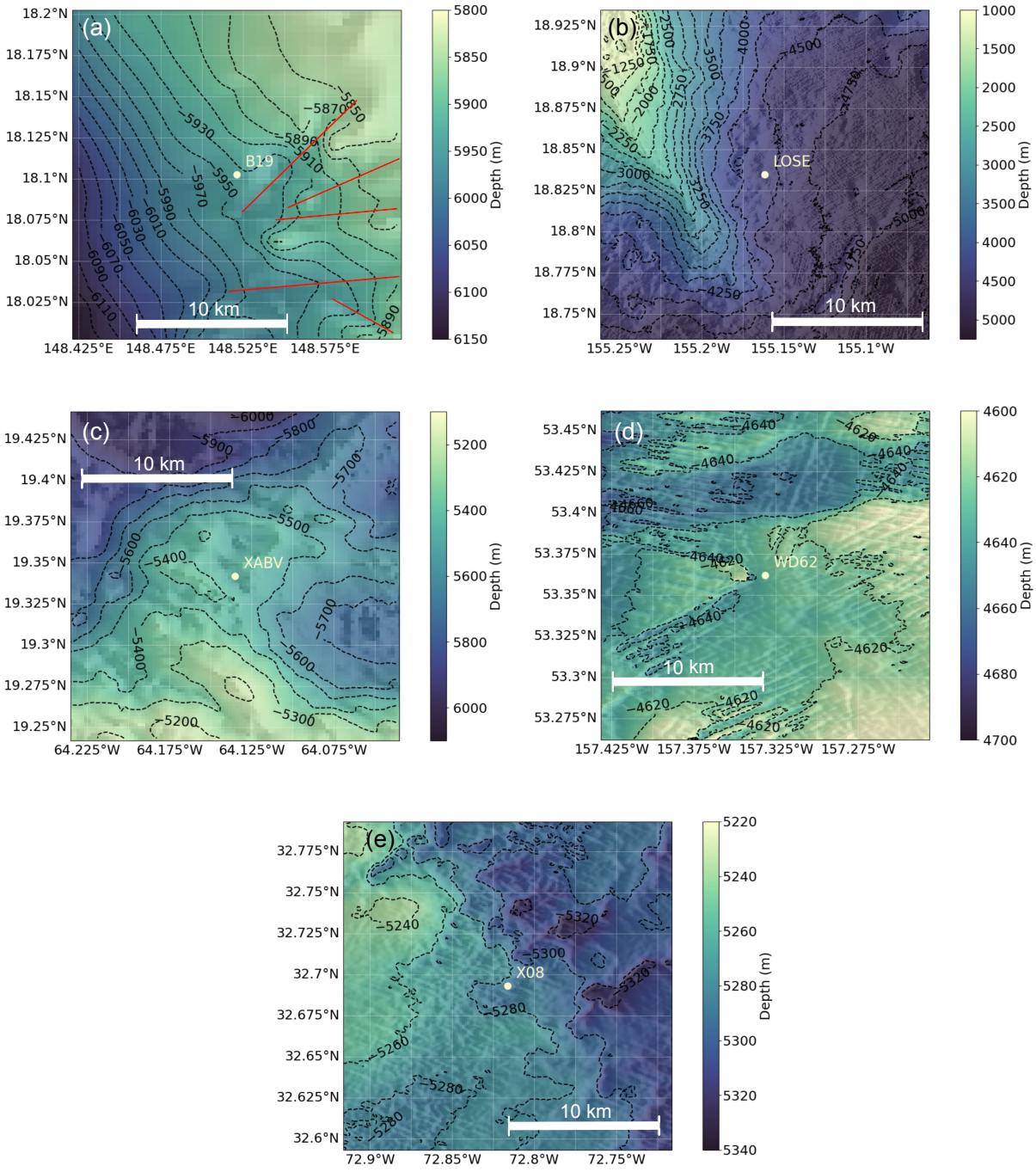

Fig. 2.4: Maps for the OBS sites showing bathymetry within 10 km for (a) Marianas (red lines show faults that offset the bathymetry), (b) Hawaii, (c) Puerto Rico, (d) Alaska, and (e) US East Coast.

2.3 | RESULTS

A. Marianas

Marianas is an ideal site for multipath ranging because the reflective chert/porcellainite layer produced up to four visible multipaths following the direct arrival for nearby whales. We used this site as a baseline for our multipath ranging methods with which other sites were compared. Because the depth of the reflector at our site was not documented, we calculated ranges assuming a reflector depth of 100 meters beneath the seafloor (mbsf), which falls within the range of regional measurements between 30-200 mbsf (Abrams et al., 1992; Oakley et al., 2008).

We first evaluated our methods by ranging to a fin whale over 9 hours on January 18, 2012 (Fig. 2.5(b)); this was the fin whale song with the strongest detections. We calculated ranges using 20-minute windows to combine calls for both the summed spectrogram and autocorrelation methods, assuming the MP1-direct arrivals are measured (Fig. 2.5(a)). To avoid the biases that would result when detections are only at one end of the window, ranges were obtained one minute apart but only when there was at least one detection within 30 seconds of the center of the window. The song started at 0020, and up until 0120 both methods yielded ranges that decreased from 9 km to 8 km. Between 0120 and 0340, the summed spectrogram ranges continued to decrease steadily to 3 km while autocorrelation ranges jumped to 18 km and then decreased to 10 km. At 0340, the summed spectrogram ranges jumped to 9 km, and both methods then showed consistent ranges that decreased steadily to <2 km at 0540. From 0540-0555, both methods yielded ranges of 0 km. At 0555, the ranges for both methods jumped to 2 km and then increased steadily to 7.5 km. At 0800, the ranges jumped to 4 km. The ranges for the summed spectrogram method steadily increased to 5.2 km at 0855. However, the ranges for

the autocorrelation method jumped back to the 12.5 km range at 0830 and steadily increased to 13.5 km at 0855. At 0855 the fin whale stopped singing.

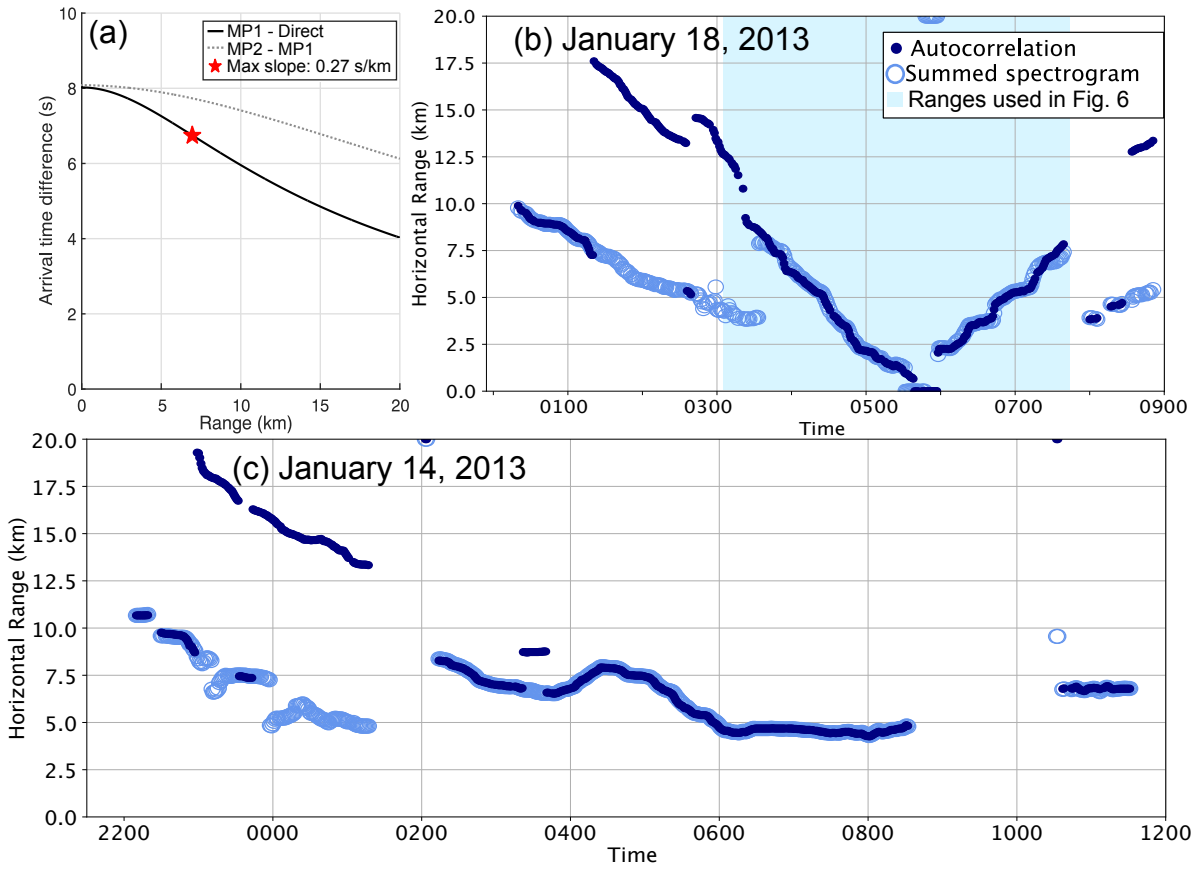

FIG. 2.5. Ranging results for the Marianas (a) Ray tracing timing model for MP1-direct and MP2-MP1 multipath arrivals with the maximum absolute gradient of the MP1-direct times indicated (red star). (b) Fin whale ranges for a 9-hour period on January 18, 2013 obtained using 20-minute windows for the autocorrelation (dark blue) and summed spectrogram (light blue) methods. (c) As for (b) but for a 14-hour period on January 14-15, 2013. Times on the x-axes in this and other ranging plots follow the 24-hour convention of HHMM.

This track illustrates the importance of identifying which arrivals are being measured. At the start, both methods provided incorrect ranges using the MP1-direct timing model because the direct path is weaker than both MP1 and MP2 arrivals. This period was ranged correctly using the MP2-MP1 timing model for both methods (Fig. 2.6(a)). Starting at 0130, the autocorrelation ranges were correctly modeled with MP1-direct times because the direct path arrival is weaker

than MP1 but stronger than MP2 (Fig. 2.6(b)). Autocorrelation measures the relative arrival time difference between the two strongest arrivals, regardless of which occurs first. In contrast, the summed spectrogram method still measures MP2-MP1 times because the summed spectrogram method differences the strongest detection (MP1) and the arrival that follows it. Between 0340-0800, both methods agreed and measured the MP1-direct times because the direct path detection is strongest, followed by MP1 (Fig. 2.6(c)). After 0800, MP1 was again stronger than the direct path, so the summed spectrogram method measured MP2-MP1 for the remainder of the song, while autocorrelation was inconsistent between MP1-direct and MP2-MP1 because the direct and MP2 arrivals have similar amplitudes.

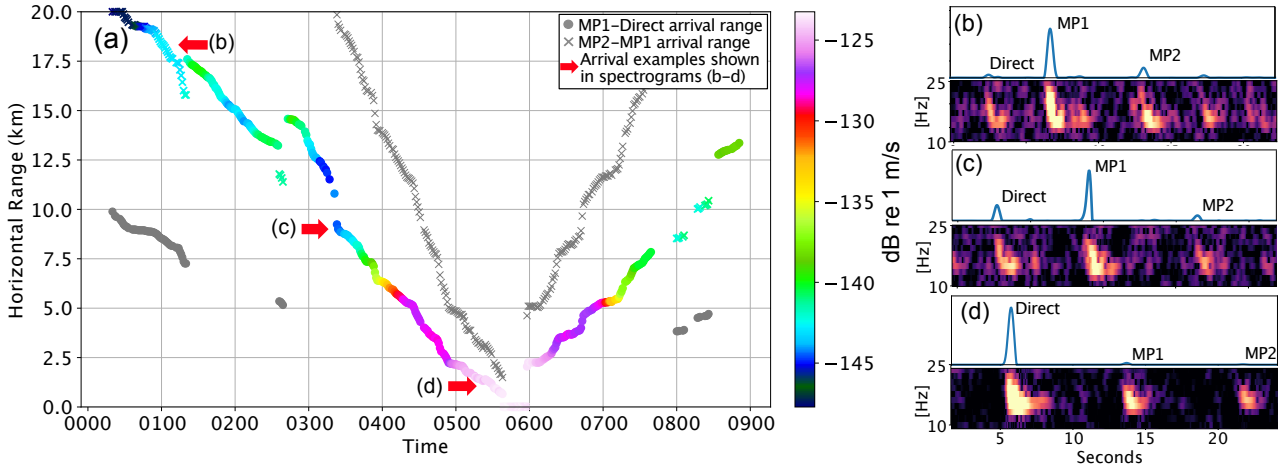

FIG. 2.6. (a) Ranges calculated for both MP1-direct and MP2-MP1 arrival assumptions for the autocorrelation method for period shown in Figure 2.5(a) with the color scale showing the average amplitudes in dB re 1 (m/s)/Hz for the strongest arrivals of calls included in the 20-minute window used for each range. Colored markers show correct multipath arrival models, gray markers show incorrect multipath arrival models. Insets show example relative detection scores and spectrograms for periods when b) MP1 is strongest and the MP2 arrival is stronger than the direct arrival, c) MP1 is strongest and the direct arrival is stronger than MP2, and d) the direct arrival is strongest.

There are several discontinuities in the autocorrelation ranges that require further explanation (Fig. 2.6). First, there was a >1 km jump from 13.2 km to 14.5 km at 0240. Since the whale appeared to be swimming at a constant speed towards the OBS, this sudden change is unlikely to represent whale movement. This offset can be explained by a shallowing of

bathymetry (and the reflector) by ~100 m at the location of the multipath bounce. There are a few sharp bathymetrical features around our site (Fig. 2.4(a)), including linear offsets of ~100 m that may correspond to normal faults caused by plate flexure (Oakley et al., 2008).

Second, there were zero ranges between 0540-0555 that jumped suddenly to 2 km at 0555 (Fig. 2.6). Zero ranges are a result of measuring MP1-direct times that equal or exceed the maximum predicted two-way travel time when the whale is overhead (Weirathmueller et al., 2017b). As for the first discontinuity, the measured MP1-direct time may have increased suddenly because the seafloor was offset by a normal fault. Another explanation is that the whale swam westward from the OBS where bathymetry deepened by ~200 m over a few kilometers (Fig. 2.4(a)). The reflective layer may deepen even more due to trenchward thickening of the sediments (Oakley et al., 2008) and the regional undulation of surface sediment thickness (Abrams et al., 1992; Harding et al., 1990). To avoid zero ranges, the reflector must be modeled at 250 mbsf. We note that the ranging could be affected by the modeled sound speed profile from World Ocean Atlas differing from in-situ values. However since sound speeds at >500 m depth are fairly well known and vary less than 5 m/s seasonally (Affatati et al., 2022), the expected ranging error is likely only equivalent to a depth change of a few tens of meters.

Third, for a few ranges at 0240 and between 0800 and 0830, discontinuities were introduced because the two strongest detections were temporarily MP1 and MP2; using the MP2-MP1 model, the ranges were estimated correctly (Fig. 2.6). This might be explained by a relatively sharp minimum in the direct arrival amplitudes that is predicted by the Zoeppritz equations at the ranges corresponding to the critical angle for refraction (Weirathmueller et al., 2017b). Assuming a velocity of 2.9 km/s in the chert layer measured in ODP hole 777B (Harding et al., 1990), the critical distance is 3.6 km. Because this discontinuity is observed to occur at

ranges up to 8-12 km, this is likely a function of the critical range for the soft surface sediments on which the OBS rests.

Ranges for a second fin whale that sang for ~14 hours on January 14-15, 2012 (Fig. 2.5(c)), showed similar features to the first. At the start, autocorrelation and summed spectrogram ranges decreased from 11 km to 8 km using the MP1-direct model. Again, the MP2-MP1 model would correctly calculate ranges because relative detection scores were MP1 > MP2 > direct. From 2315-0100, the summed spectrogram ranges continued to decrease from 8 km to 5 km, while autocorrelation ranges decreased from 19 km to 13 km. As for the first period (Fig. 2.5(b)), the ranging methods differed because relative detection scores were MP1 > direct > MP2. The summed spectrogram and autocorrelation ranges agreed after 0200 because relative arrival strengths were direct > MP1 > MP2. The whale meandered between 8 and 5 km range from 0200-0835 and then, after an interval of quiet, was at ~7 km for a final period from 1030-1145.

Multipath ranging requires a method to correctly decide between ranges calculated by MP1-direct or MP2-MP1 models and we investigated whether this could be done using amplitude, assuming that more distant whales would be recorded as weaker calls. Figure 2.6 shows amplitudes calculated between 15-20 Hz for call detections averaged with the moving 20-minute window used for ranging. Calls within 5 km were uniquely characterized by amplitudes ≥ -130 dB re 1 m/s, but at ranges between 5-20 km, the amplitudes were insufficient to determine the appropriate model. For example, amplitudes of ~-145 dB re 1 m/s were seen at ranges of 10 km, 15 km, and 19 km on the first half of the track (Fig. 2.6). At 10 km and 15 km the MP1-direct timing model was appropriate, while at 19 km the MP2-MP1 timing model was appropriate. Our approach to deciding which model to use was to determine which arrivals had

the highest amplitudes by briefly inspecting the spectrogram and detection scores of calls (Figs. 2.6(b) and 2.6(c)).

Our choice of a 20-minute window for combining calls can be justified by comparing ranges obtained with different window lengths. Figure 2.7 shows results for the proximal part of the first period obtained with windows ranging from 1 to 80-minute length. Ranges using shorter windows were more scattered, while the ranges using longer windows were skewed closer to the OBS, presumably because they tend to be biased by higher amplitude calls recorded at closer ranges. Using a 20-minute window for our ranging method minimizes scatter in range estimates without a significant bias towards smaller ranges.

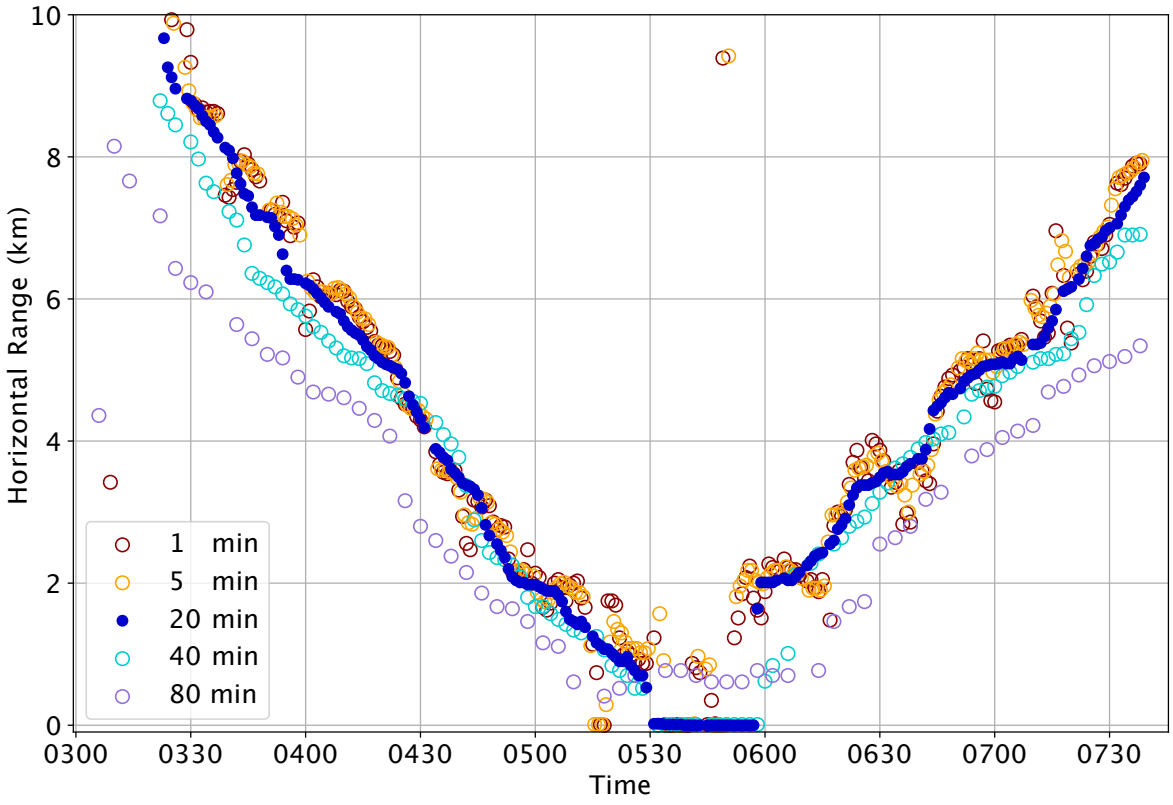

FIG. 2.7. Comparison of autocorrelation ranges calculated with different time window lengths for the portion of the Marianas track on January 18, 2013 Marianas shown by light blue shading in Figure 2.4(a).

We estimated a maximum bias in ranges that might arise by considering the effects of an uneven distribution of fin whale calls within the 20-minute window. Since we ranged only if there was at least one call detection within 30 seconds of the center of the 20-minute window, a worst-case scenario would have all the calls in one half of the window when the central call was the first or last call in a bout. This should bias the range by one quarter of the change in the whale's range over the 20-minute window. Fin whales can swim at up to 20 km/hr, but they generally swim slower than 10 km/hr while singing (Clark et al., 2019). Singing fin whales have most commonly been observed to swim between 4-8 km/hr (Guazzo et al., 2021; Soule and Wilcock, 2013; Varga et al., 2018), which is consistent with our January 18 track where the speed of the whale appeared to be 4.4 km/hr directly towards and then away from the OBS (Fig. S2.1(a)). For speeds of 5-10 km/hr, a whale swimming for 20 minutes would transit 1.7-3.3 km. The resulting maximum range bias from uneven calling if the whale was swimming radially to the OBS would thus be 0.4-0.8 km.

Another problem with using a longer window is that changes in the whale's range change the spacing of multipaths, smearing the peaks in the autocorrelation function or stacked spectrogram detection score. In the worst-case scenario, this could result in peaks with multiple maxima that might be picked inconsistently. Comparisons for the first period showed that 20-minute windows lead to only a modest increase in the width of the multipath relative to 1-minute windows (Fig. S2.1(b)), and we found no examples of peaks with multiple maxima. Travel time modeling showed that the maximum rate of change of MP1-direct times with range was 0.27 s/km at 7.2 km range (Fig. 2.5(a)). For a whale swimming at 5-10 km/hr radially to the OBS, this would lead to a change in the multipath timing of 0.5-0.9 s which is comparable to the

observed width of the multipath peak for 1-s windows, lending support to our conclusion that windows longer than 20-minute are potentially problematic.

B. Hawaii

Multipaths are clear at the Hawaii site because the basaltic seafloor is reflective. However, ranging was challenging because of the bathymetric relief of the Loihi seamount (Fig. 2.4(b)). We estimated ranges for two simplified endmember models that would be appropriate for whales located to the southeast and northwest of the OBS (Fig. 2.8). The first had flat bathymetry and the second approximated the bathymetry of Loihi seamount by a linear slope extending from the OBS with a gradient of 320 m km^{-1}.

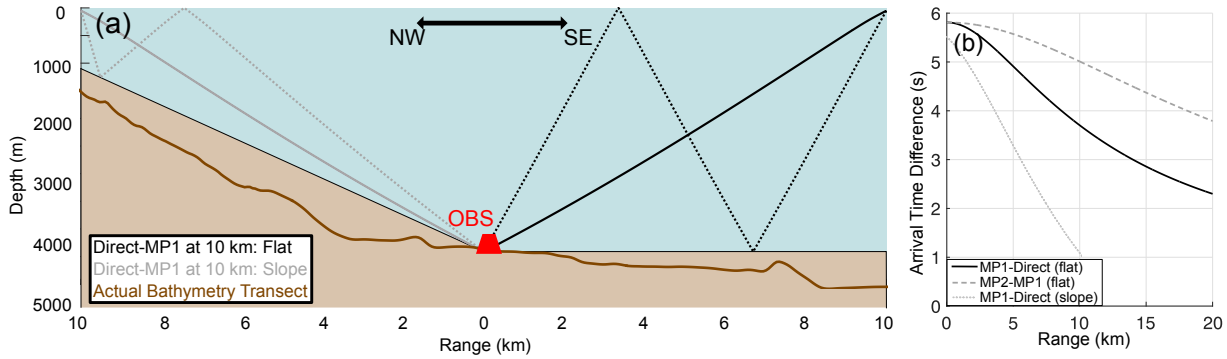

FIG. 2.8. (a) Northwest to southeast cross section through the OBS at Hawaii showing the actual and simplified bathymetric profiles running from Loihi seamount slope to the abyssal plain, and illustrative direct and MP1 ray paths at 10 km ranges. (b) Arrival time difference models for MP1-direct and MP2-MP1 for flat bathymetry and for MP1-direct for a constant slope.

We ranged to whales on December 7, 2010, and February 23, 2011 (Fig. 2.9), using timing models for both choices of bathymetry (Fig. 2.8(b)). For the flat model, the whales were appropriately ranged with the MP1-direct times for both the summed spectrogram and autocorrelation methods except for 1700-1755 on December 7, where MP2-MP1 times were required. Autocorrelation ranges were less scattered than summed spectrogram ranges on both dates, particularly for 1745-2030 on December 7.

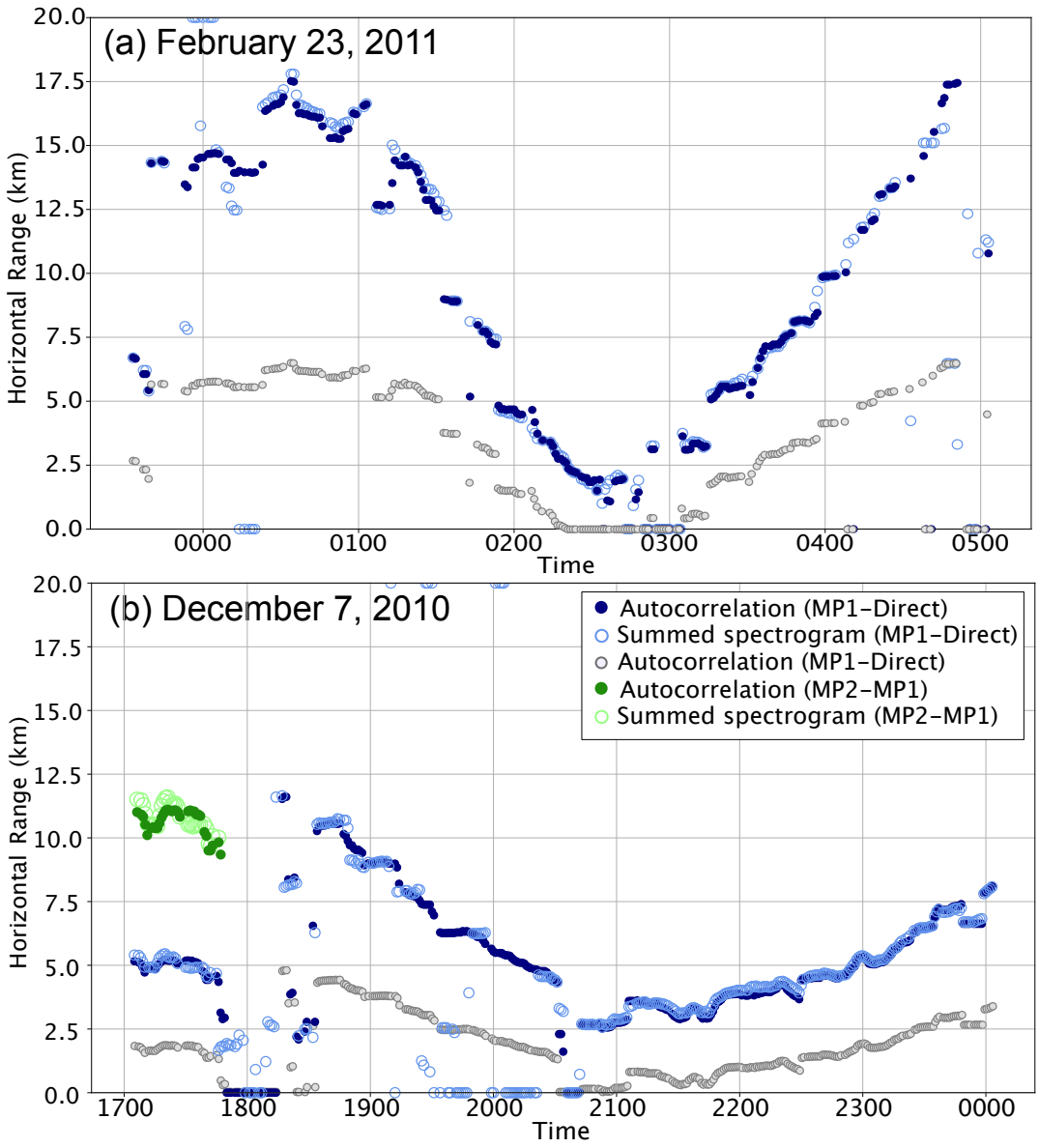

FIG. 2.9. Fin whale ranges at Hawaii calculated for flat (summed spectrogram and autocorrelation) and sloped (autocorrelation only) bathymetry models for (a) a 7-hour period on February 23, 2011, and (b) an 8-hour period on December 7, 2010. Blue autocorrelation and summed spectrogram ranges are calculated using MP1-direct timing models. Green ranges are calculated using MP2-MP1 timing models. Gray ranges are calculated using MP1-direct sloped bathymetry models.

We show only autocorrelation ranges for the sloped model (Fig. 2.9). These ranges are markedly smaller than ranges for the flat model, differing by ~2 km near the OBS and up to ~10 km at the largest distance from the OBS. The true fin whale ranges are uncertain because they

could fall anywhere between these two endmember models depending on the direction of the whale from the OBS. The ranges for the sloped model were zero from 0220-0305 on February 23 and from 2030-2045 on December 7, suggesting that the sloped model is not appropriate for these tracks.

There were several ranging failures in both tracks that we attribute to bathymetric effects. On February 23, scattered ranges during the first and last hour of the track occurred as the measured difference time was transitioning from MP1-direct to MP2-MP1 (Fig. 2.9(a)). However, relative detection scores varied erratically, likely due to complex bathymetry. Thus, the direct, MP1, and MP2 arrivals all contributed to erroneous summary ranges. From 0245-0305 on February 23 (Fig. 2.9(a)), zero ranges were calculated because more than one MP1 arrivals were observed, the strongest of which exceeded the maximum expected multipath arrival time difference. Multiples were not recorded for direct or MP2 arrivals, indicating that this was not a subsurface arrival. Instead, this was likely a propagation effect of uneven bathymetry surrounding the OBS. On December 7 from 1745-1830 (Fig. 2.9(b)), the ranges were erroneous because relative arrival strengths were generally MP2>direct>MP1. MP2-direct times were measured for autocorrelation and direct-MP2 arrivals from adjacent calls for spectrogram stacking, resulting in nonsensical ranges. MP1 arrivals were likely low amplitude because they were defocused by bathymetry.

A complex fin whale song, characterized by higher frequency notes and erratic IPIs, led to bad ranges for the summed spectrogram method on December 7 between 1800-2030 (Fig. 2.9(b)). During this period, the IPI was often as small as ~15 seconds. The time proximity filter was set to 20 s (Table 1) because this was required to ensure there was not more than one detection per call. When the IPI was shorter than this, the detection time for some calls was not on the highest amplitude arrival. The calls were thus misaligned when the summed spectrogram

was created, resulting in erroneous ranges. Autocorrelation was consequently a more robust ranging method because it is not reliant on the time proximity filter to align calls.

C. Puerto Rico

There were no 20 Hz fin whale calls detected at the Puerto Rico site, but we observed other calls with higher frequencies and shorter IPIs (Fig. 2.2(d), Fig. 2.10) that match the sei whale calls described by Baumgartner et al (2008). The calls were downswept chirps lasting >1 second, extending from above the Nyquist frequency of 50 Hz down to 25 Hz. IPIs varied, but many calls occurred as doublets, with an IPI of 4 seconds. Multipaths were visible (Fig. 2.10), so we applied our ranging methods.

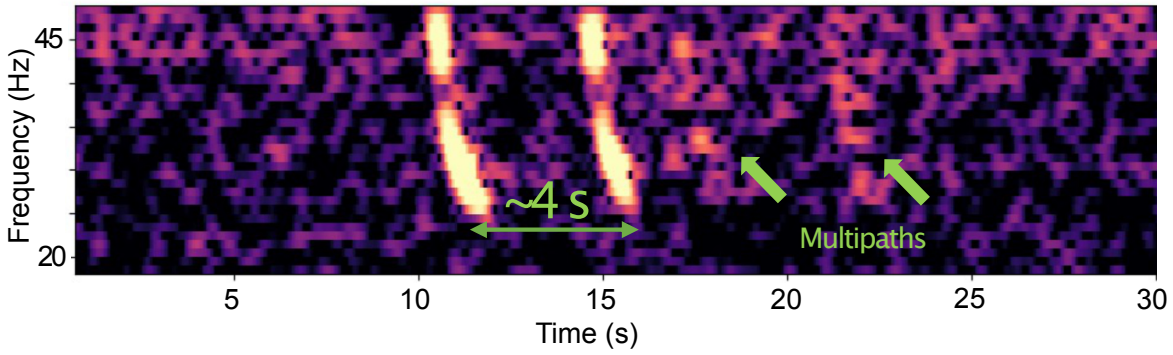

FIG. 2.10. Sei whale calls and multipaths recorded at 2350 on December 10, 2015, on the Puerto Rico OBS. The 4 second IPI pattern matches sei calls previously described by Baumgartner et al. (2008).

The maximum ranging distance is limited by the 4 s IPI doublet that can obscure multipaths for the first call at larger ranges. We restricted the multipath search window to >4.5 s to avoid picking the second call, which restricts range estimates to ≤12 km (Fig. 2.11(b)). If the whale called from farther away than 12 km, the ranging algorithm would erroneously pick MP2 from the first doublet or MP1 from the second doublet. We inspected spectrograms to ensure ranging was only attempted when MP1 arrived after the doublet.

Several intervals of faint sei calling were detected from November-March. Although the summed spectrogram method might be able to range to these distant calls if they were consistently aligned only on the second call of the doublet, the whale only approached close enough to apply both methods automatically for 4.5 hours from December 10-11, 2015 (Fig. 2.11(a)). The ranges from the autocorrelation and summed spectrogram methods using MP1-direct times agreed. The whale began singing at 2155 at a range of 7.3 km, approached at a constant speed to a minimum range of 1.5 km at 0130, and then moved away and ended its song at 4.3 km range at 0225. No subsurface arrivals were observed for multipaths at this site, likely because the carbonate seafloor of the northern Puerto Rico continental rise (ten Brink, 2005) is more reflective than typical seafloor sediments.

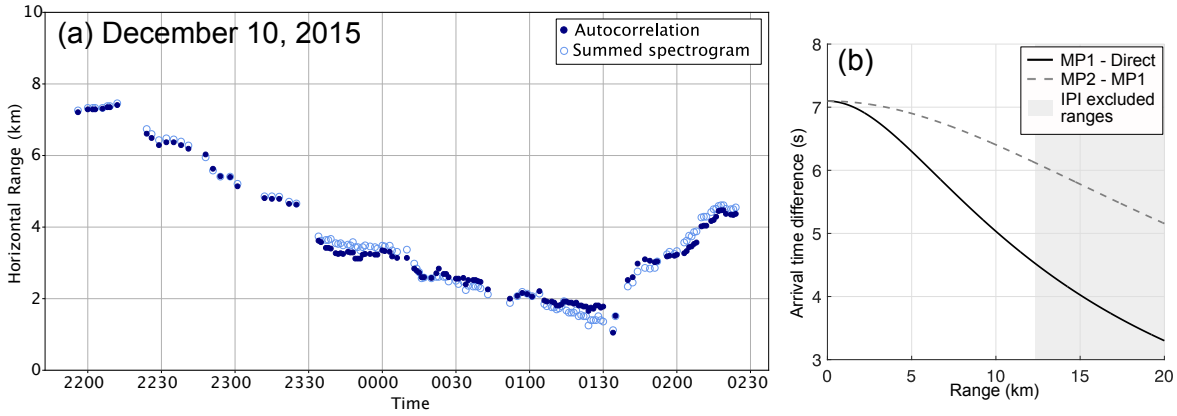

FIG. 2.11. (a) Sei whale ranges at Puerto Rico for 4.5 hours of song on December 10, 2015, and (b) arrival time difference models for MP1-direct and MP2-MP1, with the gray box showing ranges where the 4-second IPI of the doublet prevents ranging (see text).

D. Alaska

Most song bouts at the moderately sedimented site in the Gulf of Alaska (Fig. 2.4(b), Table S2.1) were composed of doublets (Oleson et al., 2014), with alternating high and low frequency notes and an alternating IPI (Figs. 2.12(a) and 2.12(b)). We used a specialized detection template

for each note (Table 2.1) but ranged using the higher frequency note because its greater frequency sweep results in clearer multipaths (Fig. 2.12(b)).

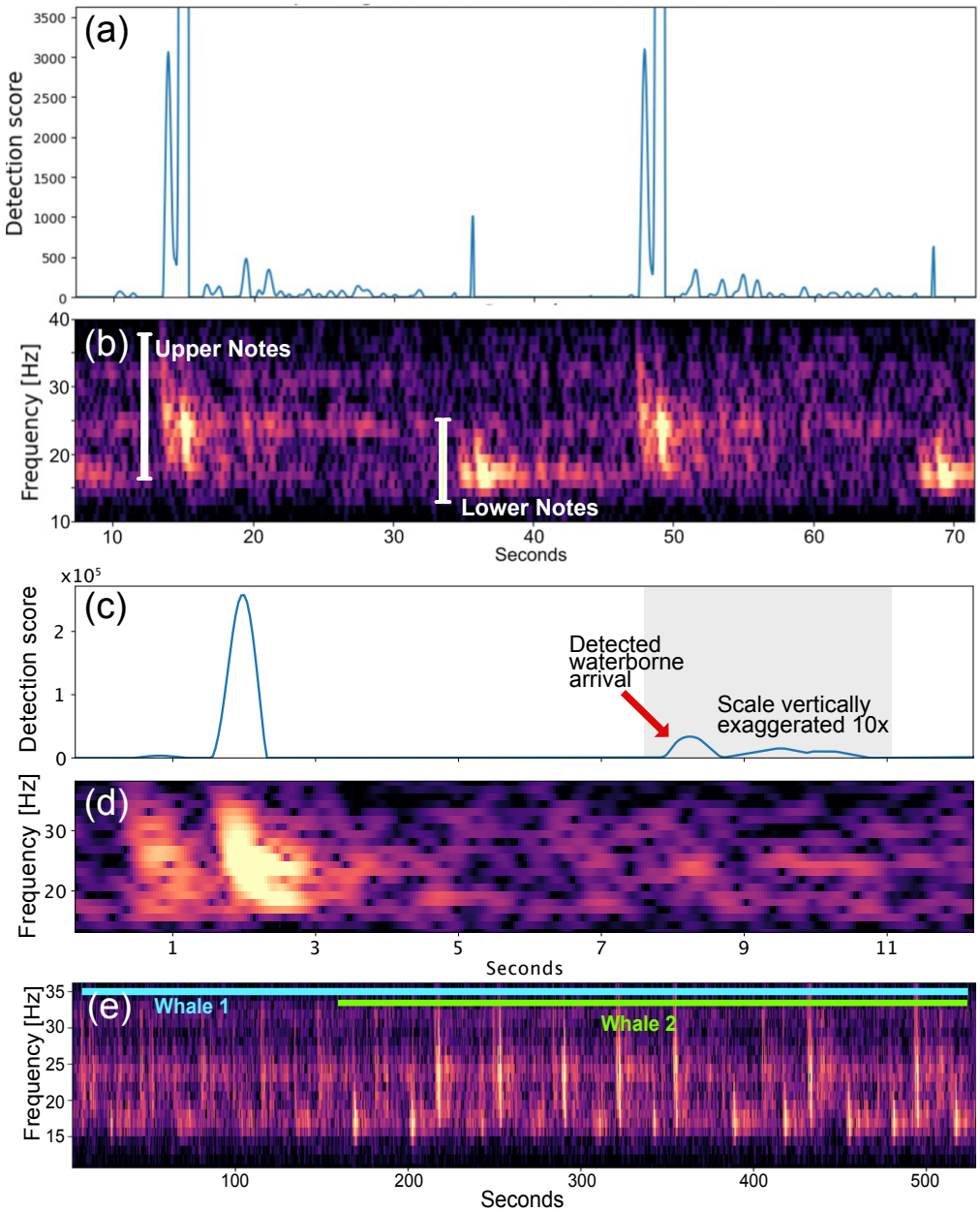

FIG. 2.12. (a) Detection score and (b) spectrogram at 0705 during the February 9, 2019, ranging period showing multi-arrival calling patterns ubiquitous in the Gulf of Alaska region characterized by fainter arrivals ~1 second before main arrival. (c) Detection score and (d) spectrogram of representative call and detected waterborne multipath arrival included in range at 0820 when the whale is almost above the OBS. In (c) the shaded region indicates the time interval over which the vertical scale is increased ten-fold. (e) Spectrogram showing example chorusing from two singing whales that causes multipath ranging failure from 1145-1205.

Surprisingly, we observed double arrivals for both note types in many songs. Direct and multipath arrivals both arrived in two pulses and were uniformly separated by ~1 s (Figs. 2.12(c) and 2.12(d)). Doubled arrivals are hard to explain as artifacts of propagation because they were also recorded on other OBSs in the experiment with varying depths and sediment thicknesses, and we also observed some song bouts with single arrivals at this site. They cannot be basement reflections because the 1-s spacing exceeded the two-way time of 0.35 s through the local sediment layer (Shillington et al., 2015). The second pulse was often stronger than the first (e.g., Fig. 2.12(d)), providing further evidence against reflection. They also cannot be crustal refracted arrivals (or head waves) in front of the direct path because the first arrival is too strong (sometimes stronger than the second, Fig. S2.2), they occur at ranges less than the critical range (e.g., Fig. 2.8(d)), and the relative timing does not vary with time as would be expected as the distance to the whale changes. Fin whales call near the surface, so the second of the double arrivals was too delayed to be a path that initially traveled upwards from the whale and reflected downward from the sea surface. Both pulses generated multipath arrivals with the same spacing, indicating they were produced at the same range, either by a whale calling twice or by two whales swimming together and calling sequentially. We avoided including the second direct path arrival of the double in the ranging by setting a 2-s minimum multipath timing search (Table 1).

We ranged to a single calling period on February 9, 2019 (Fig. 2.13). The whale meandered between 0.5-5 km over 7 hours. The summed spectrogram and autocorrelation methods disagreed often, with more scatter in the summed spectrogram ranges (Fig. 2.13(a)). Summed spectrogram ranges often failed because of unsystematic variations in whether the first or second of the double arrivals is strongest, which resulted in multipath misalignments in the summed call.

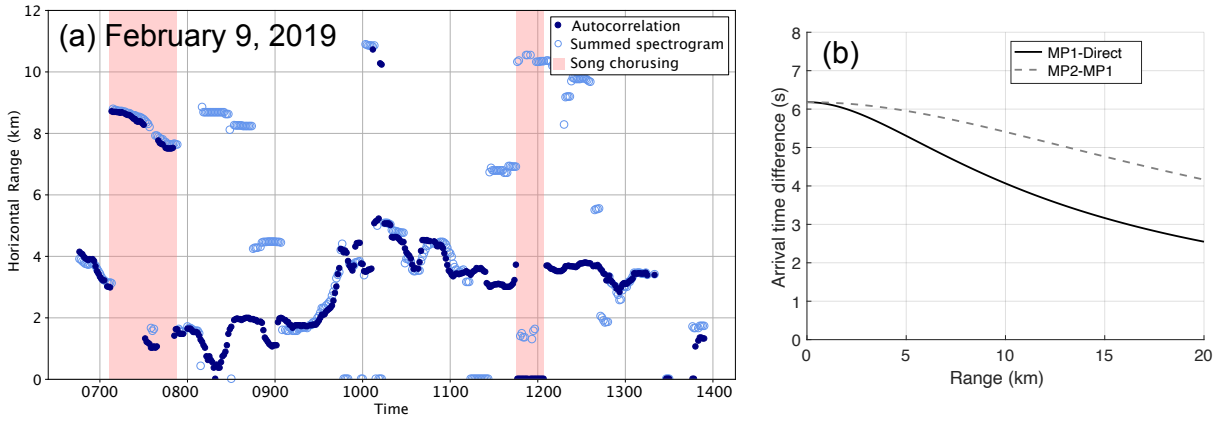

FIG. 2.13. (a) Fin whale ranges at the Alaska site for an 8-hour period on February 9, 2019, with failures due to chorusing shown in pink and (b) Arrival time difference models for MP1-direct and MP2-MP1.

Two notable failures of both summed spectrogram and autocorrelation ranges occurred between 0705-0755 and 1145-1205 when a second whale was singing at a different range (Fig. 2.12(e)). Multiple whales singing at once made it impossible to isolate multipaths from individual whales using either methods, since all the calls were combined into the summed spectrogram or autocorrelation. This resulted in spurious ranges. Additionally, distant chorusing raised the background noise level making faint multipaths harder to detect. Attempts to range to other whales at the Alaska site were unsuccessful due to almost constant chorusing during the fall/winter calling season.

E. US East Coast

For the thickly sedimented US East Coast site (Fig. 2.4(e)), waterborne multipaths were followed by multiple subsurface arrivals that were stronger when the whale was nearby. We created a model of subsurface arrivals using the reflectivity method (Fig. S2.4) and picked the MP1-direct time for the strongest reflection (Fig. 2.14). If ranging with the waterborne multipaths failed when the call was near the receiver, we then ranged using subsurface arrivals.

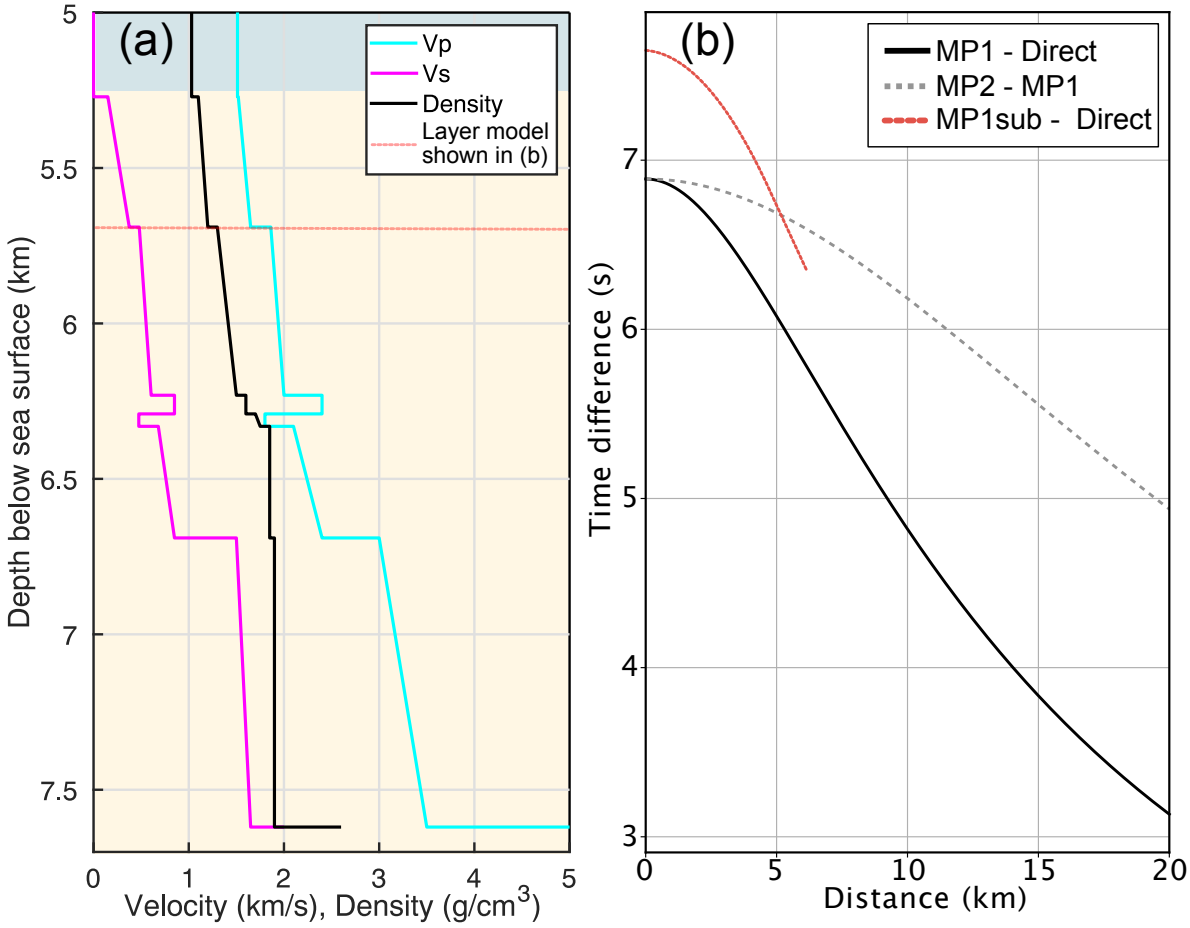

FIG. 2.14. (a) V_P, V_S, and density profiles for the sediments used for the reflectivity model at the US East Coast site informed by ODP borehole 603 and an overhead MCS profile (Bécel et al., 2020), with the strongest reflector marked in red. (b) Arrival time difference models from BELLHOP for MP1-direct and MP2-MP1 (black and gray) and from seismic reflectivity for $MP1_{sub}$-direct for the strongest subsurface reflector (red).

A track for February 28-March 1 (Fig. 2.15(a)) highlights two effects of subsurface reflections on multipath ranging. First, near 2250 and 2345, when the whale was at a range of ~3.5 km, the waterborne MP1-direct model produced zeroed ranges because higher amplitude subsurface arrivals were detected (Fig. 2.15(a), Fig. 2.16(a) and 2.16(b)). Ranges estimated with the $MP1_{subsurface}$-direct model (Fig. 2.14(b)) matched the expected ranges at 2345 but they were ~1 km too small at 2250, possibly due to a change in the depth of strongest subsurface reflection layer. The layer depth undulates slightly along the overhead MCS profile. Between 2255 and

2340, the waterborne MP1-direct model worked because the range was < 3 km and the subsurface reflection arrived outside the multipath search window which ended at 7.2 seconds (Table 2.1).

Second, between 0000-0315 on March 1, the summed spectrogram and autocorrelation ranges often disagreed, with the summed spectrogram ranges at 12 km and the autocorrelation ranges jumping between 8 km to 12 km. Manual inspection of arrivals verified that the whale remained at ~8 km and the ~12 km ranges are spurious, arising because a reflected subsurface arrival is detected more strongly than the waterborne arrival (Fig. 2.16(c) and 2.16(d)). We infer that this occurred because of a local minima in the amplitude of the waterborne direct wave due to destructive interference from Lloyd's mirror effect (Pereira et al., 2020) removing the lower frequencies that are emphasized in our call detection template. This inference is supported by the presence of Lloyd's mirror interference in calls at a similar range from 2055-2115 while the whale was approaching the station (Fig. S2.5). The seismic reflectivity model also predicts a local minima in waterborne direct wave amplitudes and stronger subsurface reflected arrivals at ~8.5 km (Fig. S2.6(a)) although it may be fortuitous that we match the range because we do not know that the whale depth of 50 m assumed in the reflectivity model is correct.

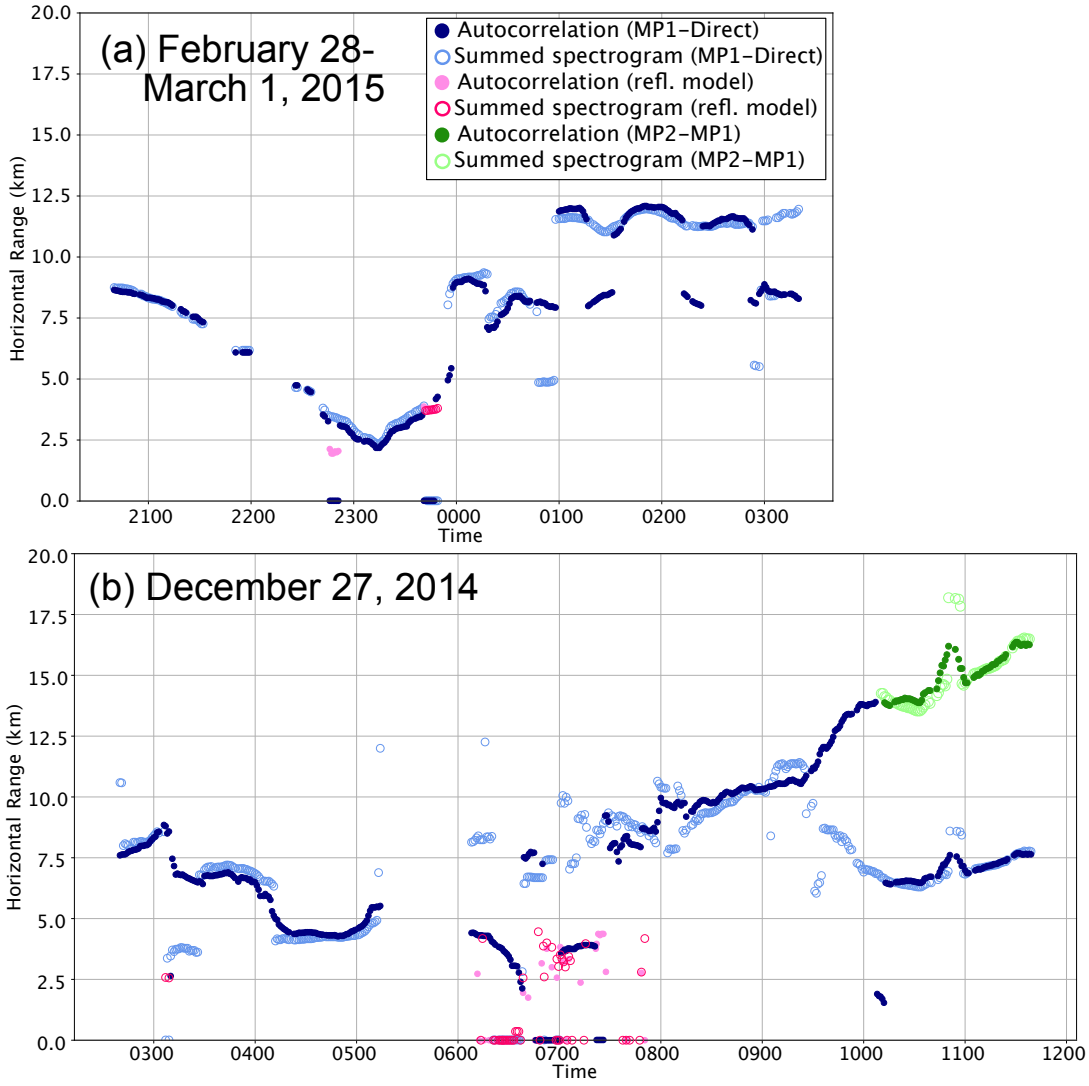

FIG. 2.15. (a) Fin whale ranges (blue) at US East Coast for a 6-hour period on February 28, 2015. Zeroed ranges are reattempted using a subsurface arrival model calculated using seismic reflectivity (pink). (b) Same as (a) but for a 9-hour period on December 27, 2014. Green ranges are calculated using MP2-MP1 timing models.

Subsurface reflections influence ranges for a second track on December 27 (Fig. 2.15(b)) which has additional complications which arose from the presence of two calling whales. The first whale called alone from 0245-0515 while generally moving towards the OBS. At 0610, this whale began singing again, moving towards and away from the OBS at distances of 2 km to 4.5 km. At the same time, a second whale started singing at ~7.5 km and moved away from the OBS.

The chorusing continued until 0730 when the first whale stopped singing. The chorusing confused the summed spectrogram method which yielded a mixture of zero ranges and scattered ranges for the more distant whale. The autocorrelation performed better, mostly yielding reasonable ranges for the nearer whale with a few distant and zero ranges. We applied our reflectivity MP1-direct times to zeroed ranges (Fig. 2.15(b)) but it only sometimes yielded more reasonable estimates for the nearer whale, presumably because of the effects of chorusing.

After the nearer whale stopped singing, the more distant whale continued to sing as it moved away from the OBS and was initially well ranged by both methods. At 0930 and 1010, MP1-direct ranges were suddenly offset to smaller values for the summed spectrogram and autocorrelation methods, respectively. These offsets correspond to times when the MP1 and MP2 amplitudes exceed that of the direct path. Using the MP2-MP1 model after 1010 showed that the whale reached a range of 17 km before it stopped singing.

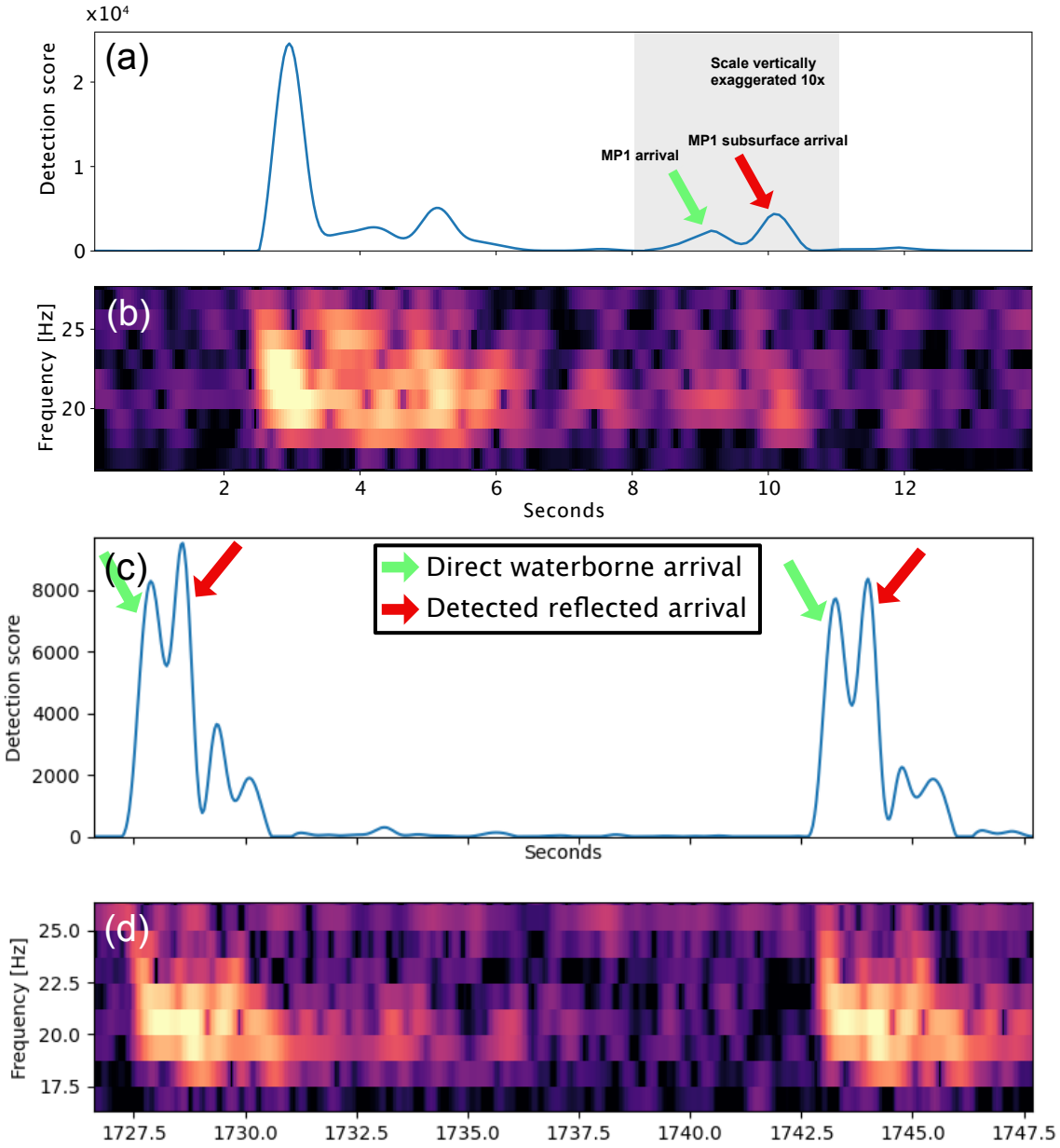

FIG. 2.16. Examples of calls with problematic subsurface arrivals at the US East Coast site. (a) Detection score and (b) spectrogram of a call at 2345 on February 28 where the subsurface MP1 arrival is stronger than the waterborne arrival. (c) Detection score and (d) spectrogram of two calls at 0130 on March 1 when a subsurface arrival with a short delay is stronger than the direct waterborne arrival.

2.4 | DISCUSSION

In this study we assessed the challenges of multipath ranging at full ocean depths to fin whale calls, and in one example sei whale calls, using five OBSs from sites with varying characteristics. We showed that 20-minute windows were effective at enhancing the signal-to-noise ratio of multipath arrivals sufficiently to detect faint multipaths while limiting uncertainty from whale motion. The autocorrelation method worked best at all sites because the summed spectrogram method was more sensitive to errors from misaligned calls and other non-multipath signals that were included in summed spectrograms. At each site, challenges arose from biological and environmental features, most of which were accounted for with additional analysis.

A. Challenges

i. *Multipath identification*

For our methods, it is important to distinguish whether we measured MP1-direct or MP2-MP1 arrival time differences. This is highlighted by ranges calculated at Marianas, Hawaii, and the US East Coast sites (Fig. 2.6, Fig. 2.9(b), Fig. 2.15(b)). For ranges <5 km at Marianas, a call amplitude threshold successfully identified the MP1-direct measurements (Fig. 2.6), but at longer ranges, amplitudes were not useful for deciding between MP1-direct and MP2-MP1. Instead, we decided between using MP1-direct and MP2-MP1 by inspecting example spectrograms and detection scores; the summed spectrogram method measures MP1-direct amplitudes when the direct arrival has the highest amplitude, while the autocorrelation method measures MP1-direct amplitudes provided either the direct or MP1 amplitude is greater than the MP2 amplitude. To automate the methods for tracks that approach within a few kilometers of an OBS, it should be possible to use a high amplitude threshold to identify MP1-direct times and then use these as a

baseline to choose between the MP1-direct and MP2-MP1 models so that ranges change smoothly. For tracks that are always distant, automation would require a robust approach to estimating the relative amplitudes of direct, MP1 and MP2 arrivals.

ii. Subsurface reflections

The importance of understanding subsurface multipath reflections is highlighted at Marianas and East Coast sites. At Marianas, ranging accuracy was somewhat limited by the uncertainty in the depth of a strong shallow chert reflector that arose from increased sediment accumulation towards the trench, undulations in reflector depth, and faults in the chert layer that are only sometimes evident in seafloor bathymetry (Abrams et al., 1992; Oakley et al., 2008). Despite this, ranges were reliably calculated out to 20 km using both MP1-direct and MP2-MP1 arrivals (Fig. 2.5, Fig. 2.6).

Ranging challenges from subsurface reflections were more complex at the US East Coast site, where several subsurface multipaths arose from reflective boundaries in the sediment column (Fig. 2.15, Fig. 2.16). Ranging using subsurface multipath arrivals when the waterborne MP1 was not measured required the development of a reflectivity model to determine MP1-direct times for the strongest subsurface reflector (Fig. 2.14, Fig. S2.4). Well-constrained reflectivity modeling was possible when the whale was nearby because of extensive characterization of sedimentary structure through borehole and MCS studies (Bécel et al., 2020; van Hinte et al., 1987). This only yielded reasonable ranges for a subset of the problematic solutions but was enough to understand the cause of problematic ranges and could be the basis for identifying times at which ranges should be interpolated. This shows the utility of ranging with subsurface models at thickly sedimented sites when profiles of subseafloor properties (V_P, V_S, and density) are available from seismic profiles or borehole data.

Stronger subsurface arrivals also caused errors for more distant ranges at the US East Coast site. This occurred only while a fin whale called for an extended period at a constant ~8 km range on March 1, 2015, after 0000 (Fig. 2.15(a)). Errors are not due to refracted waves, which emerge at ~12 km range and have much lower amplitudes than the direct arrivals (Fig. S2.6(b)). Instead, we observed local minimums in direct waterborne arrival amplitudes and destructive interference from the Lloyd's mirror effect, consistent with the reflectivity model predictions (Fig. 2.16(c) and 2.16(d)), Fig. S2.5(a)). Though these arrival patterns are evident in calls at this range in other tracks (Fig. S2.5), they do not seem to affect calculated ranges when the whale's horizontal range is changing, likely because we combine calls over 20 minutes and thus include calls at ranges that do not show the interference effect. However, stationary and slow-moving fin whales are at risk of spurious ranges from direct waterborne arrival minimums and stronger subsurface arrivals at very specific ranges which are ~8.5 km, ~10.5 km and ~12.5 km in our reflectivity model (Fig. S2.6(a)) which assumes a vocalization depth of 50 m. This is not a concern at distances >14 km where measured multipath arrivals are MP2-MP1.

iii. *Bathymetric relief*

Bathymetric relief leads to significant ranging challenges (Weirathmueller et al., 2017b) due to complicated acoustic propagation. This was well illustrated at the Hawaii site where ranging fails at times due to the strongest arrivals being non-consecutive (e.g. MP2 > direct > MP1 or direct > MP2 > MP1) or when more than one arrival was recorded for a multipath (Fig. 2.9). Even when ranging successfully yields a solution, the ranges at Hawaii had up to ~10 km uncertainty due to variations in the differential arrival times that arose from variations in seafloor depth rather than range.

Less extreme bathymetric features also may affect ranging. Bathymetry at the Marianas site gradually deepens westward towards the trench, which leads to increased disagreement with our flat bathymetry model as range increases. Additionally, smaller features of <200m relief within 20 km of the OBS are linked to seamounts and faults. These features would have a smaller effect on ranging than is observed at Hawaii but are a possible explanation for discontinuities in calculated ranges and ranges that jump to zero for some solutions when the whale was near the site.

iv. *Closely spaced calls*

Multipath detection is hindered for songs with IPIs that are shorter than multipath arrival windows. A variety of call patterns highlight this challenge at Puerto Rico, Hawaii, and Alaska. At Puerto Rico, maximum ranges were limited by the small separation of sei whale doublets (Fig. 2.10, Fig. 2.11(b)). Limiting the search window to >4.5 s avoided the doublet spacing being misidentified as the multipath spacing, but limits ranging to ≤12 km.

At both Hawaii and Alaska, call spacings within the expected multipath separation confused summed spectrogram ranges (Fig. 2.9(b), Fig. 2.13(a)) and are one reason why autocorrelation is a more robust method. At Hawaii, this resulted from complex song bouts on December 7, 2012 from 1745-1830 with short note spacings that led to misalignments in the summed spectrograms and thus, bad ranges. Misalignments occurred because the time proximity filters were set with a minimum call spacing that was informed by the IPI of the dominant single or doublet song and needed to be long enough to avoid detections on more than one arrival for the same call. If the minimum time for the time proximity filter exceeded the spacing of calls, then some calls were detected on a lower amplitude later arrival. The autocorrelation method is not sensitive to misalignment because it does not rely on time proximity filters.

The double calling pattern observed in the Gulf of Alaska also led to bad ranges throughout the ranging period with the summed spectrogram method but not autocorrelation. Double arrivals spaced 1-2 s apart (Fig. 2.12(a)-2.12(d)), occurred commonly on each of 10 OBSs investigated at varying locations and depths throughout the AASCE network. They led to misalignments in the summed spectrogram method because the largest amplitude arrival varied between the two arrivals.

Though not described in previous publications, similar double calling patterns have been observed in other regions such as the Bering Sea (personal communication, Daniel Woodrich) and the Azores (personal communication, Andreia Pereira)(Fig. S2.3). As discussed in section III(D) the double arrivals cannot be easily explained by a single call taking two paths or refraction, and a downward sea surface reflection would require the whale to be unreasonably deep. This pattern could arise from two whales singing together or by a single whale modifying its vocal behavior. Further studies are required to understand this phenomenon.

v. *Chorusing*

Chorusing from two or more whales singing at different locations causes two problems for multipath ranging. First, elevated background noise levels in the fin whale frequency band can obscure both waterborne and subsurface multipath arrivals. Second, ranging attempts to a whale with stronger calls can be confused by fainter but distinguishable arrivals from other whales. The first problem was partially overcome in our analysis by combining all calls within a 20-minute ranging window. However, when distinct calls were visible from more than one whale, both our multipath ranging methods failed. This caused problems along a portion of one track at the ENAM site (Fig. 2.15(b), 0610-0730) and all but prevented ranging at the Alaska site because of almost constant chorusing. We only found one track where we were able to

successfully range and even this was interrupted by two short intervals of chorusing (Fig. 2.13(a)). This is consistent with previous studies that found extensive fin whale call presence throughout the late summer-late winter in the Gulf of Alaska (Pearson et al., 2023; Rice et al., 2021).

B. Applications and future work

The three-component particle motion method is an alternative approach to ranging to fin whales with a single OBS that has complementary strengths to the multipath method (Harris et al., 2013; Matias and Harris, 2015). One disadvantage of the particle motion method is that it only works out to the critical range, the range corresponding to the critical angle for total reflection. At sites with strong velocity contrasts at or just beneath the seafloor, this is quite restrictive. For example, for a basaltic seafloor with a velocity of 2.5 km/s (Christeson et al., 1994) the critical range is 4.5 km for a seafloor depth of 6 km and for the chert layer at Marianas with a velocity of 2.9 km/s (Harding et al., 1990) this is reduced to 3.6 km. At the Marianas site, multipath ranges were obtained to nearly 20 km. Thus, in areas of low calling density, the multipath method may be a more useful technique. Conversely, in areas of high call density such as the Gulf of Alaska where chorusing prohibits effective ranging with the multipath method, the more limited range of the particle motion method may be advantageous and would likely still provide enough data for reliable density estimates.

An advantage of the three-component method is that it can localize calls if the OBS orientation is known because it determines the azimuth to the fin whale relative to the horizontal channels. It is also not sensitive to bathymetric relief, which, as our Hawaii site demonstrated, leads to very large uncertainties in the ranges estimated from multipaths. In the future, the strengths of the particle motion and multipath methods could be combined to extend the range of

single-station fin whale call localization capabilities in areas of high relief and seafloor reflectivity (McDonald and Fox, 1999). To localize a fin whale call at distances greater than the critical range, the horizontal components of an OBS can be used to calculate the bearing of a fin whale call with a 180° azimuthal uncertainty (Matias and Harris, 2015). The azimuth and ranges could be determined by comparing the relative timing of three or more multipaths with multipath arrival time models for the two alternative bathymetry profiles.

A systematic comparison of multipath and particle motion methods is necessary to compare their effectiveness in settings with different depths, seafloor seismic properties, sediment thickness, and bathymetry. Where both methods yield similar solutions, such a comparison would also provide some verification of their reliability, although ideally, they should be compared for OBS networks where the stations are sufficiently close to allow multi-station TDOA localization.

Large networks of OBSs can have dozens of instruments and extend over hundreds of kilometers. Applying ranging to all the OBSs in a network would provide call density estimates over a large region. Though OBSs in large networks are usually too widely spaced for TDOA localization, directional movement might be inferred via analysis of all the OBSs in the network as whales transit in and out of range of nearby sensors. If the OBS spacing allowed, it might be possible to hand off the ranging of one whale from one OBS to the next. Capturing calls from the same whale on different OBSs over time would allow for more advanced density estimation methods, namely mark-recapture or spatially explicit capture-recapture (Marques et al., 2013).

Though multipath ranging is a tool that is used to estimate spatial call densities, animal densities are of more interest for ecological and conservation purposes (Thomas and Marques, 2012). Converting measurements of call densities to animal densities requires independent

knowledge of the calling or cue rates of the calling species, which is difficult to constrain because calling behavior changes over time and by region (Helble et al., 2020; Oleson et al., 2014; Sirovic et al., 2013; Weirathmueller et al., 2017a). Efforts to further develop single station ranging techniques should be conducted in concert with studies that measure cue rates using acoustic tags and/or visual observations combined with recordings on passive acoustic instruments (Guazzo et al., 2021; Marques et al., 2013; Stimpert et al., 2015; Thomas and Marques, 2012).

Instrument sampling rates for passive OBS studies have typically varied from 50-200 Hz; increasing the sampling rate would increase the number of whale species that could be studied with OBSs. In this study, we successfully ranged to sei whale song which would not have been possible with an OBS that sampled at 50 Hz. A sampling rate of 200 Hz would allow ranging to other species such as pygmy blue whales and Bryde's whales which both make downswept impulsive calls centered around 70-80 Hz (Gavrilov et al., 2011; Wang et al., 2022). The addition of a higher-frequency hydrophone channel to OBSs, or a separate hydrophone attached to the OBS frame, sampling at 1000-2000 Hz would enable studies of essentially all baleen whales and sperm whales, with the exception of some humpback whale song that can reach frequencies >15kHz (Au et al., 2001; Davis et al., 2020; Moore et al., 2006).

2.5 | ACKNOWLEDGMENTS

We thank Danielle Harris, Dave Mellinger, Andreia Pereira, and Shima Abadi for helpful conversations that improved our methods and manuscript, Arthur Nowell for editorial comments, Uri ten Brink for facilitating access to the USGS Puerto Rico Trench OBS experiment data, and two anonymous reviewers for constructive comments. This research was funded by the Office of Naval Research under Award No. N00014-21-1-2564.

Chapter 3:

Applying distance sampling to estimate densities of fin whale calls recorded by ocean bottom seismometers in the Marianas region

Authors: Rose Hilmo[1], Danielle Harris[2], William S.D. Wilcock[1]

[1]School of Oceanography, University of Washington, Seattle, WA, USA
[2]Centre for Research into Ecological and Environmental Modelling, University of St. Andrews, United Kingdom

3.0 | ABSTRACT

Ocean bottom seismometers (OBSs) are opportunistic instruments for passive acoustic monitoring of fin whales. To estimate animal population densities from acoustic data using distance sampling, a standard density estimation method, it is essential to estimate ranges to detected calls. Regional OBS networks are too widely spaced to localize fin whale calls through trilateration of arrivals on multiple instruments. This motivates the development of ranging methods using single instruments. We previously developed and published a single-OBS ranging method for fin whale calls that uses the relative timing of multipath arrivals for calls reverberating in the water column to estimate horizontal ranges to fin whales. In this study, we applied multipath ranging and distance sampling methods to fin whale calls recorded on seven OBSs deployed over a 200 x 300 km^2 area east of the Marianas trench from February 2012-Janurary 2013. We detected and ranged to calls within 40 km at each OBS, then applied point-transect distance sampling methods to fit detection functions and estimate the probability of call detection. We calculated monthly fin whale call densities during the Marianas calling season from December-April, except for February when airgun shots prevented ranging. We discuss sources of uncertainty in call density estimations and identify encounter rate variance as the largest contributor. Increasing the number of OBSs used for ranging would improve the precision

of call density estimates. Looking forward, converting call densities into estimates of animal abundance will require independent estimates of fin whale call rates.

3.1 | INTRODUCTION

Passive acoustic monitoring (PAM) is an important tool for studying large baleen whales. PAM records whale vocalizations that usually use hydrophones but sometimes uses opportunistic instrumentation such as ocean bottom seismometers (OBSs) (McDonald et al., 1995; McDonald and Fox, 1999). PAM is ideal for monitoring far-ranging migratory species with limited visual observation options (Mellinger et al., 2007), and can provide long-term continuous data that are difficult to obtain by other means (Lewis and Širović, 2018; Mcdonald et al., 2009; Rice et al., 2021, 2022b; Weirathmueller et al., 2017a). High intensity baleen whale calls can propagate for tens of kilometers, allowing PAM to monitor large regions (Blackwell et al., 2021; Marques et al., 2011; Risch et al., 2014).

Using acoustic data to estimate whale populations usually requires techniques to localize or range to calls (Marques et al., 2013). Closely spaced instruments can be used to localize calls that arrive on multiple instruments through trilateration (Blackwell et al., 2021; Dreo et al., 2017; Dréo et al., 2019a; Dunn and Hernandez, 2009; Soule and Wilcock, 2013; Stafford et al., 1999a; Warner et al., 2017), but this is often not possible with sparse regional OBS networks (instrument spacing of tens of kilometers) that were not designed with marine mammal monitoring in mind. This motivates the development of methods to localize or range to calls recorded on single instruments. To date, single station methods have been developed for calls of various toothed and baleen whale species using acoustic transmission loss models (McDonald and Fox, 1999; Samaran et al., 2010; Wiggins et al., 2004), timings of multipath arrivals of calls (Hilmo and Wilcock, 2024; Iwase, 2015; Kuna and Nábělek, 2021; McDonald and Fox, 1999; Širović et al., 2007; Tiemann et al., 2006; Weirathmueller et al., 2017b), and particle motions for orthogonal tri-axial sensors (Harris et al., 2013, 2018; Iwase, 2015; Matias and Harris, 2015).

Once ranges to whale vocalizations are calculated, point-transect distance sampling methods (Buckland et al., 2001) can be applied to estimate call densities and abundances (Blackwell et al., 2021; Harris et al., 2013, 2018; Marques et al., 2013). With an independent estimate of typical call production rates, call density estimates can then be transformed into estimated animal densities.

Fin whales are large baleen whales that are found in all ocean basins. They generally feed on zooplankton and small schooling fish at high latitudes in the summer-fall and breed at temperate latitudes in winter-spring (Edwards et al., 2015; Herr et al., 2022; Joiris and Dochy, 2013; Mizroch et al., 1984, 2009; Pérez-Jorge et al., 2020). Fin whale males produce song composed of repeating high-amplitude calls centered around ~20 Hz that downsweep ~10 Hz over ~1 second (Croll et al., 2002) that is easily identified in PAM studies. PAM methods are ideal for studying fin whales, since fin whale calls are regularly recorded in regions where visual studies report minimal presence (Brodie and Dunn, 2015; Dréo et al., 2019; Hamilton et al., 2009; Jackson et al., 2004; Miksis-Olds et al., 2019).

Fin whale calls are low enough in frequency to be recorded by OBSs, which typically sample at 50 Hz or higher (McDonald et al., 1995). This makes global deployments of OBS networks particularly useful for opportunistic PAM studies of fin whales (Dréo et al., 2019; Iwase, 2015; Weirathmueller et al., 2017a). Indeed, several studies have employed single station methods to range to fin whale calls recorded on OBSs in various settings where localization via trilateration is not possible (Harris et al., 2013; Hilmo and Wilcock, 2024; Kuna and Nábělek, 2021; Matias and Harris, 2015; Weirathmueller et al., 2017b), and have demonstrated applications of distance sampling to range datasets (Harris et al., 2013).

In this study we use OBSs to characterize fin whale call densities in the equatorial Pacific at the Marianas trench. There have been few observations of fin whales in this region, but calls have been reported on an OBS (Hilmo and Wilcock, 2024). We implement the semi-automated multipath method developed by Hilmo and Wilcock (2024) to detect and range to fin whale calls using an OBS network deployed from 2012-2013. We apply point-transect distance sampling methods to estimate monthly fin whale call densities in the region (Buckland et al., 2001; Harris et al., 2013; Marques et al., 2013). We demonstrate the potential of this method for characterizing fin whale populations in under-surveyed regions using OBS experiments, discuss its limitations, and suggest future steps to take to improve its utility.

3.2 | METHODS

A. Data

We analyze OBS data from the Mantle Serpentinization and Water Cycling Through the Mariana Trench and Forearc experiment (Wiens, 2014) deployed from February 2012 through the end of January 2013. The seismic network comprised 20 OBSs and 5 moored deep hydrophones extending 400 km east-west and 300 km north-south across the Marianas Trench. For this study, we excluded 8 instruments on the west side of the experiment because they were deployed on shallower, mountainous bathymetry that complicates acoustic propagation. We analyzed only deep instruments deployed on the relatively flat seafloor to the east. Of the 12 instruments deployed in deep water we excluded 2 due to deployment on mountainous bathymetry and 3 due to poor data quality. We also attempted to use data from moored hydrophones in the trench but rejected them all due to poor data quality. In total, 7 instruments were used for analysis (Fig. 3.1), all of which were SIO OBSs with Nanometrics Trillium 40 seismometers. Vertical channel 100 Hz data for the full deployment year were retrieved for each

OBS from the Incorporated Research Institutions for Seismology Data Management Center database (now part of the Earthscope Consortium Data Services).

We obtained winter sound speed profiles at each site from the World Ocean Atlas (Boyer et al., 2018). Borehole (Abrams et al., 1992) and multichannel seismic studies (Oakley et al., 2008) show that the seafloor sediment in this region is acoustically transparent with a strong subsurface reflector below the seafloor. This structure is composed of a surface layer of unconsolidated sediments and a subsurface lithified chert/porcellainite layer. The depth of the lithified layer below the seafloor varies between 35 meters to a few hundred meters. However, because we do not have measurements of the lithified layer depth at our OBSs, we use a simplified assumption of 100 meters depth based on estimates from OBS B19 obtained by Hilmo and Wilcock (2024).

For each OBS, we estimated site-specific arrival time models for the direct arrival and first, second and third multipaths at 10 meter range intervals out to a distance of 40 km (Fig. 3.2) using BELLHOP (Dushaw and Colosi, 1998; Porter and Bucker, 1987), a ray-tracing acoustic propagation model. We assumed a flat seafloor with the depth equal to that of the OBS and a call source at 50 m depth (Pereira et al., 2020; Stimpert et al., 2015). We modeled the acoustically transparent surface sediments as part of the water column, with the OBS suspended 100 m above the reflective chert layer (Fig. 3.2a).

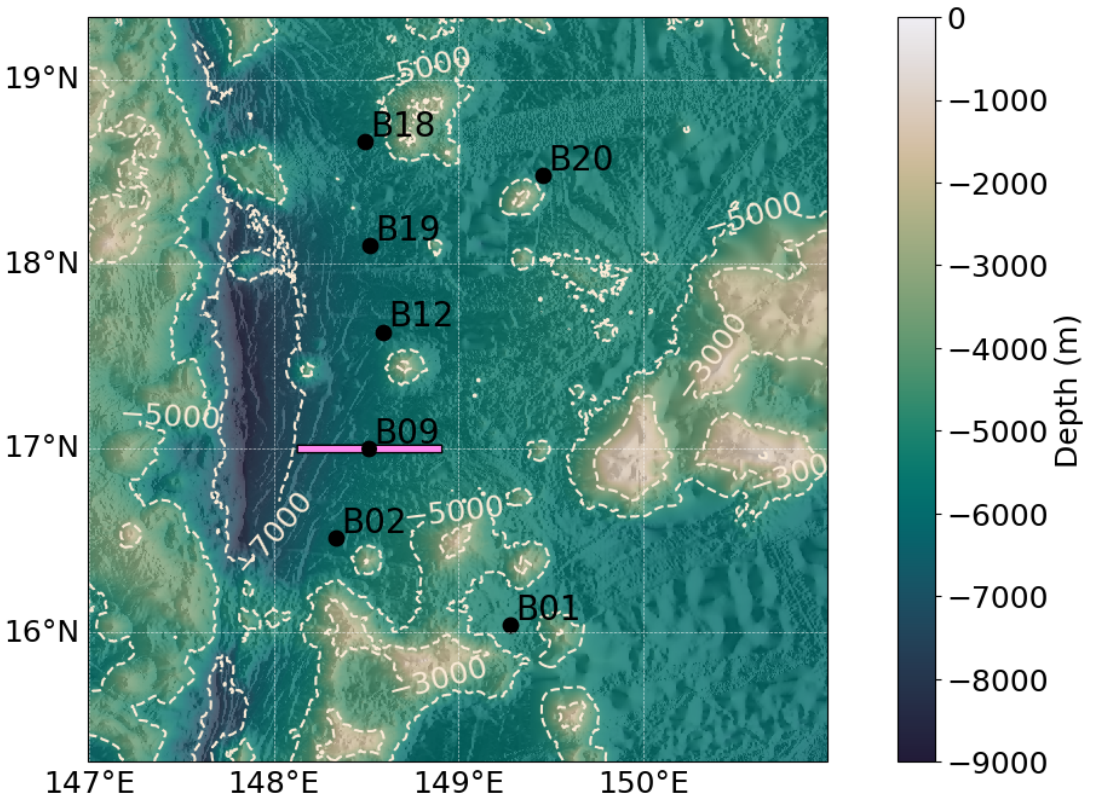

FIG. 3.1: Bathymetric map showing the OBSs used for fin whale call density estimation using multipath ranging as labelled black circles. The pink line extending 40 km east and west of station B09 shows the depth transect used to estimate the ranging uncertainty resulting from bathymetry (Figure S3.3).

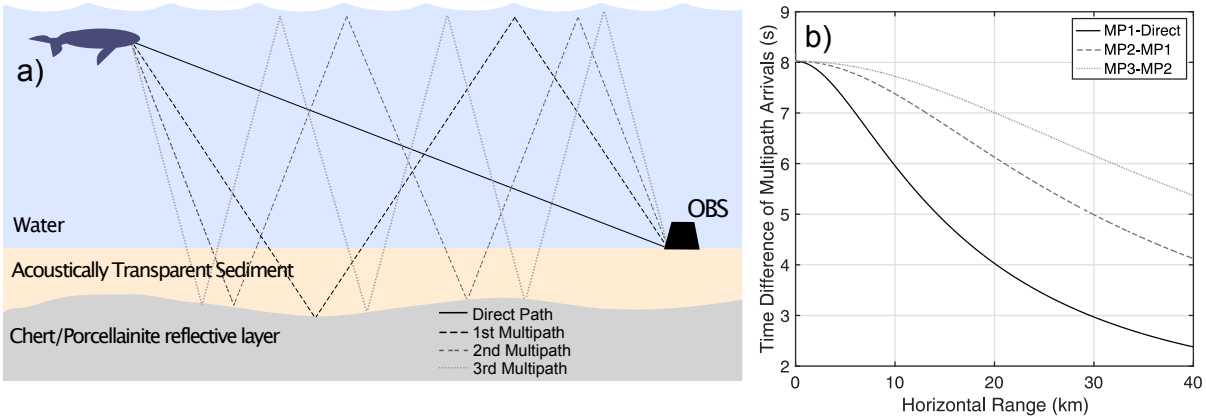

FIG. 3.2: (a) Simplified diagram illustrating ray paths of the first four multipath arrivals from a fin whale to an OBS. (b) Time difference of arrival against horizontal range for consecutive multipaths for an OBS at 5949 m depth (OBS B19). Modeled time differences of multipath arrivals are reported for the first multipath minus direct arrival (MP1-Direct), second multipath minus first multipath (MP2-MP1), and third multipath minus second multipath (MP3-MP2).

B. Multipath ranging

Estimating the range to a fin whale from an OBS through multipath ranging relies on measuring the timings of repeated arrivals of a single call that echo off the sea surface and the sea floor (Fig. 3.3). Arrivals with more reflections arrive at the OBS later (Fig. 3.2). The observed time difference of multipath arrivals can be compared with those predicted by ray tracing to estimate horizontal range. This approach requires identification of which multipaths are being detected, which is complicated by the fact that relative strengths of multipaths change with distance. This is because earlier multipaths with shallow source angles decrease in relative amplitude with distance as rays are refracted to intersect the seafloor at shallower angles. Here, we estimate distances to fin whale calls following the autocorrelation multipath ranging method described in Wilcock and Hilmo (2024). The method combines consecutive calls in fin whale songs to obtain robust ranges. Here, we refine this approach by developing a semi-automated method to identify which multipaths were measured and select the appropriate timing model hypothesis (Fig. 3.2b).

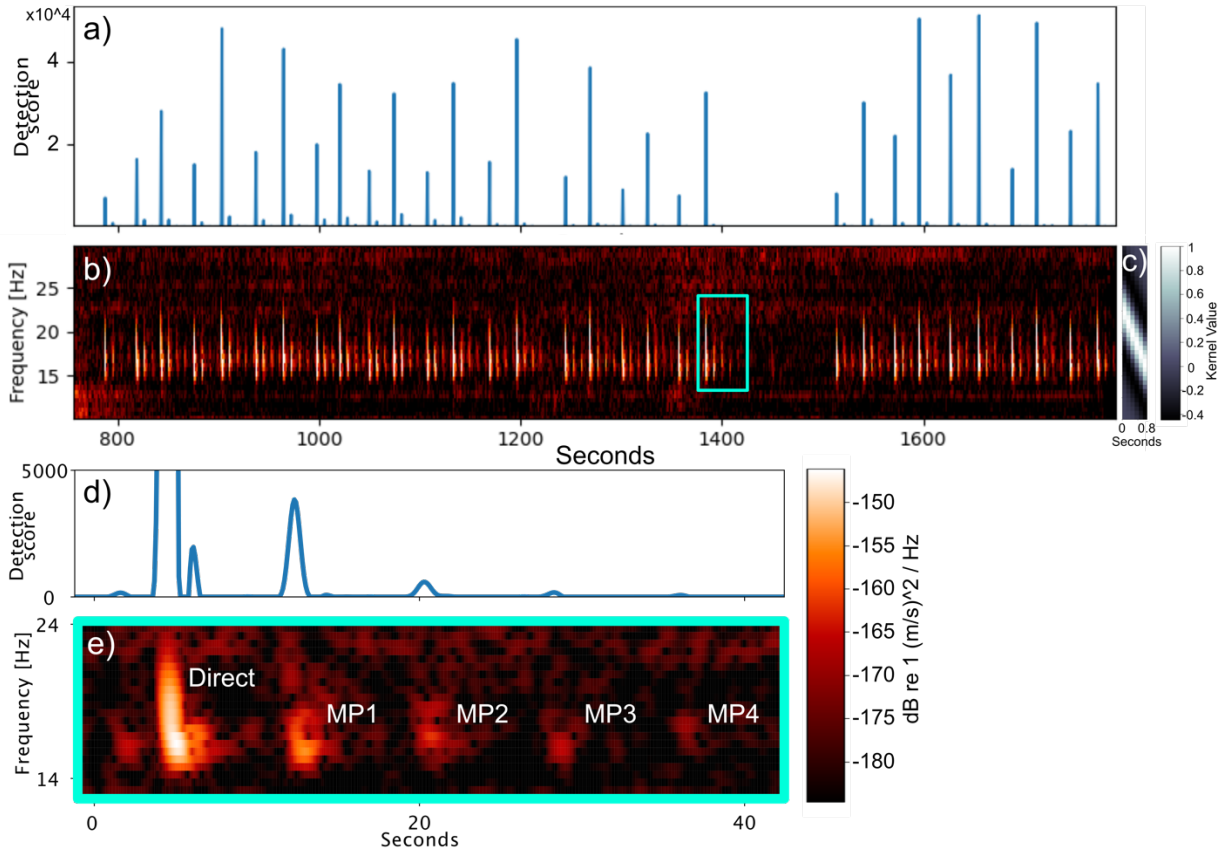

FIG. 3.3: (a) Detection score and (b) spectrogram of 15 minutes of fin whale song recorded by OBS B19 at 0600 on January 18, 2013. Calls within a song are typically spaced at 15 to 25 s (c) 2-D kernel (time axis exaggerated 30x) that was cross-correlated with the spectrogram to calculate the detection score. (d) Detection score and (e) spectrogram of the direct and multipath arrivals of a fin whale call (highlighted in cyan in (b)).

For each site, we downloaded the timeseries and removed the sensor response using ObsPy, a Python toolbox for seismology (Beyreuther et al., 2010). We calculated a spectrogram with a 0.8-s Hanning window and 95% overlap. We detected fin whale calls by cross-correlating the spectrogram with a 2-D template synthetic call and then picked peaks in the resulting "detection score" (Fig. 3.3) (Mellinger and Clark, 1997). The template call (Fig. 3.3(c)) was 0.8 seconds in duration and downswept linearly from 20 to 15 Hz. We implemented at time proximity filter of 13 seconds to exclude all but the highest amplitude detection for each call.

To avoid false positives, we implemented our multipath ranging method only if at least two calls are present in a minute and at least 10 total calls are detected within the 20-minute

surrounding time window. We estimated the horizontal range to the whale as follows. We autocorrelated 21 minutes of the detection score series centered on the minute of interest. Then, we measured the time difference between the highest peak at zero lag and the highest peak within a feasible time window for multipath arrivals. We did this by restricting the search to lags that ranged from 2 s to the overhead two-way travel time plus 0.5 s. Since we did not know what two multipath arrivals were being measured *a priori*, we calculated ranges for each of three modeled arrival time difference hypotheses (Fig. 3.2b).

We designed an automated algorithm to choose our initial whale track by selecting the multipath hypotheses that resulted in the smoothest path (Fig. S3.1). First, sequential ranges with the same hypothesis that were close in space (within 1.5 km) and time (within 1 hour) were linked together into groups. Sequential groups containing at least 12 ranges with <3 hours gap between them were linked into tracks. This avoided confusing the automated algorithm with occasional groups of spurious ranges resulting from high amplitude signals like earthquake swarms or T-phases. Isolated groups were later manually discarded or assigned to groups. Finally, the best multipath hypothesis was assigned to each group in each track by selecting the set of hypotheses that minimized the RMS difference between the end and start ranges of consecutive groups.

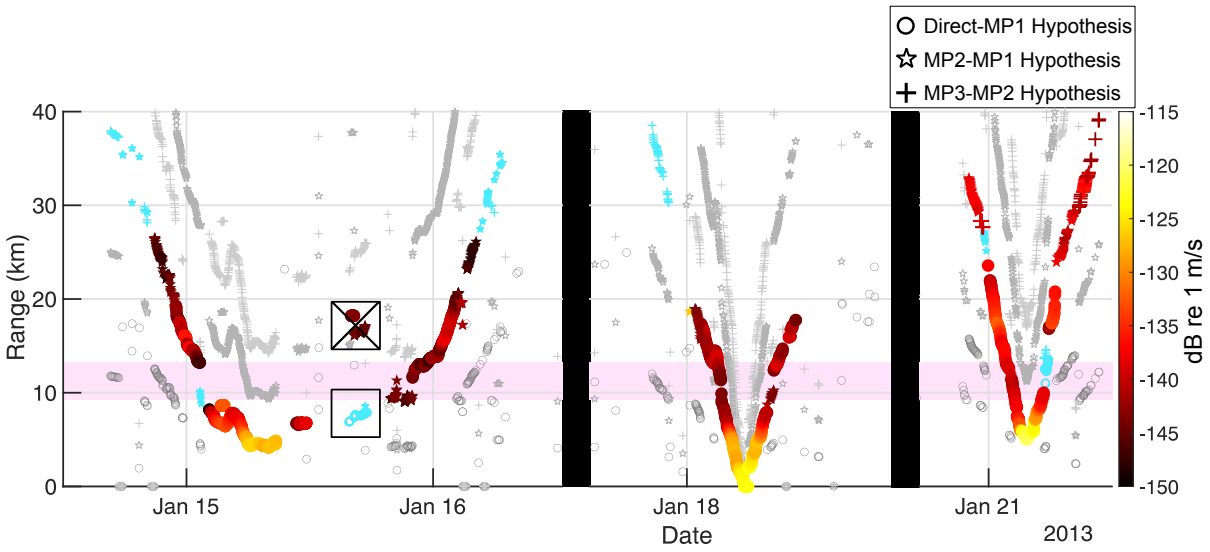

FIG. 3.4: Scatter plots showing ranges calculated for three tracks recorded on OBS B19 in January, 2013. Filled symbols colored by average amplitude show ranges to tracks following the method in the text. Grey symbols show ranges for multipath hypothesis that were not selected. Cyan symbols show groups of ranges that were not linked into tracks by the automated analysis but were subsequently added by manually. Black boxes on January 15th show a group of incorrect ranges (crossed out box) which was corrected by manual analysis (open box). A pink bar highlights a distance band where recorded calls have amplitude minimums. This leads to lower rates of call detection and thus fewer ranges.

We inspected the automated tracks manually to ensure the selected hypotheses produced a smooth path. Sometimes, we corrected miscategorized groups; for example, on January 15th, 2013, at ~1600 a group of calls were wrongly assigned to the MP2-MP1 hypothesis rather than Direct-MP1 (Fig. 3.4). If the correct hypothesis for a group was not clear within the context of the automated whale path, we selected it after inspecting spectrogram of the fin whale song. Where appropriate, we manually added smaller groups (<12 ranges) that were not included by the automated process (Fig. 3.4). Finally, each track was interpolated with a cubic-spline to estimate a range for each detected call. Histograms of fin whale call ranges for each OBS are shown in Figure 3.5.

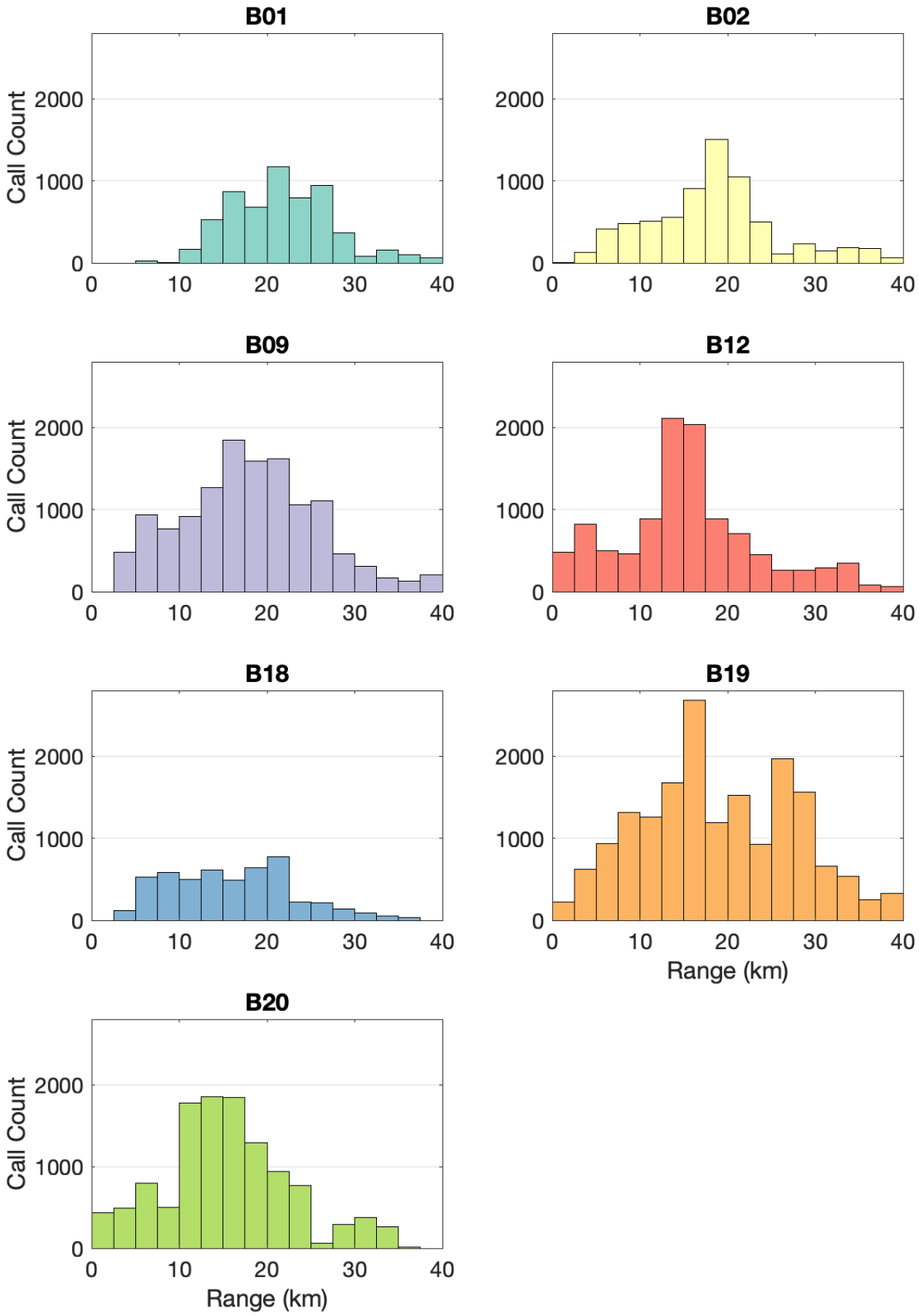

FIG. 3.5: Histograms of call ranges for each OBS.

C. Call density estimation

We estimate fin whale call density by treating OBSs as point-transect observers that detect and range to animal "cues" (Marques et al., 2011). The formula we used for estimating the density of animal cues ($\widehat{D}$) is

$$\widehat{D} = \frac{n(1-\hat{c}_{fd})}{\pi w^2 \hat{P}_{det} k m} \quad , \tag{1}$$

where n is the number of detected cues, $\hat{c}_{fd}$ is the proportion of false detections, w is the truncation distance, $\hat{P}_{\text{det}}$ is the probability of detecting a cue within the monitored region, and k is the number of point-transect observers (OBSs) (Buckland et al., 2001). If an independent estimate of "cue rate" is known, $\widehat{D}$ can be scaled to estimate animal density and abundance. In our case, n is the number of automatically detected fin whale calls (Table 1). We estimated $\hat{c}_{fd}$ to be 1.9% manually through examining 80 hours of fin whale song. We set w to 35 km to improve the reliability of the detection function fitting (Buckland et al., 2001), which excludes the ~2% of detected calls that were estimated at a larger range. We standardize $\widehat{D}$ for difference in month length by dividing by effort (m), which we define as number of days in the month divided by 31 (Table 1). We estimated $\hat{P}_{\text{det}}$ through fitting detection functions to range distributions using the *Distance* software package in R (Thomas et al., 2010).

We used $\hat{P}_{det}$ to estimate monthly call densities using equation (1). We calculate the coefficient of variation for monthly densities ($CV(\widehat{D})$) using the Delta method (Buckland et al., 2001) which uses both the coefficients of variation of the preferred detection function $CV(\hat{P}_{det})$ and encounter rate $CV(\frac{n}{k})$ for each month according to

$$CV(\widehat{D}) = \sqrt{[CV(\tfrac{n}{k})]^2 + [CV(\hat{P}_{det})]^2} \quad , \tag{2}$$

where $\frac{n}{k}$ is the encounter rate (ER) (Table 1) and other parameters are as in equation (1). The standard error $SE(\widehat{D})$ of monthly call densities is related to the coefficient of variation according to

$$SE(\widehat{D}) = \left[CV(\widehat{D})\right] * \widehat{D} \quad . \tag{3}$$

Lognormal lower and upper 95% confidence intervals (LCL, UCL) are calculated as $(\frac{\widehat{D}}{C}, \widehat{D} * C)$, where

$$C = \exp\left[1.96\sqrt{\ln\left(1 + CV(\widehat{D})^2\right)}\right] \quad . \tag{4}$$

3.3 | RESULTS

We analyzed data from March 1, 2012 to February 1, 2013. In total, our method ranged to 69,809 fin whale call detections. All calls were found in March, April, and December of 2012, and January of 2013 (Fig. 3.8, Table 3.1). Ranging was not feasible in February 2012 because airgun noise from a seismic survey that spanned almost the whole month prevented accurate fin whale call detection and ranging. Though our automated method occasionally reported detections and ranges outside of these months, all of them were categorized as isolated, unassigned groups that required manual verification. All were rejected after manual inspection of the spectrograms and identified as other acoustic signals such as swarms of earthquakes, T-phases, and ship noise.

The months of January and March had the lowest coefficients of variation for encounter rate (<30%), indicating counts of detected calls were similar between OBSs (Table 3.1). For December and April, the counts of detected calls varied more between OBSs which resulted in higher coefficients of variation of encounter rate of 37% and 67% respectively. This is expected because they are the shoulder months of the calling season, when call presence is more irregular

in the region. The April encounter rate variation was particularly high because calls were only detected on 4 out of the 7 OBSs.

Month	**Site Area (km^2)**	***k***	**Total Area (km^2)**	**Effort (*m*)**	***n***	**ER (*n/k*)**	**SE(ER)**	**CV(ER)**
Dec	3849	7	26939	1	15146	2163.7	802.6	0.37
Jan	3849	7	26939	1	22759	3251.3	730.2	0.22
Mar	3849	7	26939	1	25185	3597.9	956.7	0.27
Apr	3849	7	26939	0.97	5204	768.2	512.8	0.67

TABLE 3.1: Parameters for estimating density. Columns from left to right are the month, the site area monitored (π*35km^2), the number of OBSs (*k*), the total area monitored (*k**Site Area), the effort standardized by length of month (total days divided by 31), the total number of call ranges, the encounter rate (ER) which is *n/k*, the standard error of the encounter rate (SE(ER)), and the coefficient of variation for the encounter rate CV(ER).

The subset of 68,294 ranges (~98% of all detections) within our truncation distance (*w*) were used to fit our detection function. We tested multiple detection functions and picked the best fitting one through minimizing the Akaike information criterion (AIC) while manually verifying the model did not overfit the range distribution (Fig. 3.6, Table 3.2). We evaluated models of simple hazard-rate and half-normal key functions with no adjustments or covariates, hazard-rate and half-normal key functions with up to 4 cosine adjustments, and adjusted models with site as a covariate (18 models total). We report four representative test models here (Fig. 3.6, Table 3.2). We found that half-normal key functions overfit more distant ranges and did not fit the distributions of closer ranges well (Fig. 3.6(a&c)). They were rejected because it is critical for detection functions to fit nearby ranges well.

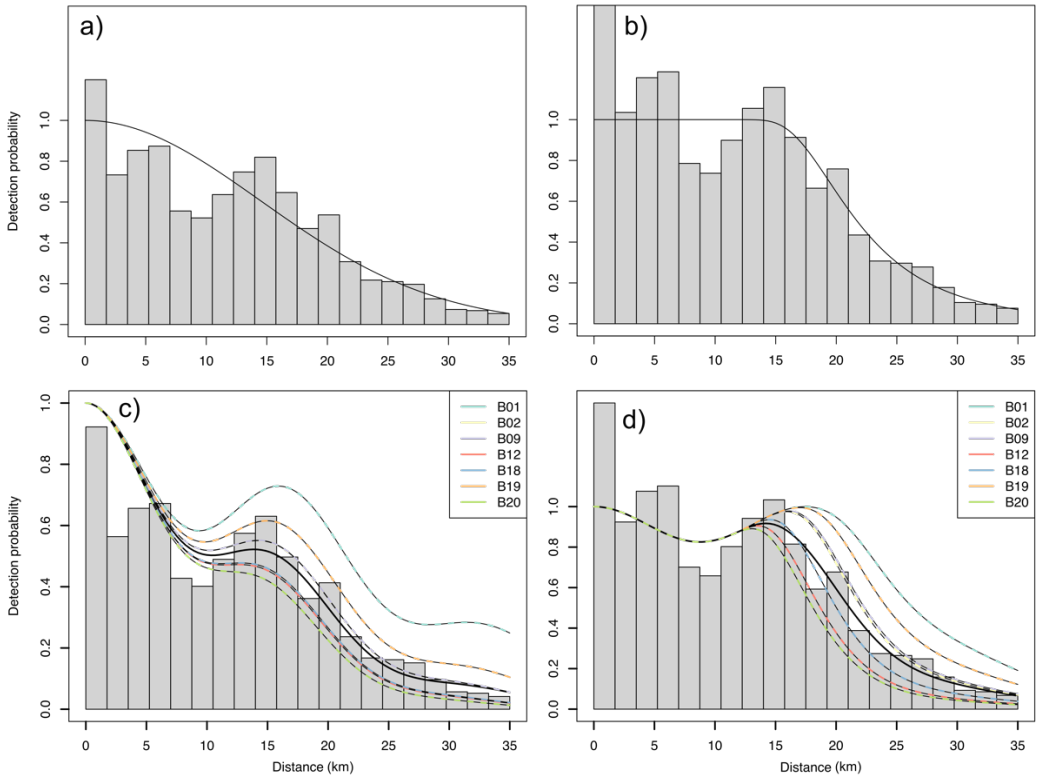

FIG. 3.6: Fitted detection functions plotted for the (a&c) half normal and (b&d) hazard-rate key function models presented in Table 2. The hazard rate model shown in (d) was selected for call density estimates. It includes the site as a covariate and 4 cosine adjustment parameters .

Key function	**Covariates**	**C-vM p-value**	$\widehat{P}_{det}$	**SE($\widehat{P}_{det}$)**	**CV($\widehat{P}_{det}$)**	**ΔAIC**	**Figure 6**
Hazard-Rate, cosine(4)	Site	8.49E-06	0.408	0.003	.007	0	d)
Half-normal, cosine(4)	Site	7.53E-02	0.249	0.002	.007	1947.3	c)
Hazard-Rate	None	7.08E-05	0.458	0.002	.004	4678.7	b)
Half-normal	None	1.36E-01	0.324	0.002	.005	6636.6	a)

TABLE 3.2: Summary of the detection function models plotted in Figure 6 reported in order of quality as indicated by ΔAIC. The columns list the model key functions, covariates, the Cramer von-Mises p-value (C-vM p-value), the average probability of detection ($\widehat{P}_{det}$), the $\widehat{P}_{det}$ standard error (SE($\widehat{P}_{det}$)), the $\widehat{P}_{det}$ coefficient of variation (CV($\widehat{P}_{det}$)), the difference in Akaike information criterion between reported models (ΔAIC), and corresponding detection function plot in Figure 6.

We selected the half-normal key function with four cosine adjustment terms and the site as a covariate as the best fit because it had the lowest AIC, best Cramer von-Mises p-value, a

good visual fit to the range distributions, and a close alignment of the data with the 1:1 line on the Q-Q plot (Fig. 3.6(d), Fig. 3.7, Table 3.2). This detection function is non-monotonic, with a detection probability minima at ~10 km. This is typically not ideal for distance sampling because it indicates that the detection function is overfit. However, it is justified for our data because there is a decrease in ranging success rates at this distance. As described by Wilcock and Hilmo (2024), this occurs because the direct arrival has an amplitude minima at ~10 km associated with the critical range for full reflection from the soft sediments on which the OBS rests. Indeed, the method often did not observe the direct arrival (Fig. 3.4) and recorded lower detection scores at ranges between 8-12 km (Fig. S3.2).

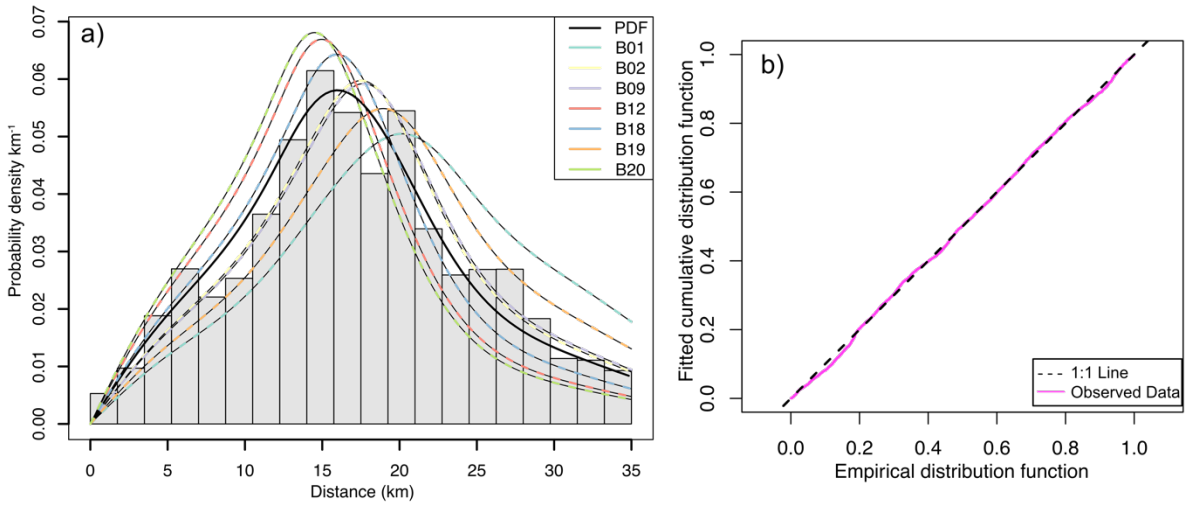

FIG. 3.7: (a) Preferred detection function with 4 cosine adjustment parameters (black line) and site as covariate (dashed colored lines) plotted as a probability density function with a histogram of range distributions from all sites. (b) Quantile-quantile plot used to assess the goodness of fit of the preferred detection function. A good fit is indicated by the close alignment of the observed data points (magenta line) with the 1:1 line (black dashed line).

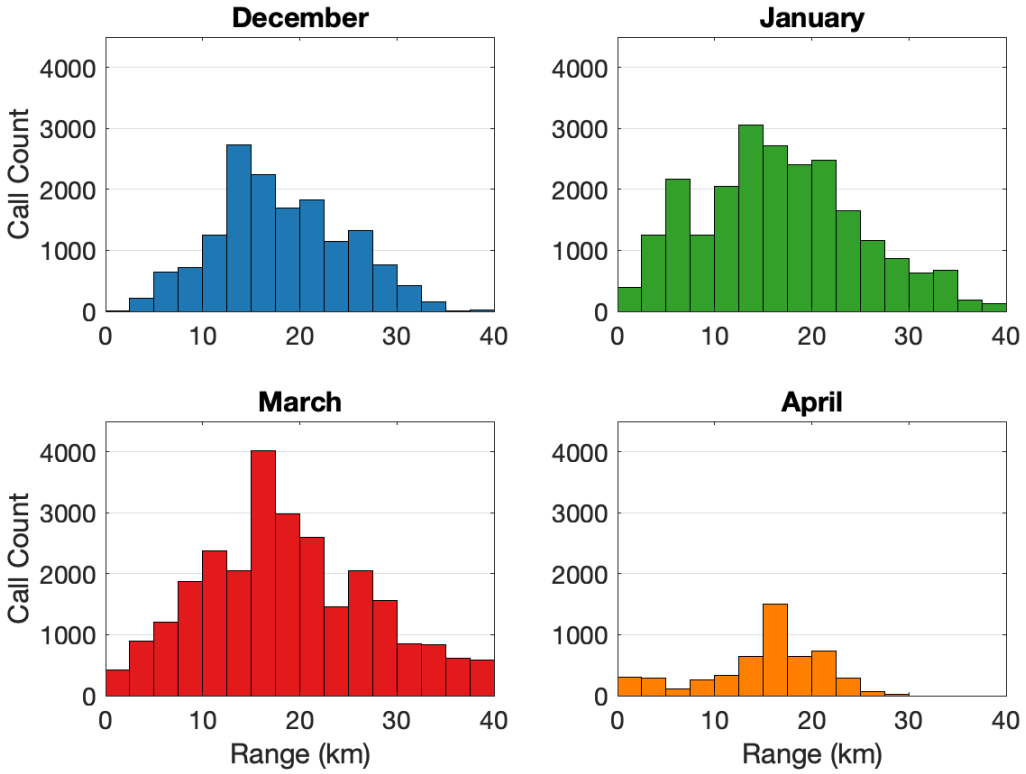

FIG. 3.8: Histograms of range distributions for each month when fin whales were detected (March, April, and December of 2012, and January of 2013). Airgun shooting prevented fin whale detection during February 2012 and all OBSs were recovered by February 4, 2013.

Our preferred model estimated the probability of detection ($\hat{P}_{det}$) within our study region to be 40.8% (Table 3.2, Fig. 3.7). We applied the $\hat{P}_{det}$ to calculate the densities of fin whale calls for each month using equation (1) (Table 3.3, Fig. 3.9). The highest density of calls occurred in March, and the lowest density in April. We simplistically estimated that February call densities were likely between 2.17 km^{-2} (averaged from January and March values) and 2.55 km^{-2} (estimated by polynomial fit) depending on whether peak calling season occurs during February or March (Fig. 3.9). However, this assumes the 2011-2012 and 2012-2013 fin whale song seasons are similar as March-April represent the end of the one season and December-January the start of the next. For all months, $CV(\hat{D}) \approx CV(\frac{n}{k})$ because the variation from the detection function fit ($CV(\hat{P}_{det})$) was negligible (<1%) compared to the variation from monthly encounter

rates ($CV(\frac{n}{k})$) (equation (2)). $CV(\widehat{D})$ have acceptable values for distance sampling for all months except April due to low call counts. Call density $SE(\widehat{D})$ and 95% confidence limits calculated using equations (3) and (4) are also reported (Table 3.3, Fig. 3.9).

Month	Call Density (per km^2)	$SE(\widehat{D})$	$CV(\widehat{D})$	LCL	UCL	DF
Dec	1.35	0.50	0.37	0.67	2.72	6.0
Jan	2.03	0.45	0.22	1.33	3.11	6.0
Mar	2.25	0.61	0.27	1.34	3.78	6.0
Apr	0.48	0.32	0.67	0.15	1.58	6.0

TABLE 3.3: Monthly call densities calculated using our preferred detection function. Also reported are the standard error $SE(\widehat{D})$, the coefficient of variation $CV(\widehat{D})$, the lower 95% confidence limits (LCL), the upper 95% confidence limits (UCL), and the degrees of freedom (DF).

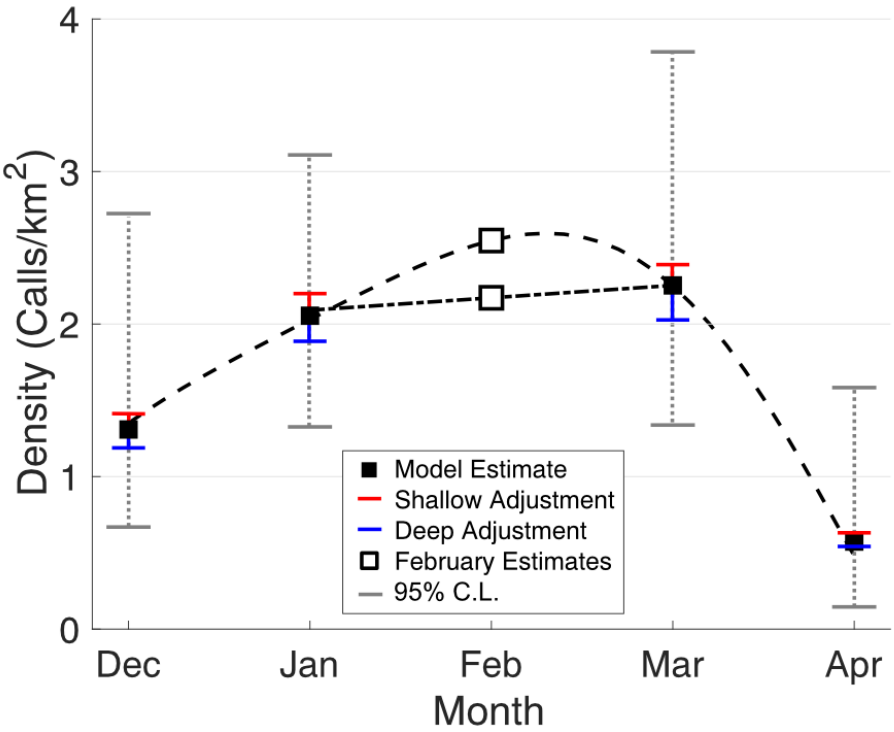

FIG. 3.9: Monthly spatial call densities estimated by our preferred detection function (Fig. 3.7) and 95% lognormal upper and lower confidence limits. Also shown are estimates of the effects of shallower (red) and deeper (blue) bathymetry on call densities calculated by fitting additional detection functions to depth-adjusted range distributions (Fig. S3.3). The full results of depth adjusted models are presented in Table S3.1 and S3.2.

We investigated how range calculation uncertainties may have influenced our density estimates. The maximum error in ranging caused by combining calls within a 20-minute window at stations of these depths was estimated to be ~0.8 km due to whale movement (Hilmo and Wilcock, 2024). However, even larger errors can result from variations in bathymetry that are not accounted for in a flat seafloor propagation model (Hilmo and Wilcock, 2024). In this study, OBSs are distributed on a subducting plate, which deepens westward toward the trench.

To understand the uncertainties that might be introduced by bathymetry, we considered OBS B9 which is the site with the steepest slope (Fig. 3.1). The bathymetry deepens by ~1000 m over 40 km downslope and shallows by ~400 m over 40 km upslope (Fig. S3.3(a)). To approximate these depth changes, we calculated new multipath arrival timing models for flat bathymetry with the depths changed by average increase downslope (500m) and decrease upslope (-200 m). For each model, we calculated the average difference in range for each arrival hypothesis for the ranges over which it dominantly correct: MP1-Direct from 5-20 km, MP2-MP1 from 20-30 km, and MP3-MP2 from 30-40 km (Fig. S3.3(b)). We made the simplifying assumption for end member models that half the calls are from the north and south where the bathymetry is flat, while the other half are either all to the east in shallower water or all to the west in deeper water. Thus, we randomly adjusted half the ranges, first with the difference for the dominant arrival time hypothesis for shallow bathymetry assumptions and second for the deep bathymetry assumption. This yielded two new range distributions (Fig. S3.4) which we fitted with detection functions using the same parameters as our preferred model (Fig. S3.4). We found that $\hat{P}_{det}$ was 37.2% and 43.5% for the shallow and deep bathymetry assumptions. We calculated call densities and found that they varied ≤ ±10% from our original estimates for each month (Fig. 3.9, Table S3.1, Table S3.2).

3.4 | DISCUSSION

This study combines multipath ranging (Hilmo and Wilcock, 2024) and point-transect distance sampling methods (Buckland et al., 2001; Marques et al., 2013; Thomas et al., 2010) to estimate fin whale call densities in the Marianas region using a temporary OBS network. The call densities show fin whales are consistently present throughout the late fall-early spring song season observed elsewhere in the northern hemisphere (Rice et al., 2021; Romagosa et al., 2024; Stafford et al., 2009b; Weirathmueller et al., 2017a). Thus, fin whales are clearly present in this region despite their absence in visual surveys and minimal historical catches recorded in the equatorial Pacific (Hamilton et al., 2009; Jackson et al., 2004; Mizroch et al., 2009). Distance sampling using acoustics is a relatively new field for marine mammal monitoring, and there are several considerations that must be taken into account that differ from visual surveys (Harris et al., 2013; Marques et al., 2011, 2013). Here we address the assumptions, limitations, and potential future utility of distance sampling using OBS multipath ranging methods.

A. Distance sampling assumptions

Key assumptions for point-transect distance sampling through monitoring animal cues are as follows: 1) cues made at zero distance from the sensor are detected with certainty, 2) cue detections are independent from each other, 3) transects are conceptually "snapshots" during which animals do not move, and 4) cue distance is measured exactly (Buckland et al., 2001). Our multipath ranging dataset likely satisfied the first assumption, as we found through manual verification of 80 hours of song spectrograms, that all calls between 0-5 km range were detected. Our dataset violates the other three assumptions, but we argue that our analysis is still robust.

Our ranges are not independent of each other, both because of the inherent nature of fin whale song and the reliance of our ranging method on combining calls. Dependent detections can

result in overdispersion of ranges and affect the statistical tests that evaluate the fit of estimated detection functions (Buckland et al., 2001). Some of our sites do seem to show data overdispersion (OBS B12 and B20 in Fig. 3.5), as their distributions vary greatly from the fitted model displayed in Fig. 3.7. However, our combined range distribution is typical of point-transect distance sampling data (Fig. 3.7); detection counts increase semi-linearly with increased range near the site where detection probability is high, then decreases past ~15 km as detection probability drops sharply. This indicates our dataset is likely robust to violation of the assumption of cue independence. Similar robustness is reported by other acoustic point-transect distance sampling studies of baleen whales (Harris et al., 2013; Marques et al., 2011).

Our dataset obviously violates the assumption that transects represent instantaneous "snapshots" in relation to animal movement. Our monthly call density estimates were calculated using continuous OBS observation, during which whales swam into and out of the monitoring region (Fig. 3.4). The largest concern for most studies is that animals are responsive to the observer/sensor, which could result in underestimation or overestimation of density depending on whether the animals avoid or are attracted to it. This is not a concern for recording fin whale calls with OBSs that are left in place for long durations to record autonomously. Another concern is that the same animal is measured multiple times. This is certainly a limitation of our dataset, as each track that is attributed to a single individual often contains hundreds of calls, moves tens of kilometers, and lasts for multiple days. Our estimates of *call* density are robust regardless of measuring the same individual multiple times, but we would need to account for these associations if we were to attempt to estimate *animal* density with this dataset.

Our range estimates are also not exact. Previously studies that account for random errors in range estimates found that they tend to result in slightly overestimating calculated densities

(Borchers et al., 2010; Marques, 2007). Our autocorrelation call-combination method greatly reduces the random errors in calculated ranges, but ranges may have systematic errors. We addressed this by estimating how our largest source of uncertainty, seafloor depth variations, may affect calculated range distributions. Though depth changes can change estimated ranges by a few kilometers (Fig. S3.3), we found that shallowing or deepening bathymetry surrounding our sites would likely change our density estimates by <10% (Fig. S3.4, Table S3.1, Table S3.2). The uncertainty from bathymetry is much less than the uncertainty resulting from encounter rate variance. Thus, our dataset is likely also robust to violation of the assumption that cue distance is measured exactly.

B. Limitations and future method development

The ranging dataset acquired by our multipath method differs from those that distance sampling was designed to address. Distance sampling methods were designed to maximize the potential of small datasets, usually composed of up to a few hundred observations. Our large dataset of ~70,000 ranges challenged the standard evaluation and selection of detection functions. For example, adding additional adjustment parameters to improve the detection fit continued to improve AIC, even when the data were overfit. This required us to rely more on subjective visual evaluations to select the best model. Our large dataset also resulted in a much lower coefficient of variation in the detection function $CV(\hat{P}_{det})$) than is typical. $CV(\hat{P}_{det})$ is generally expected to account for ~50% of $CV\left(\widehat{D}\right)$ for point-transect studies, but accounted for <1% of $CV\left(\widehat{D}\right)$ in our study (Buckland et al., 2001). A much larger source of uncertainty in our data set is variation in encounter rates, $CV(\frac{n}{k})$), which increases then studies perform fewer transects. We use only 7 OBS instruments as point-transect observers, which is less than typically recommended (Buckland et al., 2001; Marques et al., 2013). Despite this, coefficients

of variations have acceptable values for density estimation for all months but April, when calls were only detected and ranged to on 4 out of the 7 OBSs. Additionally, the DISTANCE package in R is not optimized for large datasets, resulting in models failing to converge when they included continuous variables as covariates in the detection function. This is unfortunate, because call amplitudes and ambient noise levels would be good choices for detection function covariates.

Another limitation of our method is that in can only range to a single whale at any given time. In temperate and high-latitude regions of higher fin whale population densities, overlapping calls in chorus can preclude multipath ranging because of the difficulty in determining which arrivals belong to which individuals (Hilmo and Wilcock, 2024). Fortunately, our observations of spectrograms during verification found no examples of overlapping multipaths from multiple whales in our data. The chorusing limitation was likely not an issue in our Marianas study area due to low fin whale densities.

Sources of uncertainty in calculating multipath ranges were discussed by Wilcock and Hilmo (2024). Bathymetrical variation is the largest source, and we found our call density estimation to be robust to systematic variations in depth at our site. However, rough bathymetry like seamounts interferes with ranging in ways that would require more advanced acoustic propagation modeling. Thus, we did not incorporate data from many of OBSs including all OBSs on the west side of the network. Future work could address this by including acoustic propagation modeling with azimuth-specific bathymetry. The orthogonal horizontal seismometer channels could be used to determine two potential azimuths 180° apart (Harris et al., 2013; Matias and Harris, 2015), and measured multipath arrival time differences with the two

corresponding azimuth-specific models to select the best fitting and determine range (McDonald and Fox, 1999).

Our multipath ranging method is semi-automated, but still requires significant analyst supervision in its current form. The two manual analyses critical for accurate ranging are 1) verifying the automated method selected the correct multipath hypotheses for groups in tracks, and 2) accepting or rejecting the ranges of smaller groups of calls that were not automatically assigned. Together these took a week of time for this relatively small dataset comprising 1 year of data on each of our 7 OBSs. Many other OBS experiments have either involved many more sensors (ex. the Alaska Amphibious Community Seismic Experiment, Cascadia Initiative Community Experiment) (Barcheck et al., 2020; IRIS OBSIP, 2011), or in the case of cabled observatories such as the Ocean Observatories Initiative Regional Cabled Array and NEPTUNE Canada (Barnes et al., 2013; Cowles et al., 2010), much longer periods of observation. This motivates further automation of the multipath ranging method to increase its efficiency.

One way to reduce time required for manual supervision, would be to reduce the sensitivity of the fin whale call detector to non-call signals. Extended high-amplitude acoustic signals such as T-phases, earthquake swarms, and ship noise can trigger several consecutive minutes of false detections with high detection scores that pass our temporal association thresholds for attempting ranging. They occasionally produce coherent ranges in large enough groups to be included in tracks, which can break up the smooth whale path and upset hypothesis selection by the automated algorithm. In this study, we corrected for this manually through analyst verification. Improving signal processing to robustly reject detections associated with these signals would improve the automated multipath hypothesis selection algorithm and reduce analyst verification workload. Recently developed machine learning algorithms with high success rates in identifying

marine mammal vocalizations could be implemented to overhaul the detection process (Bermant et al., 2019; Lu et al., 2021; Miller et al., 2023).

This study reported fin whale call densities in the Marianas region, but we did not convert these estimates to animal abundance due to the lack of knowledge of fin whale call rates (cue rates) in the region. Robust cue rate estimation studies require long-term tagging of whales with hydrophone/accelerometer instrument packages that can confidently associate recorded calls with the tagged whale and exclude calls that may be produced by nearby conspecifics (Blackwell et al., 2021; Goldbogen et al., 2014; Stimpert et al., 2015). To best estimate fin whale populations with future distance sampling studies, cue rate studies should be undertaken 1) systematically in different regions to best characterize acoustic subpopulations (Constaratas et al., 2021; King-Nolan et al., 2024; Rankin et al., 2011, 2018) and 2) repetitively over time to account for evolution in calling behavior (Best et al., 2022; Helble et al., 2020; Romagosa et al., 2024; Weirathmueller et al., 2017a).

C. Potential for monitoring fin whales in the equatorial oceans

Though fin whales are often characterized as being distributed from pole to pole (Aguilar, 2009), some studies instead suggest that there is an equatorial gap from 20°S to 20°N that separates the ranges of southern and northern hemisphere subpopulations of fin whales (Edwards et al., 2015; Mizroch et al., 1984). This proposed gap is based on extensive visual transect studies that rarely observe fin whales in the equatorial oceans (Hamilton et al., 2009; Jackson et al., 2004).

Acoustic studies regularly detect fin whales in regions where visual studies report minimal presence. Acoustic observations detected fin whale calls in the equatorial Atlantic, though they decreased sharply approaching the equator compared to temperate latitudes (Nieukirk et al.,

2004), and are completely absent just north of Puerto Rico (Hilmo and Wilcock, 2024). Fin whales have also been detected where there are minimal sightings in the equatorial Pacific near Fiji (Brodie and Dunn, 2015), the Marianas Trench (Hilmo and Wilcock, 2024), Wake Island (Miksis-Olds et al., 2019), and in regions <30°S in the Indian Ocean (Dréo et al., 2019). This highlights the strengths of PAM studies in regions of low population density.

Our success in estimating fin whale call densities in the Marians region suggests that point-transect distance sampling through multipath ranging may be an ideal tool for monitoring fin whales in the deep equatorial oceans. Because fewer individuals migrate near the equator compared temperate and high latitudes, long-term monitoring methods that cover large areas are essential for observing them. Even with only the 7 OBSs analyzed in this study, we monitored ~27,000 km^2 continuously for a year (Table 3.1) and ranged to ~70,000 fin whale calls. Other OBS networks that have been deployed with tens of instruments would be capable of monitoring even greater areas. Additionally, OBS distributions within networks often reflect ideal survey design for point-transect distance sampling studies; instruments are deployed systematically, but randomly with respect to fin whale populations (Buckland et al., 2001; Marques et al., 2013).

3.5 | ACKNOWLEDGMENTS

We thank Andreia Pereira for helpful conversations about density sampling that improved our methods and manuscript. This research was funded by the both Office of Naval Research under Award No. N00014-21-1-2564 and Living Marine Resources under Award No. N39430-21-C-2208.

Chapter 4:

Acoustically investigating distributions and behavior of overwintering northeast Pacific blue whales using ocean bottom seismometer networks

Rose Hilmo[1], William S.D. Wilcock[1]
[1]School of Oceanography, University of Washington, Seattle, WA 98195, USA

4.0 | Abstract

Northeast Pacific (NEP) blue whales are one of the world's most accessible and well-studied populations of blue whales. They are specialist krill feeders and have historically been described as capital breeders that feed off Southern California in the summer and breed in the Eastern Tropical Pacific in the winter. Recent studies have challenged this stereotypical characterization by describing large variations in NEP blue whale migration strategies. Our study investigates the behavior of whales that skip southward migration and overwinter off the coast of the Pacific Northwest through analyzing song produced by males. We acoustically localize B-calls recorded by a large opportunistic dataset of ocean bottom seismometers that were deployed offshore from Northern California through British Columbia in 2013-2014. We associate localizations into tracks that describe the movement of individual whales. We use tracks to analyze metrics of distribution, movement, and song and identify two distinct regions of different habitat use: the Gorda Basin as a migration corridor, and the Cascadia basin as an overwintering and foraging ground. We also leverage our ability to associate call metrics with whale movement to investigate links between song and behavior. We conclude that trends in song metrics including increases in call and phrase spacing may be driven by high energetic costs of repeating B-note production. We also suggest that different calls and phrase types may be used in different contexts, as we observe that singular A-calls are associated with social interaction, AB phrases are associated with overwintering, and ABB phrases are associated with migration.

4.1 | INTRODUCTION

There are currently two recognized subpopulations of blue whales in the north Pacific identified by their distinct calls: the Northwest and Northeast blue whales (Monnahan et al., 2014; Stafford et al., 2001). These populations dominate opposite sides of the ocean basin, with some overlap in central Pacific (Carretta et al., 2023). The endangered Northeast Pacific (NEP) blue whale population is one of the most accessible and well-studied population of blue whales in the world (Monnahan et al., 2014; Thomas et al., 2016). They are highly migratory specialist krill feeders that generally feed near the southern coast of California in the summer and overwinter in the Costa Rica Dome (CRD) for calving and breeding (Bailey et al., 2009; Fiedler et al., 1998). Blue whales have historically been considered capital breeders, relying on fat stored during the feeding season while fasting on breeding grounds.

Tagging and biopsy studies show that this capital breeding and migration pattern is not consistent for all NEP blue whales. A large dataset of biopsy stable-isotope analyses collected in the CRD indicates that many blue whales actually feed year-round, suggesting a mixed income-capital breeding strategy (Busquets-Vass et al., 2021). An extensive tagging dataset of 159 individuals off of California (Mate et al., 2019) found that several whales stayed in the Gulf of California year-round, while others travelled north through the late autumn months as far as the Gulf of Alaska, with some individuals moving hundreds of kilometers offshore (Abrahms et al., 2019; Hazen et al., 2017; Irvine et al., 2014; Palacios et al., 2019). Tagged whales all migrated out of northern waters by late December. Recent stable isotope analysis of baleen plates of thirteen individuals found these migration patterns to be sex specific (Blevins et al., 2022), with some juveniles and adult males altogether skipping migration to the CRD for years at a time. Females skipped migration to the CRD less frequently. Benefits of skipping migration may be

related to improving intraspecific competition for resources and reproductive status, or mitigating high energetic costs associated with reproduction (Blevins et al., 2022; Busquets-Vass et al., 2017).

Little is known about how the NEP blue whale population subsets that skip winter migration or migrate northward are utilizing the temperate region. Whales may be following krill biomass maximums that move northward up the West Coast throughout the fall (Bailey et al., 2009; Irvine et al., 2014). Temperate latitude overwintering individuals may also be returning to regions where they were historically harvested, or they may be responding to shifts in prey distributions caused by changing oceanographic conditions (Abrahms et al., 2019; Calambokidis et al., 2009; Szesciorka et al., 2020). Observed decadal changes in the timing of this migration may also be related to climate change (Szesciorka et al., 2020). These recent shifts in our understanding of blue whale migration and reproductive strategies suggest that the traditional approach of estimating population structure based on north-south migration may no longer be well supported. Understanding why some blue whales migrate differently and how they are using the northeast Pacific habitat is critical for revising our understanding of the population structure. Knowledge of the population structure is, in turn, critical to manage the species and best mitigate anthropogenic impacts.

Acoustic monitoring is a powerful tool that may help in revising assessments of population structure. Several acoustic studies have recorded NEP blue whales skipping southward migration on a population level. NEP blue whale song, a reproductive display produced by males, is stereotypical which allows for identification of their range through detecting calls (McDonald et al., 1995; Stafford et al., 1999a, 2001). Song is recorded throughout the temperate latitudes in the East Pacific during the overwintering season as late as February or

March in some years (Burtenshaw et al., 2004; Monnahan et al., 2014; Stafford et al., 2009; Stafford et al., 1999). Song occurs later in the year with increasing latitude, which is further evidence of a population-level northward migration of throughout the fall and winter (Burtenshaw et al., 2004; Pearson et al., 2023; Rice et al., 2021).

Different NEP blue whale call types are associated with different behavior. Common vocalizations are A, B, and D calls. A and B calls are produced seasonally by males in reproductive song display and acoustically identify the NEP blue whale subpopulation (McDonald et al., 2001). A-calls are pulses centered at ~14 Hz that last at for <20 seconds, while B-call fundamental frequencies are higher-amplitude tonal notes that are downswept from 16-14 Hz for <25 seconds (Mcdonald et al., 2009; Rice et al., 2022b; Stafford et al., 2001). A and B calls can either be produced individually or as notes in song where individuals sing consecutive phrases that can continue for hours or days (Lewis et al., 2018; Oleson et al., 2007a); each phrase starts with an A-note and is followed by one or multiple B-notes. D calls are highly-variable ~1 second downswept calls centered around ~50 Hz and are not produced in song phrases. They are produced by individuals of both sexes, and are thought to be contact calls in social groups during breaks from foraging (McDonald et al., 2001; Oleson et al., 2007a, 2007b). However, because they are less common (Lewis et al., 2018; Lewis and Širović, 2018), have a lower source level (Thode et al., 2000), and are less stereotypical than A and B song notes (McDonald et al., 2001), they are therefore not as well monitored in acoustic studies.

Historically, acoustic studies have had limited ability to interpret occurrence of song in the context of whale behavior because of the difficulty in associating vocalizations with individuals. However, recent studies combining acoustic and tagging data have contextualized patterns in male NEP blue whale song off southern California with migration and foraging.

Acoustic studies have long noted a diel pattern in song; individuals sing less during day than at night, dawn, and dusk (Stafford et al., 2005; Wiggins et al., 2005). Acoustic tags have confirmed that this is because whales preferentially deep lunge feed on diely migratory krill swarms during daylight hours, during which behavior they do not sing (Oleson et al., 2007a). Song is produced exclusively during non-lunging shallow dives (Lewis et al., 2018). Additionally, the cessation of diel singing has been linked to a seasonal transition in life history from foraging to migration (Oestreich et al., 2020, 2022). This association enables acoustic investigation into whether whales are utilizing the temperate north Pacific for foraging during the fall-winter song season and if they do, identify spatial patterns in when whales transition from foraging to southward migration.

NEP blue whales may also vary song parameters with behavior. For example, most long-term song is produced by lone traveling males, while singular calls and phrases are produced by whales in pairs (Oleson et al., 2007a). Note patterns also vary; some individuals sing alternating A and B notes (AB phrases), while others sing A notes followed by multiple B notes (ABB phrases). Studies have observed spatial patterns in AB and ABB phrase production off of Southern California (Lewis et al., 2018), with more AB phrases recorded nearshore, and more ABB phrases recorded offshore. Variations in spatial patterns in AB and ABB phrases reflect spatial distributions of behavior; solitary transiting males tend to be observed further offshore, while social and/or foraging individuals tend to be observed to the coast (Lomac-MacNair and Smultea, 2016; Oleson et al., 2007a; Wiggins et al., 2005).

Variations in song patterns may be useful for identifying regions of specific behavioral settings. High amplitude, tonal B-calls can propagate for hundreds of kilometers in the open ocean, much further than in coastal environments (McDonald et al., 2001; Širovic et al., 2015;

Stafford et al., 1998). They may be the most advantageous call type for solo transiting males in deep water to communicate with conspecifics over great distances, or to advertise for mates. This may motivate increased B-call production of offshore males through singing ABB phrases. For male fin whales, most individuals occasionally sing at fast swimming speeds, though song duration decreases with increased speed. It may be that fin whales sing at high speeds to advertise reproductive fitness, but for shorter durations due to increased energetic costs (Clark et al., 2019). Blue whale song production might be similarly contextualized and constrained by energetic costs. Spacing between A-B and B-B notes tend to be stereotypical within acoustic studies, but spacing between phrases vary (Lewis and Širović, 2018; Oleson et al., 2007b; Stafford et al., 2001). Investigating links between song metrics and behavior may expand the applications of acoustic studies in determining how NEP blue whales utilize different regions, and how they may be responding to changing habitats.

Ocean bottom seismometer (OBS) networks that are deployed for approaching a year or more to monitor earthquakes can provide unique acoustic datasets on large spatial scales. Most instruments sample at 50 Hz or higher, which allows them to resolve low frequency signals at or below their Nyquist frequency of 25 Hz. This includes A call and B call fundamental frequencies produced by NEP blue whales (McDonald et al., 1995). Closely spaced instruments have been used to localize blue and fin whale calls that are recorded on multiple instruments (Dreo et al., 2017; Dunn and Hernandez, 2009; MacDonald et al., 1995; Soule and Wilcock, 2013; Wilcock, 2012). Localizing vocalizing individuals is a powerful tool to contextualize calling with whale behavior.

In this study, we leverage a two contemporaneous OBS experiments off the coast of the Pacific Northwest through fall-winter 2013-2014 to investigate NEP blue whales in the

temperate pacific during the overwintering season. We associate localizations into tracks to investigate spatial and temporal patterns in movement of long-term singing whales. We also explore diel and song pattern metrics to investigate links between vocalization and movement. This unique dataset provides new insight into the movement, calling, and foraging behaviors of overwintering NEP blue whales in this region.

4.2 | METHODS

A. Seismic Data

We acquired ocean bottom seismometer (OBS) data from the Cascadia Initiative (CI) and Gorda Deformation Zone (GDZ) experiments. The CI network of ~70 OBSs was deployed in fall-summer seasons from 2011-2015 to monitor seismicity and image the Cascadia subduction zone. During the 2013-2014 season the OBSs were deployed across the Juan de Fuca plate from the spreading center to the continental margin. Deep instruments were spaced ~70 km from each other, while instruments on the shelf and slope were spaced at ~35 km except for dense targeted arrays deployed at ~10 km spacing near Grays Harbor and Cape Mendocino. Instruments contained either Nanometrics Trillium Compact or Guralp CMG-3T seismometers, which each measured velocity in one vertical and two horizontal orthogonal directions. Most OBSs sampled at 50 Hz, though some sampled at 125 Hz.

The Gorda Deformation Zone network was deployed to monitor seismicity and image the Gorda plate and Blanco transform zone in fall-summer seasons from 2013-2015. The ~60 GDZ network OBSs were almost entirely deployed in the deep ocean, focusing on the oceanic plate, spreading center, and transform fault. GDZ instruments were more closely and irregularly spaced than CI instruments, ranging from 20-50 km. GDZ instruments included SIO Sercel L-28LB and

Nanometrics Trillium 40, Trillium Compact, and 240 seismometers. OBSs all sampled at 100 Hz for 2013-2014.

We chose OBSs deployed in both CI and GDZ networks from the fall 2013 to summer 2014 season for tracking analysis because together they provided maximum coverage of the Pacific Northwest coast (Fig. 4.1). The CI network was deployed in its northern configuration, extending from the Blanco Transform northward to Vancouver B.C., and the GDZ network extended from the Blanco Transform southward to Cape Mendocino. Together, the networks spanned ~1000 km of the US West Coast and extended up to ~500 km offshore, with the majority of OBSs spaced near enough to localize NEP blue whale B-calls (Fig. 4.1).

We downloaded vertical channel seismometer data from the Incorporated Research Institutions for Seismology Data Management Center database (now part of the Earthscope Consortium Data Services) and analyzed a total of 77 instruments combined from both networks (~400,000 total hours of data), after excluding those deployed shallower than 1500 m depth which are not effective for localization (Wilcock and Hilmo, 2021) and a few with poor quality data. We analyzed data from October 1, 2013 – May 15, 2014. All CI instruments were deployed by October 1, but the all the GDZ instruments were not deployed until the start of November (Fig. 4.1).

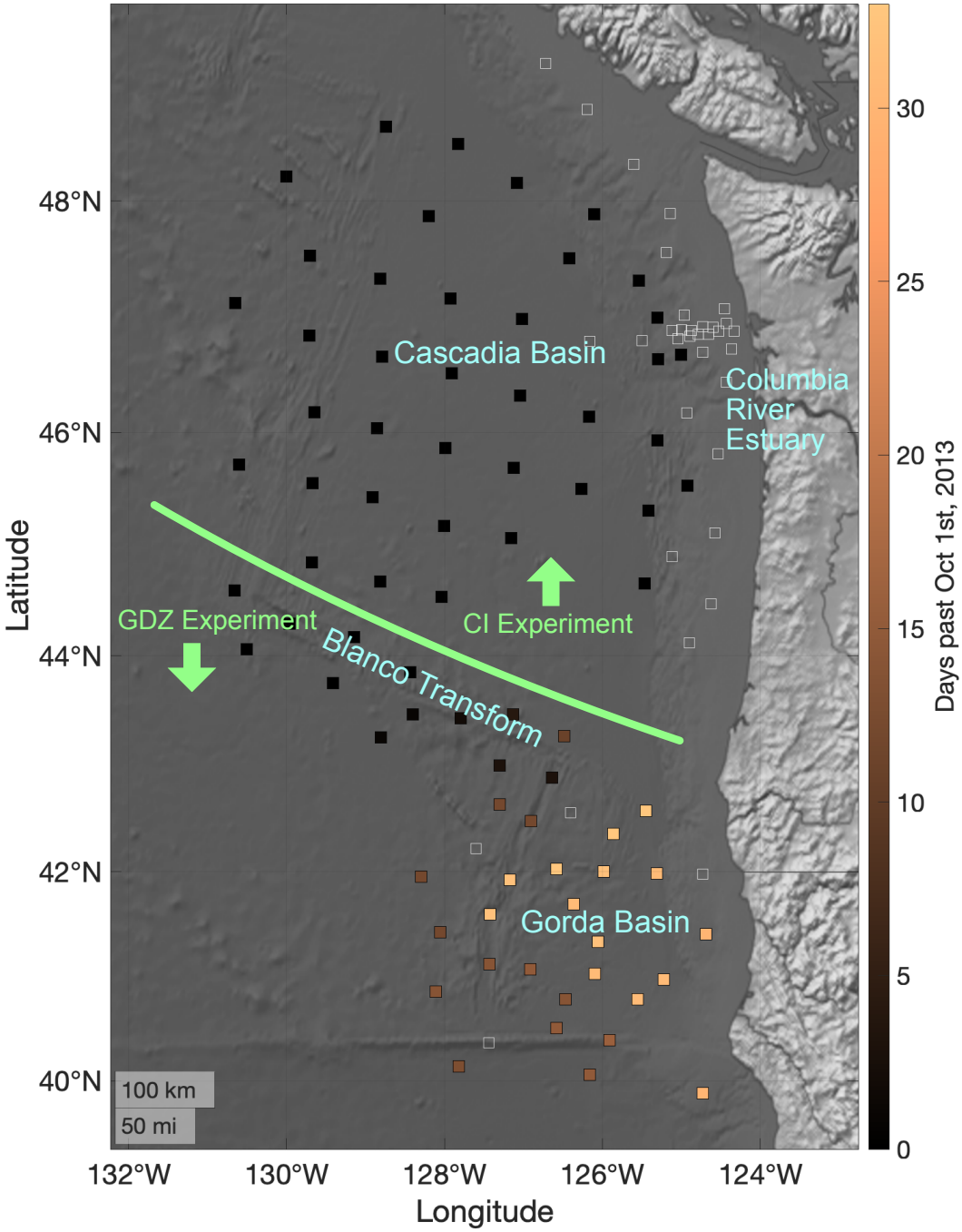

FIG. 1: Map showing ocean bottom seismometers (OBSs) deployed in 2013-2014 for the Cascadia Initiative and Gorda Deformation Zone experiments separated by green boundary line. Filled squares indicate stations used in this study, with color indicating the date of deployment when later than October 1, 2013. Open squares indicate instruments that were not used, either because they were too shallow for the localization method (<1500 m depth) or had poor quality data. Blue labels show geographic features referenced in text.

B. Analysis

i. Localization

We implemented the localization methods described in Wilcock and Hilmo (2021) with a few modifications to localize NEP blue whale B-calls and extract likely tracks. We detected B-calls through building spectrograms of OBS vertical channel ground velocity timeseries and cross-correlating them with a generalized template kernel. Spectrograms were calculated using a 5-second Hanning window with 95% overlap. We did not apply instrument frequency response curves to data as they were flat surrounding 15 Hz. We applied exponential decay filters to spectrograms vertically (to dampen fin whale calls in upper frequencies within the band of interest) and horizontally (to dampen noise bands from shipping). We then cross-correlated spectrograms with the template kernel which downswept linearly between 16-14 Hz over 20 s (Mellinger and Clark, 1997), and detected calls through picking peaks in the cross-correlation series, which we refer to as the "detection score". Thresholds were set low to detect even very faint calls, which resulted in high numbers of false detections. For each detection we recorded peak detection score, timing of the peak, and duration.

As in Wilcock and Hilmo (2021), we estimated the probability detections were true by comparing rates of B-call detection of different detection scores during the fall-winter calling season to those detected from May 1-15 when no blue whale calls are expected in the region. This process relies on the assumption that triggering noise sources are consistent throughout the year and that there are no B-calls outside the standard singing season. True probabilities p_r for different detection scores are determined by,

$$p_r(a) = \frac{(r_c(a) - r_{nc}(a))}{r_c(a)} \quad (1)$$

where a is peak detection score, r_c and r_{nc} are the rates of detection during calling and non-calling seasons (Fig. S4.1). Detections with a true probability >80% were categorized as master detections, each of which trigger the localization process.

We localized B-calls using a Bayesian approach (Nosal, 2013) as described in Wilcock and Hilmo (2021). A master detection on an OBS triggered a search for all detections arriving up to 100 seconds later on surrounding OBSs within 150 km. The 100 s threshold was based on how long it would take a call to travel 150 km at a standard ocean sound speed of 1.5 km/s. A likelihood function was constructed for all associated detections, which was then maximized to fit the master detection time and as many other detections as possible (Wilcock and Hilmo (2021), Eq. (3)). We used a second process to maximize the number of high probability detections on nearby stations to avoid overfitting more distant low probability detections (Wilcock and Hilmo (2021), Eq. (6)). We used both sets of detections times to calculate separate spatial probability distributions which were integrated for localizations. Localizations were required to fit at least 4 arrivals on 4 different OBSs to be considered.

Because of the large number of spurious low-probability detections, most of resulting localizations are likely false. We initially allowed detections to be localized into multiple solutions, but used an iterative process to find localizations that were clustered in tracks by grouping them with a spatio-temporal filter that required at least 4 localizations to occur within 10 kilometers within 15 minutes (Fig. S4.2). This filter is not informed by biological metrics of whale speed, but rather the low precision of consecutive whale localizations (~10 km uncertainty) (Wilcock and Hilmo, 2021). We assumed track segments to be correct localizations and then found additional localizations using the remaining calls not already associated with previous tracks. We repeated this process 3 times before reapplying the spatio-temporal filter.

ii. Track analysis

Because of the parameters of the spatio-temporal filter for track segments, breaks in whale song of >15 minutes resulted in separate track segments. Track segments were then manually associated into full tracks by an analyst guided by the following rules:

- If there were no other coincident track segments from other whales within 100 km, consecutive track segments were linked with gaps up to 24 hours if they were consistent with a consistent swimming direction and speed.
- If other coincident track segments were present within 100 km we used stricter parameters for grouping:
    - If track segments showed clear directional movement, they were linked with consecutive segments with similar directional movement within 12 hours within 30 km.
    - If track segments did not show clear directional movement, they were linked with consecutive non-directional segments within 8 hours within the typical range of localization uncertainty (~10 kilometers).
    - Otherwise, nearby track segments were kept in separate tracks.

Although the choice of parameters for grouping segments into tracks is somewhat subjective, subsequent analysis showed that it grouped segments with similar calling patterns. This procedure resulted in a total of 81 tracks composed of at least 150 consecutive localizations that are each likely to represent the movement of a single whale.

There was scatter of up to ~10 km in consecutive localizations within a track due to uncertainty in B-call detection timing (Wilcock and Hilmo, 2021), which necessitated estimating the whale's path. We calculated the smoothed path of the whale using the least-squares method

described in Wilcock and Hilmo (2021) which fits the localizations taking into account their uncertainty while smoothing changes in both the direction and speed of tracks. For each track the smoothing weight was adjusted so that the track fits the localizations to their expected uncertainly after iteratively removing outliers that are inconsistent with a smooth path at the 98% confidence level as determined by a chi-squared test.

For each smoothed track, we calculated the ratio of net distance travelled (the straight-line distance from the start of the track to the end of the track) to the total distance travelled (the length of the smoothed path fit to each track). If the ratio was ≤0.5, which means that total swimming distance predicted by the smoothed track more than doubles the net directional movement of the whale, we categorized the track as non-transiting. Ratios >0.5 were categorized as transiting. Transiting tracks were analyzed for movement. We used K-means clustering to group sections of smoothed track with similar movement using azimuth, speed, and distance travelled. The analyst selected the number of k-means; one cluster for each unique direction of travel (a change of at least 45 degrees) that persisted for at least 8 hours. Total distance traveled, average velocity, and average azimuth were recorded for each cluster.

To assess the success rate of localizations in the tracks, we examined spectrograms of every 5th hour of each track from the nearest OBS. We plotted predicted B-call arrival times obtained from the smooth track on the spectrogram. For each localization, if the predicted arrival time occurred within 10 seconds of a verified B-call detection time we flagged it as true. We flagged locations as false if the predicted arrival times did not align with a B-call, indicating a spurious location was included in the track by the spatio-temporal filter. Additionally, we counted the total number of B-calls during every 5th hour from the tracked whale's song and compared them with the number of localizations to determine the localization success rate. If

songs from multiple whales were present in an hour, it was often not possible determine which of the notes not localized within the examined track were produced by the tracked whale and which were produced by other individuals. In these cases, we could not calculate localization success rate, so the hour was not included in this verification.

iii. Song behavior analysis

We also categorized every 5th track hour for song type. We assigned each hour as AB song, ABB song, chorus, or unverifiable. We categorized an hour as AB song if the whale sang exclusively phrases composed of a single A note followed by single B note. If the whale sang any ABB phrases in the hour, which are composed of a single A note followed by two or more B notes, we categorized the hour as ABB song. We use this simple binary classification due to the difficulty of accurately describing proportions of AB vs. ABB song for categorization. For example, because ABB phrases are much longer in duration that AB phrases, an hour of mixed AB and ABB phrases might be categorized as AB if it is assigned based on phrase count but ABB if it is assigned based on the proportion of time the whale is singing each phrase type. If recorded song phrases could not be confidently associated with the tracked whale due to multiple nearby singing conspecifics, we categorized the hour as chorus. We included chorus hours in analysis as a metric for whale behavior in the presence of other singing individuals. We categorized an hour as unverifiable and did not use it in analysis if song was not visible due to noise, earthquakes, or instrument failure. We determined spatial and temporal patterns in AB song, ABB song, and chorus hours and compared them with average hourly track metrics including transiting vs. non-transiting movement, whale speed, and azimuth (Fig. S4.3).

We selected ten tracks representing various months, movement types, and song patterns that lasted at least 24 hours and included minimal chorusing hours from nearby conspecifics for

further song pattern analysis out of ~30 tracks that satisfied this criteria. We manually annotated hourly spectrograms from the nearest OBS for the entire track, recording start times of each A and B note (Fig. 4.2). We used note types and timings to calculate song metrics including A and B note counts, AB and ABB phrase counts, inter-note intervals (lengths of spacings between A-B notes, and B-B notes), and inter-phrase intervals (lengths of phrase spacings less than 5 minutes apart). We compared variations in interphrase and internote intervals with song phrase types.

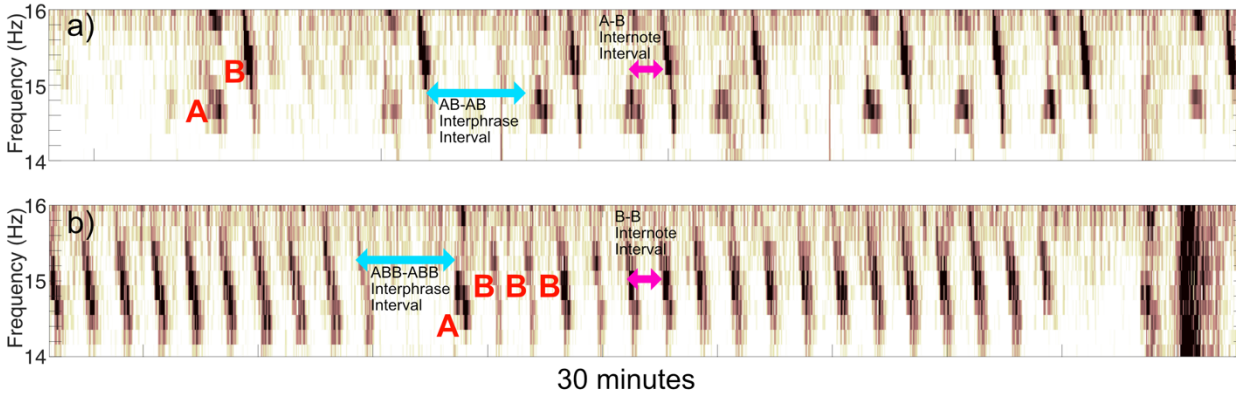

FIG. 2: Example spectrograms for 30 minutes of (a) AB song and (b) ABB song. Annotations show note types (red) and example measurements of internote (magenta) and interphrase (cyan) intervals. These examples were selected from two nearby singers that together are localized in track 92 (see section 3.2.3).

We investigated diel patterns in song on OBSs using strong B-call presence. Daily day and night B-call rates were compared on stations that had at least 20 high probability detections (P>0.8) for at least 50% of deployment days. We defined daytime B-calls as occurring between sunrise and sunset, and nighttime B-calls as occurring between nautical dusk and nautical dawn. We defined B-calls recorded between dawn-sunrise and sunset-dusk as twilight calls, which are not included in diel analysis. We scaled counts of B-calls by the proportion of recording time during respective categories (ex. Scaled Detections $_{night}$ = Detections $_{night}$ /(Hours $_{night}$ /24)). We smoothed time series of daytime, nighttime, and total B-calls with a 15-day Hamming window normalized to unity. We investigated diel pattens through using daytime, nighttime, and total B-

call series to construct a timeseries of call index to, a metric we adapted from Oestrich et al. (2020).

$$\text{Call Index} = (\text{Scaled Detections}_{night} - \text{Scaled Detections}_{day})/(\text{Scaled Detections}_{night} + \text{Scaled Detections}_{day}) \quad (2)$$

A call index of 1 would indicate that all B-call detections occurred at night. A call index of -1 would indicate all B-call detections occurred during the day. A call index of 0 would indicate equal rates of detection during the day and night. We investigated the spatial and temporal patterns in call index on each station. We compared dates and values of call index maximum and averages with OBS locations and distributions of transiting and non-transiting whales.

4.3 | RESULTS

A. Blue whale distribution and movement

The Bayesian algorithm calculated 488,614 localizations of blue whale B-calls between October 1st, 2013, and May 1st, 2014. The spatio-temporal filter assigned 47,978 localizations to track segments. Of these, 31,477 were then manually linked into 81 tracks that each contained at least 150 localizations.

We do not use shallow OBSs because the acoustic propagation in shallow waters is too poor to track whales given the OBS spacing (Wilcock and Hilmo, 2021), so the lack of localizations on the upper continental slope and shelf in our dataset cannot be interpreted as a lack of singing whales. Future studies might be able to localize with shallow shelf OBSs networks with if they are spaced at <35 km, or if more advanced shallow water acoustic propagation modelling is used. The localization algorithm is also ineffective where the station geometry is too sparse (spacings >~100 m). A large gap near 44°N between the eastern part of the north CI deployment and south GDZ deployment prevents tracking. Additionally, tracking is impacted by smaller gaps in the

OBS network centered around 48°N, 129°W and 46.5°N, 126°W. We term abyssal regions within the network where there a no network gaps, the "effective localization area" (Fig. S4.4(a), Fig. 4.3(a)).

Within the effective localization area, no spatial pattern was found in the success rate of localizations. Within the effective localization area, localization distributions are similar to distributions of high-probability ($P > 0.9$) call counts detected on OBSs (Fig. 4.3(a)). The localization success rate within tracks varies substantially from <10% to 100% for the hours analyzed, averaging 53.5% with a standard deviation of 23.8% (Fig. S4.4(a-b)). The success rate shows no clear spatial pattern (Fig. S4.4(a)) and no significant dependence upon distance from the nearest OBS (Fig. S4.4(c)). Instead, localization success likely depends on factors such as background noise levels, other signals such as earthquakes and ship noise on nearby OBSs, and calling rates of other whales nearby. These issues have been documented as problematic for the algorithm (Wilcock and Hilmo, 2021) because of its reliance on detecting and associating distant calls with low amplitudes. Only 1.5% of the localizations in tracks were false (i.e., not associated with a B-call on the nearest OBS).

NEP blue whales were localized from when OBS recording starts (October for CI, November for GDZ) until March (Fig. 4.2). A density plot of all 47,978 localizations within track segments show that whales are heterogeneously distributed throughout the effective localization area (Fig. 4.3(a)). There are higher densities in a band along the eastern side of the area (Fig. 4.3(a)). A striking feature is a high-density hotspot at ~45.7°N, 127°W. Density plots of localizations in transiting and non-transiting tracks show differences. In the northern Cascadia Basin, non-transiting whale distributions are more eastward (Table 4.1) while in the southern Gorda Basin

they are more westward (Table 4.1). A much higher proportion of localizations in the Gorda Basin are categorized as transiting than in the CI network (94% versus 52%).

	Transiting mean lon	Non-transiting mean lon	Lower 95%	Mean Difference	Upper 95%	P-value
North (>44° N)	-127.468°	-127.410°	0.041°	0.057°	0.074°	**<0.001**
South (<44° N)	-125.992°	-126.353°	-0.398°	-0.361°	-0.324°	**<0.001**

TABLE 4.1: ANOVA results comparing longitude distributions of transiting and non-transiting localizations north and south of 44°N, respectively. Mean longitudes for transiting and non-transiting tracks are reported for each region. Lower 95% and Upper 95% show the confidence intervals of the estimation of longitude mean differences, and Mean Difference shows the best estimate of the group mean differences. Both regions show significant longitude mean differences between non-transiting and transiting localizations ($P < 0.05$).

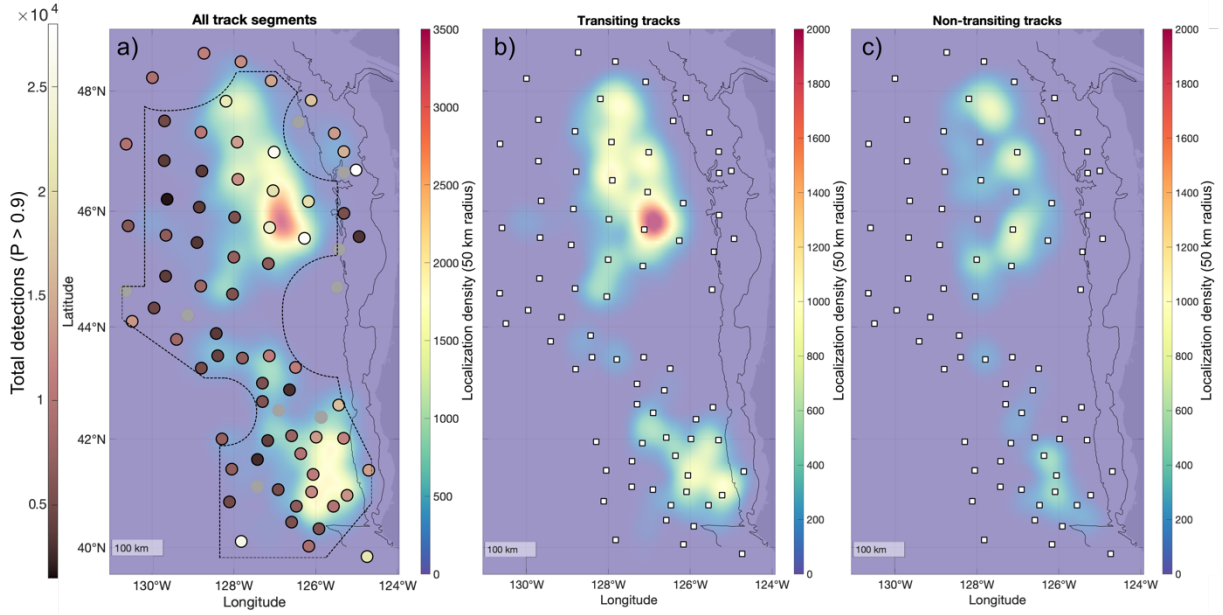

FIG. 4.3: (a) NEP blue whale B-call localization density maps (50 km radius) for all spatiotemporally filtered track segments, with stations colored by total counts of high probability ($P > 0.9$) B-calls recorded between October-March. Stations in grey with no outline had no high probability detections due to poor quality data. Dotted polygon encapsulates the "effective localization area" identified in Fig. S4.4(a). (b-c) Location density maps of (b) the 57 transiting tracks with ≥150 calls, and (c) the 24 non-transiting tracks with ≥150 calls. Black contours show 200 m and 2000 m depth contours.

A total of 81 tracks of >150 localizations were found from October-February (Fig. 4.4). Some stations record a few high-probability B-call detections in the month of March, but none are localized into long tracks (Fig. S4.1). Track distribution and movement varies spatially and

by month (Fig. 4.4). Track counts north of 44°N in the Cascadia Basin are high throughout the fall (October-December) but decrease through the winter (January-February). The proportion of tracks located south of 44°N in the Gorda Basin generally increase through the deployment. In all months, there are more transiting tracks than non-transiting tracks. However, the highest proportions of non-transiting tracks are in November and December. All non-transiting tracks are in the Cascadia Basin, except for one non-transiting track in January and one in February. In all months, non-transiting tracks in the north are on average closer to the continental slope than transiting tracks at the same latitudes (Fig. 4.4). The two non-transiting tracks in the Gorda Basin have similar longitudes to the average of transiting tracks.

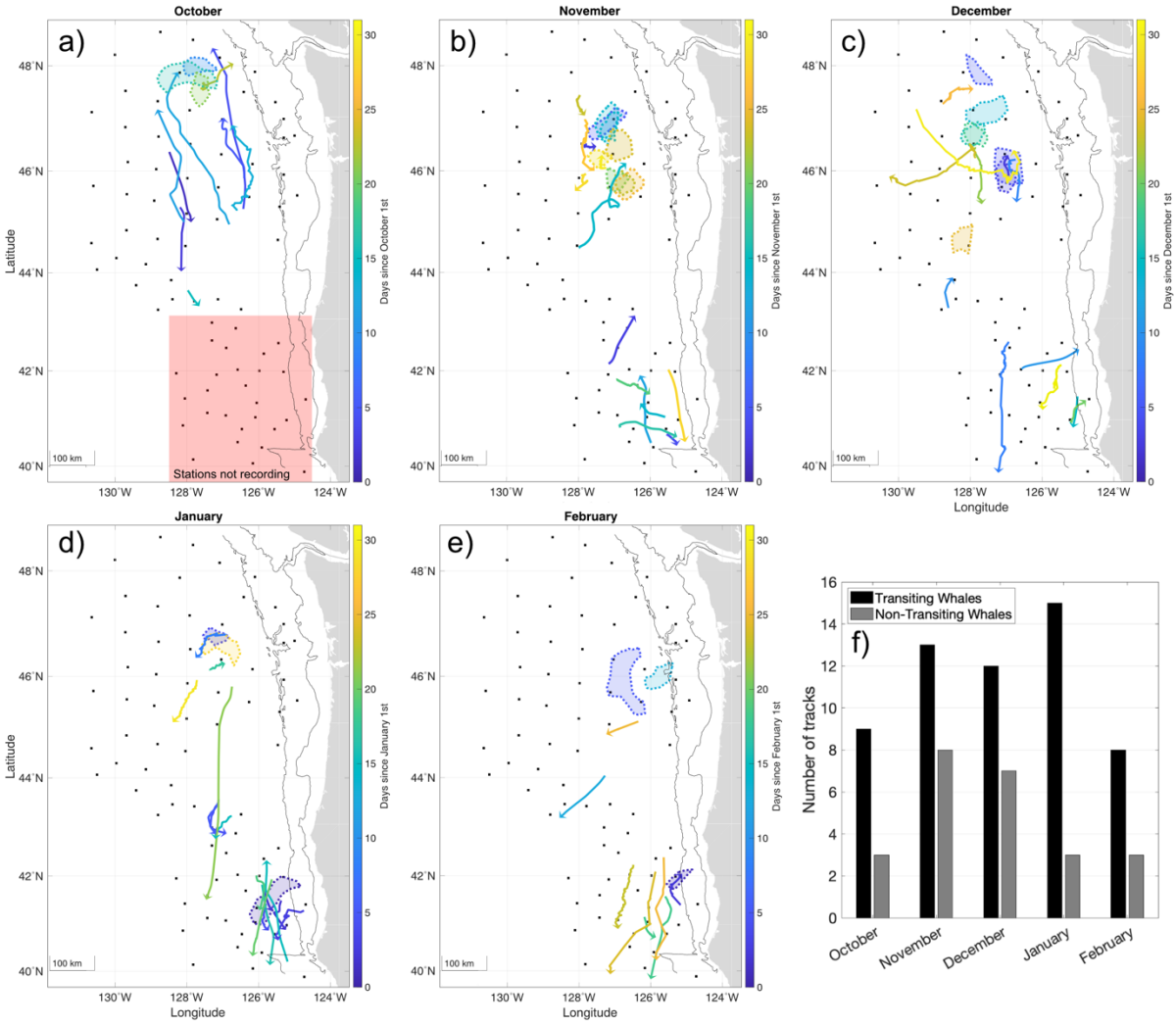

FIG. 4: Maps showing tracks with ≥150 localizations for (a) October, (b), November, (c) December, (d) January, and (e) February. Solid lines show smoothed paths for transiting tracks. Dotted filled polygons encapsulate localizations of non-transiting tracks. Line color represents the day of the month of the midpoint of the track. Black contours show 200 m and 2000 m depth contours. (f) Histogram showing counts of transiting and non-transiting tracks for each month.

The directionality of NEP blue whale movement in transiting tracks also varies over the deployment (Fig. 4.5, Fig. S4.5). K-means clustering divided the 57 transiting tracks into 101 clustered segments each with a relatively consistent direction and speed. During October, whale movement is polarized north-south, with most individuals travelling north. The average whale displacement of K-means track segments is ~110 km north-northwest, with an average speed of 3.7 km/hr. Whale movement during November is not polarized, with individuals travelling in all directions mostly at slower speed than other months. The average whale displacement in November is only ~25 km east-northeast, with an average speed of 1.4 km/hr. In December, January, and February, increasing proportions of whales travel southward with increasing average whale displacements of ~60 km south-southeast, ~85 km south-southwest, and ~120 km south-southwest and average speeds of 2.5 km/hr, 3.5 km/hr, and 3.5 km/hr, respectively.

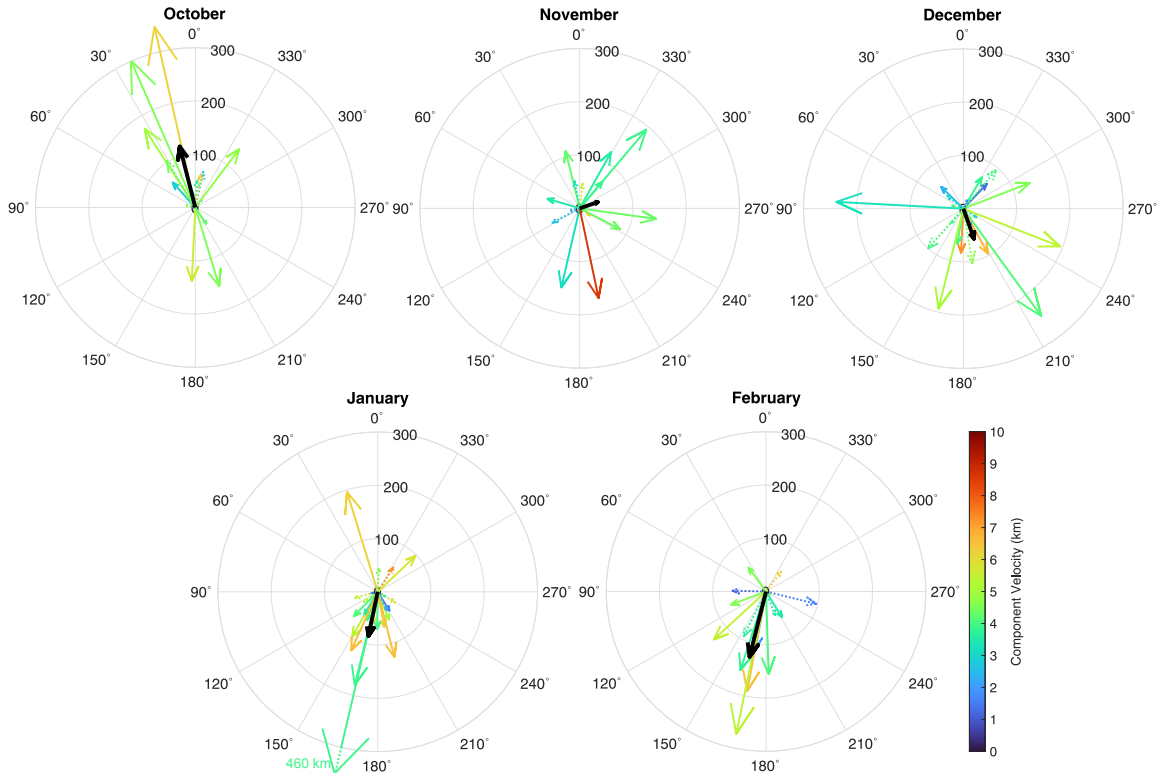

FIG. 4.5: Monthly polar plots showing the direction and net distance of the transiting smoothed blue whale tracks. Vectors represent distance (km) and color represents speed along the smooth track (km/hr). One vector is plotted for each k-means clustered segment of the tracks. The cluster with the largest directional component is plotted with a solid line, and smaller components are plotted with dotted lines. Black arrows show averaged whale displacement vector from all transiting segments.

B. Song patterns

i. Patterns in song categorization

Song categorizations of every 5th hour examined via spectrogram show strong spatial patterns. Song types have different latitudinal distributions (Fig. 4.6(a&b)), with more AB song and chorus hours in the Cascadia Basin and more ABB song hours in the Gorda Basin. ANOVA results show that mean AB song and chorus latitudes are significantly northward of ABB song latitudes (Table 4.2). Song types also have different longitudinal distributions, with more AB song hours in the west and more chorus and ABB song hours in the east (Fig. 4.6(a&c)). ANOVA results show that mean chorus and ABB song longitudes are significantly eastward of mean AB

song longitudes (Table 4.2). The eastward ABB song prevalence is due to its dominance in the southern GDZ network, which is distributed farther east than the CI network. Chorus song hours tend to be distributed closer to the continental slope in the Cascadia Basin. This reflects the locations of non-transiting tracks, which have higher proportions of chorusing hours (Fig. 4.3(c), Fig. 4.4, Fig. 4.6(i)).

Song categorizations also vary throughout the year (Fig. 4.6(h)). Proportions of AB and ABB song hours are similar in October, but proportions of AB song increase during November and December. Proportions of AB song drop off sharply during January and February, when ABB song patterns dominate. ANOVA results show that ABB song hours occur significantly later in the season than AB song (Table 4.2). Chorusing hours also vary throughout the year, increasing from October through a peak in December, then decreasing in January and February. Monthly chorusing patterns reflect monthly proportions of non-transiting whale tracks (Fig. 4.4(f)).

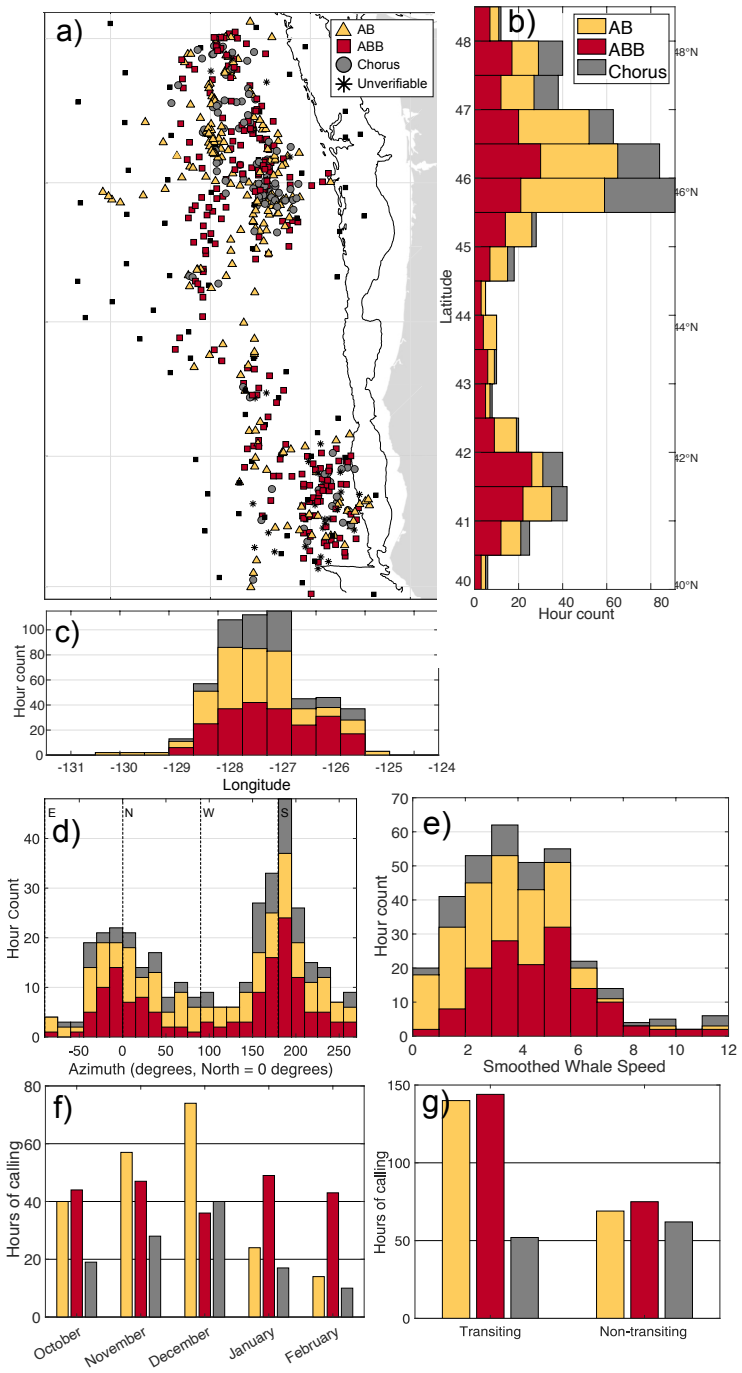

FIG. 4.6: (a) Map showing song type and location of every 5th hour of blue whale tracks with >150 localizations. Black lines show 200 m and 2000 m depth contours. (b-e) Summative histograms showing song type distributions for (b) latitude, (c) longitude, (d) average whale azimuth for smoothed transiting tracks, (e) average whale speed for smoothed transiting track. (f-g) Bar charts showing (f) hours of song types versus month, and (g) hours of song type versus track type.

Song categorizations also vary with whale behavior. Some tracks only had hours exclusively categorized as AB phrases. Other tracks only had hours that included ABB phrases. Many tracks had both exclusive hours of AB phrases and hours that contained ABB phrases. Azimuths of transiting whales are generally polarized north-south (Fig. 4.6). The dominant travel azimuth of all song types is southward (Fig. 4.6(d)). However, azimuths of whales singing AB and ABB song are both bimodally distributed, with a second northward peak. We test whether hours of AB song are less polarized north-south than hours of ABB song using a binomial proportion test (Ryan, 2007). We created two sample bimodal distributions of AB and ABB hourly azimuths, with the north-south category including all azimuths ± 45 degrees from north or south and the east-west category including all azimuths ± 45 degrees from east or west. We test the null hypothesis that proportion of north-south song hours in ABB samples is less than or equal to the proportion of north-south song hours AB samples by calculating the Z-statistic for a one-sided test. The Z-statistic was 2.4088, which corresponds to a P-value of 0.008. The P-value is significant, rejecting the null hypothesis and indicating that ABB song hours have significantly a higher north-south polarization than AB song hours.

Speeds of transiting whales also vary with song type (Fig. 4.6(e)). ANOVA results find that hours of ABB song have significantly higher average speeds than hours of AB song (Table 4.2). Localization rates also vary with song type (Table 4.2, Fig. S4.6(a)). ABB song hours have significantly higher average localization rates than AB song, which reflects greater B-call production rates associated with ABB song. Chorus hours have lower average localization rates than even lone AB song at a $P<0.1$ significance level. Song type prevalence does not vary between day and night hours (Fig. S4.6(b)).

	Group 1	Relationship Between Means	Group 2	Lower 95%	Difference in Means	Upper 95%	P-Value
Latitude (°)	***AB***	>	***ABB***	***0.18***	***0.70***	***1.22***	***0.004***
	AB		Chorus	-0.78	-0.16	0.46	0.822
	ABB	<	***Chorus***	***-1.48***	***-0.86***	***-0.24***	***0.003***
Longitude (°)	***AB***	<	***ABB***	***-0.51***	***-0.31***	***-0.10***	***0.002***
	AB	<	***Chorus***	***-0.51***	***-0.26***	***-0.01***	***0.042***
	ABB		Chorus	-0.20	0.05	0.30	0.897
Loc Rate (hr^{-1})	***AB***	<	***ABB***	***-5.00***	***-3.35***	***-1.71***	**<0.001**
	AB		Chorus	-0.22	1.76	3.74	0.094
	ABB	>	***Chorus***	***3.15***	***5.11***	***7.08***	**<0.001**
Speed (km/hr)	***AB***	<	***ABB***	***-2.07***	***-1.47***	***-0.87***	**<0.001**
	AB	<	***Chorus***	***-1.78***	***-0.95***	***-0.11***	***0.021***
	ABB		Chorus	-0.31	0.52	1.35	0.301
Day of deployment	***AB***	<	***ABB***	***-19.88***	***-10.91***	***-1.94***	***0.012***
	AB		Chorus	-14.55	-3.75	7.05	0.694
	ABB		Chorus	-3.55	7.16	17.87	0.260

TABLE 4.2: ANOVA results comparing distributions of hours categorized as AB song, ABB song, and chorus over latitude, longitude, localization rate, speed for transiting tracks, and day of deployment. Group 1 and group 2 list the song type categories being compared. We report the difference in the means between the samples of groups 1 and 2. Lower 95% and Upper 95% give the 95% confidence interval for the difference in means of the populations. Bold rows show group comparisons with significant differences between the means ($P < 0.05$). When there is a significant difference the Relationship Between Means column indicates which group has the higher mean.

ii. Patterns in song metrics

The 10 tracks selected for manual song analysis are shown in Figure 4.7. Nearly all A and B calls in these tracks were produced within song phrases. The spatial and behavioral patterns in annotated AB and ABB song phrases mirror the patterns observed in hourly song categorizations. ANOVA results show that the ABB song phrase distribution is significantly southward of the AB song phrase distribution (Table 4.3). The ABB song phrases distribution is also significantly eastward of the AB song phrase distribution due to the relative distributions of the CI and GDZ

networks. Whales singing ABB song also swim significantly faster on average than whales singing AB song.

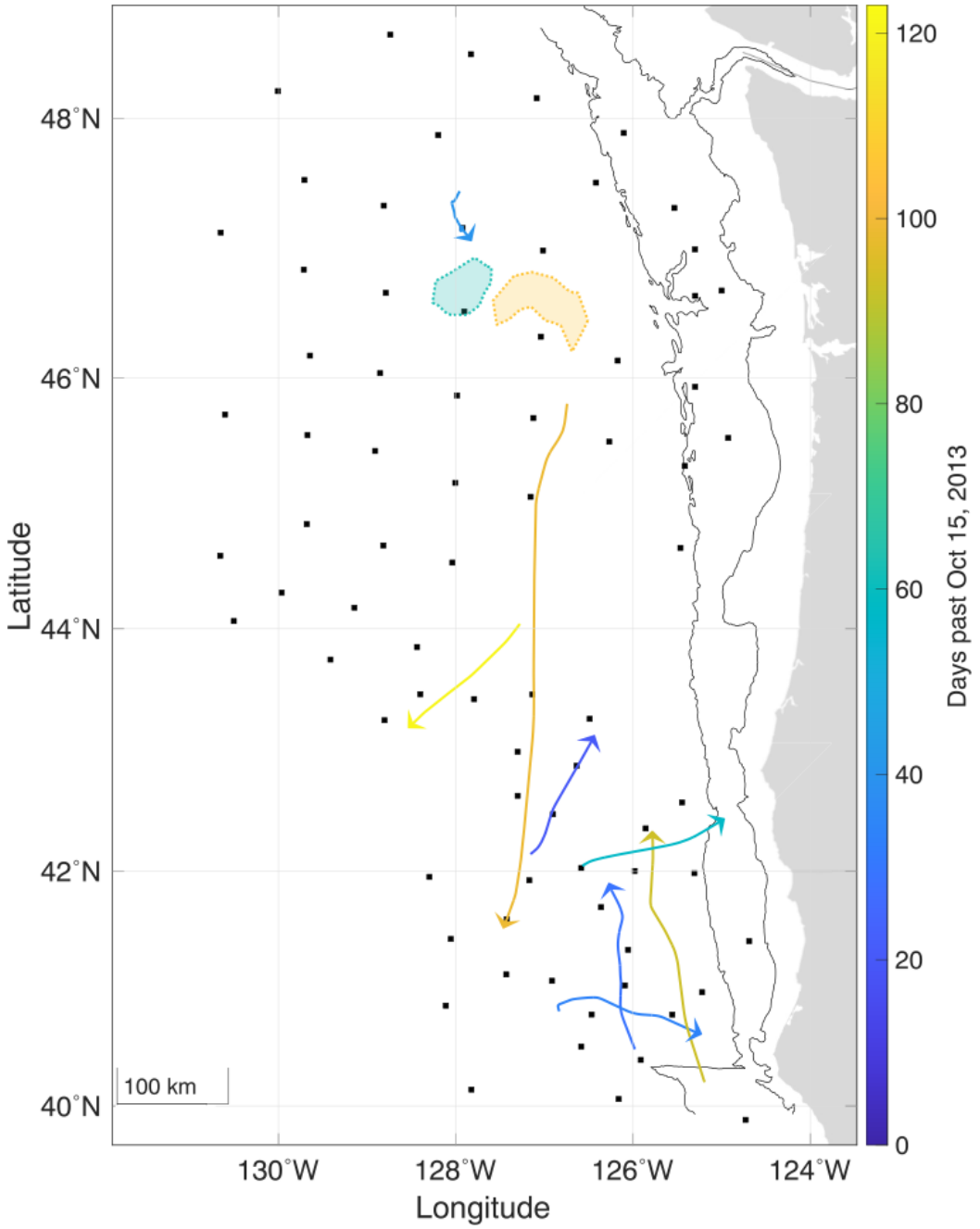

FIG. 4.7: Representative smoothed tracks selected for annotation of A and B note timings. Color shows median time of track. Solid lines show transiting tracks, dotted shapes enclose the localizations in non-transiting tracks. Black lines are 200 m and 2000 m depth contours.

The proportions of AB and ABB phrases varies greatly (Fig. 4.8). By definition, Tracks composed nearly exclusively of AB phrases have nearly equal numbers of A and B notes (Fig. 4.8(a&c)). Ratios of B to A calls in song generally increase with increased counts of ABB phrases but the relationship depends on the average number of B notes following each A note in song phrases. Some whales that sing ABB phrases often follow an A note with only two B-notes, but some whales singing ABB phrases in sing up to 15 B-notes in a single phrase (Fig. 4.2(b)). This increases the number of B-notes produced per hour for ABB singers compared to AB singers. Whales that sing more ABB phrases also sing less phrases total than whales that sing more AB phrases (Fig. 4.8(c)), because ABB phrases are longer than AB phrases.

	Group 1	**Relationship between means**	**Group 2**	**Lower 95%**	**Difference in Means**	**Upper 95%**	**P-Value**
Latitude (°)	**AB**	**>**	**ABB**	**0.46**	**0.63**	**0.80**	**<0.001**
Longitude (°)	**AB**	**<**	**ABB**	**-0.50**	**-0.45**	**-0.39**	**<0.001**
Speed (km/hr)	**AB**	**<**	**ABB**	**-0.85**	**-0.72**	**-0.58**	**<0.001**
Internote Int. (s)	**A-B**	**>**	**B-B**	**2.27**	**2.54**	**2.80**	**<0.001**
Interphrase Int. (s)	AB-AB		AB-ABB	-5.70	1.79	9.29	0.93
	AB-AB	**<**	**ABB-AB**	**-38.65**	**-31.02**	**-23.39**	**<0.001**
	AB-AB	**<**	**ABB-ABB**	**-36.25**	**-31.19**	**-26.13**	**<0.001**
	AB-ABB	**<**	**ABB-AB**	**-43.11**	**-32.81**	**-22.52**	**<0.001**
	AB-ABB	**<**	**ABB-ABB**	**-41.55**	**-32.99**	**-24.42**	**<0.001**
	ABB-AB		ABB-ABB	-8.86	-0.17	8.51	1.00

TABLE 4.3: ANOVA results comparing annotated song metrics for 10 selected tracks with column conventions as in Table 2. Distributions of AB and ABB phrases are compared for latitude, longitude, and speed for transiting tracks. Also compared are internote intervals for gaps between A and B notes (A-B) and B and B notes (B-B), and interphrase intervals for AB followed by AB phrases (AB-AB), AB followed by ABB phrases (AB-ABB), ABB followed by AB phrases (ABB-AB), and ABB followed by ABB phrases (ABB-ABB). Bold rows show group comparisons with significant differences in the means ($P < 0.05$).

The internote and interphrase intervals also show distinct patterns. ANOVA analysis shows that A-B internote intervals (53.3 +- 6.5 seconds) are significantly longer on average than B-B internote intervals (50.8 +- 4.3 seconds) (Fig. 4.8(b), Table 4.3). A-B and B-B internote

intervals are similar across tracks regardless of proportion of AB to ABB song phrases. Average interphrase intervals in tracks increase with increased proportion of ABB song phrases. ANOVA results found that interphrase intervals that start with an ABB phrase followed by either an AB or ABB phrase are significantly longer on average than interphase intervals that start with an AB phrase and are followed by either an AB or ABB phrase. Interphrase intervals following ABB phrases are on average ~32 seconds longer than those following AB phrases.

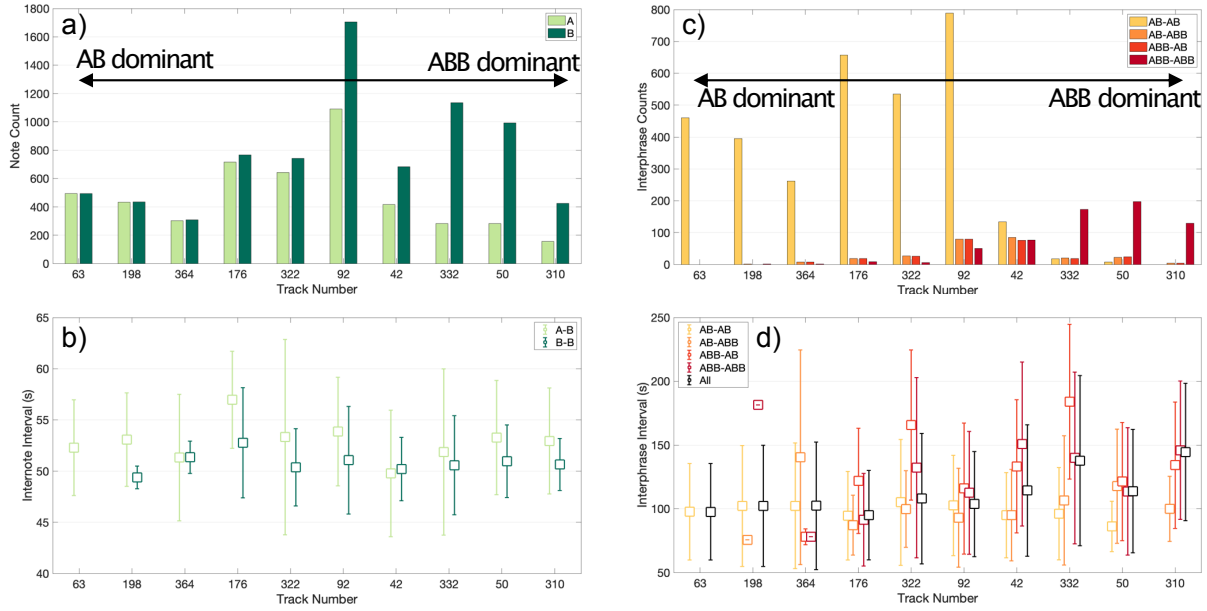

FIG. 4.8: Metrics of song composition of 10 tracks which were manually annotated for A and B call times. For each plot the tracks are ordered by the relative proportions of AB and ABB phrases. (a) The counts of A and B notes in each of the ten tracks. (b) The mean and standard deviation of internote intervals in song phrases with A-B denoting the time difference between an A note and a following B note and B-B the time difference between consecutive B notes in ABB phrases. (c) Interphrase metrics for each track showing counts of consecutive phrase types. (d) The mean and standard deviation of interphrase intervals for different consecutive phrase types. The interphrase interval measures the time between the start of the last B-call in a phrase and the A-call that starts the next phrase. Phrase spacings > 5 minutes are categorized as rests and excluded from these calculations.

iii. Track 92, two traveling singers

Each of the 10 tracks analyzed for song metrics was confirmed by inspection to be consistent with a single singing whale, except for one track on November 22, 2013 (Fig. 4.9). Track 92 is composed of two travelling whales that intersperse their singing patterns. The whales

must have been within ~10 km of each other for their localizations to be linked to the same track by our spatio-temporal filter. Songs are assigned to separate whales because they sometimes overlap and have distinct patterns and note frequencies. One whale sang exclusively AB phrases, with an average B note frequency of 15.2 Hz (Fig. 4.2(a)). The other whale sang exclusively ABB phrases, with a lower average B-note frequency of 14.8 Hz (Fig. 4.2(b)). B notes from both whales are localized within the track. Track 92 is also the only track that contains more than one isolated A note that is not followed by B note.

The whales were tracked for ~80 hours beginning at 1400 on November 22, 2013, and their song and movement is distinctly different between the earlier and later portions of the track (Fig. 4.9). We divide the track into two parts separated by an 8-hour calling break from 1600 November 23 to 0200 November 24. During the first part, the smoothed track shows that the pair transits towards the south at an average speed of 0.9 km/hr. Periods of AB and ABB song alternate, with minimal overlapping time. During the second part of the track, the smooth track meanders and the average speed slows significantly to 0.5 km/hr. AB and ABB songs overlap more frequently and the two whales also produce 9 of their 11 total singular A-calls. The scatter of localizations increases at the end of the track, which may be indicative of increased separation as the whales swim apart.

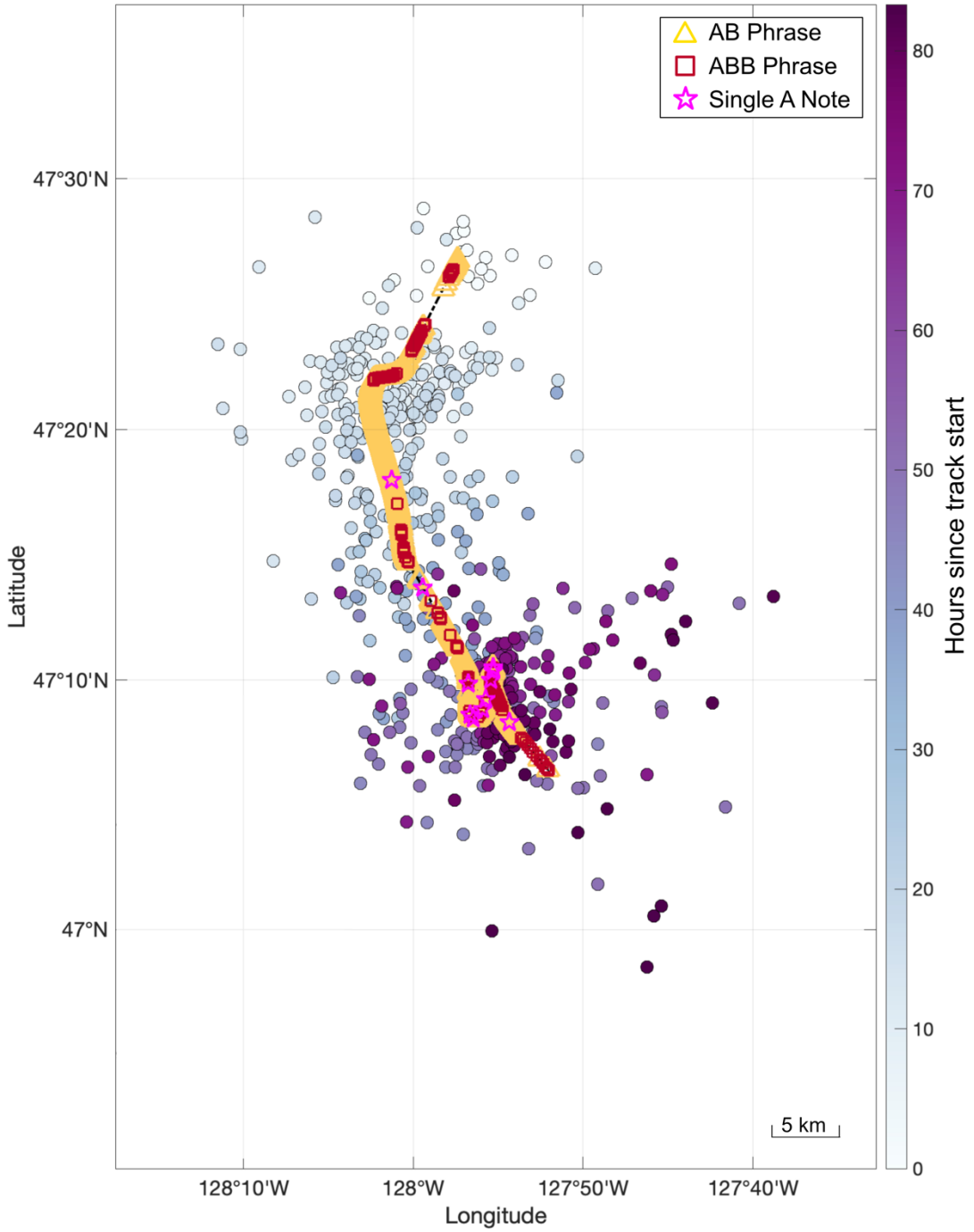

FIG. 4.9: Summary plot for track 92 which uniquely includes two singing whales. Circles show localizations colored by time relative to the beginning of the track at 1410 on November 22, 2013. The smooth track is shown by a dotted black line which is overlain by tan triangles, red squares, and magenta stars at the times of AB phrases, ABB phrases, and single A notes, respectively. One whale sang exclusively AB phrases, while the other sang exclusively ABB phrases.

C. Diel patterns

The localizations within tracks are not well suited for examining diel calling patterns because the localization success rate is variable (Fig. S4.7, Fig. S4.4) and expected to be worse when many whales are calling (Wilcock and Hilmo, 2021). Instead, spatial and seasonal patterns in diel calling are more accurately described using call index calculated from high-probability call detections on each OBSs (equation 2). Smoothed call index timeseries show diel calling recorded on OBSs varies seasonally and with latitude (Fig. S4.8). Maps of call index metrics show strong spatial patterns (Fig. 4.10). The northernmost OBSs that line the base of the British Columbia and Washington continental slopes have the highest average and peak call index values, indicating more nighttime calling (Fig. 4.10(a&c)). The two OBSs with the highest call index values are located nearest to the Juan de Fuca canyon, which is the largest submarine canyon complex along the Cascadia margin. These OBSs are not within the effective localization area, so it is impossible to compare their diel patterns with whale movement. Within the effective localization area, most of the highest average and peak call index values (Fig. 4.10(a&c)) coincide with the region of highest non-transiting track location densities on the eastern side of the Cascadia Basin (Fig. 4.3(c)). Average call index values in the south (Fig. 4.10(a)) are mostly negative indicating higher proportions of calling during the day. The majority of localizations in this region are from transiting whales (Fig. 4.3(b)). The call index also peaks later in the season as the latitude increase (Fig. 4.10(b-d)) with the notable exception of the two northernmost OBSs that have early peaks.

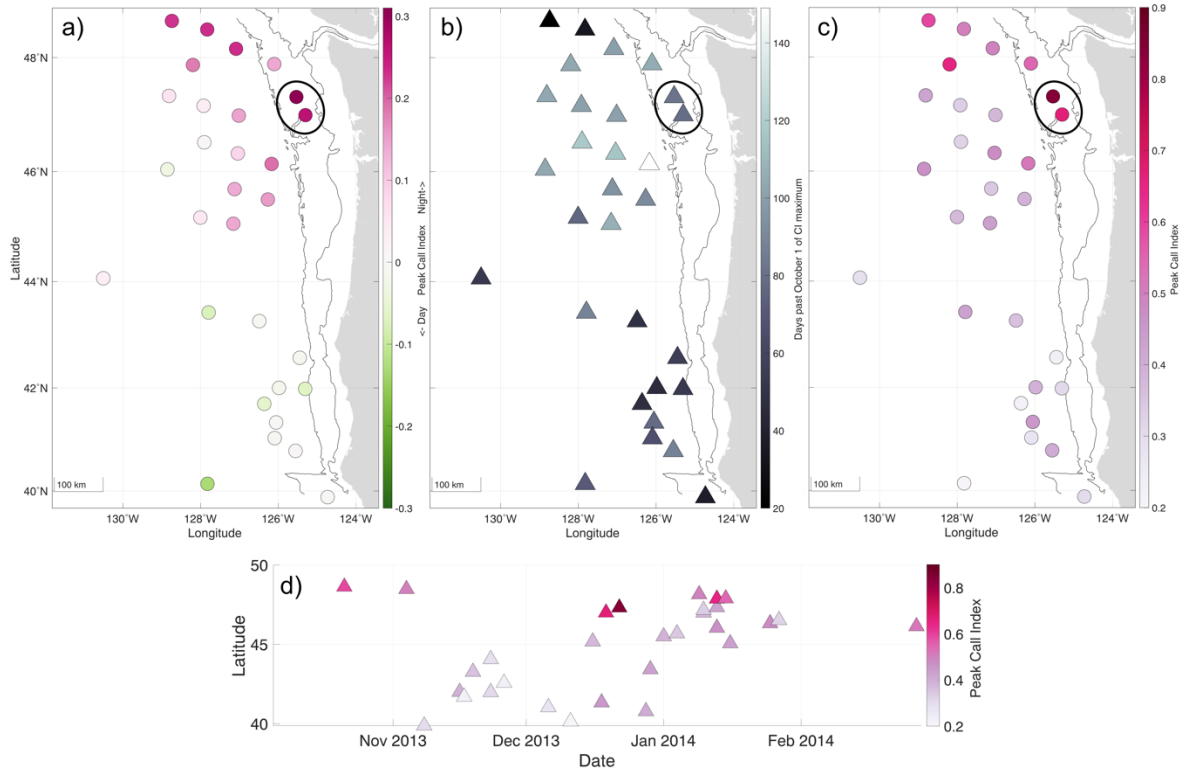

FIG. 4.10: Maps showing location of stations with at least 20 high-probability B-calls (P > 0.8) recorded on at least 50% of deployment days with colors representing (a) mean call index value, (b) date of peak call index value, and (c) the peak call index value. Black lines show 200 m and 2000 m depth contours. (d) Scatter plot showing the date of peak call index against station latitude with colors representing the maximum call index values as in (c). Stations circled on each map are deployed along the Juan de Fuca canyon complex and show the strongest nighttime calling metrics.

4.4 | Discussion

In this study we apply a recently developed acoustic localization method (Wilcock and Hilmo, 2021) to obtain tracks for singing NEP blue whales. However, there are several limitations to our tracking dataset.

First, we can only track whales withing the effective localization area (Fig. S4.4(a)) that comprises region seaward of the continental slope base where the OBSs form a grid with a spacing of ~70 km or less. Second, we do not observe the beginning of the NEP blue whale song season; NEP blue whales were tracked in the Cascadia Basin with the CI OBSs starting right

after the network was deployed in early October and the GDZ OBSs were not all deployed until early-November (Fig. 4.1). Third, we only track singing whales that produce repeating B calls and most of our analysis considers only extended tracks with at least 150 B calls localizations. Fourth because our localization success rate is highly variable, our set of extended tracks is presumably incomplete. For these reasons, we focus our interpretation on the behavior of singing whales rather than on estimates of population density.

Finally, geographic and seasonal patterns in acoustic observations of singing whales have generally been interpreted to be representative of the population in general (Clark et al., 1996; Monnahan et al., 2014; Stafford et al., 1999b). However, this may not hold true for singing male NEP blue whales overwintering in our study region since whale sex and age have been found to influence differences in individuals foraging and migration strategies (Blevins et al., 2022; Busquets-Vass et al., 2017, 2021).

A. Patterns in whale movement and distribution

Our study provides a unique data set to investigate the movement of singing NEP blue whales in deep waters off the Pacific Northwest coast. Net movement is northward in October, nearly zero in November, and southward in December, January, and February (Fig. 4.4, Fig. 4.5). Though we cannot describe whale behavior earlier than October, we can extrapolate our observations of increasing monthly whale track counts throughout the fall and changes in azimuth to estimate early fall behavior. We suggest that there would likely be fewer whales and less song in early fall months, and they would likely be moving northward through the region. Our observations are consistent with whales transiting northward into the region in the fall, remaining through early winter, then transiting southward out of the region through late winter. The timeline for departing the region is later that observed in tagged whales by Mate et al.

(2019), in which several NEP blue whales tagged off California transited northward through the Washington/Vancouver region through the late fall but all migrated southward by late December. Our timeline is supported by an acoustic study that reported B calls in the Cascadia through late winter in 1994-2000 (Burtenshaw, 2004), and stable-isotope analysis of baleen that shows some blue whales overwinter entirely in the region (Blevins, 2022).

There are a few explanations for the mismatch between our observations and movements of whales tagged off the coast of California. First, the Mate (2019) dataset included <10 tagged whales that migrated northward into the Cascadia Basin, which may not be enough to capture the patterns we describe in this study. Conversely, the whales we detected in late-winter may have originated from regions other than coastal California or represent resident whales as observed in baleen stable isotope analysis by Blevins (2022). The recent discovery of two distinct migration corridors of NEP blue whale subpopulations with slightly differing song metrics, one in the central Pacific from the Gulf of Alaska to Hawaii and one in the eastern Pacific from the US West Coast to the CRD (Carbaugh-Rutland et al., 2021), is consistent with the idea that there may be additional geographic variations in migration that have yet to be characterized. Alternatively, the mismatch may result from changes in migratory behavior over the decade or two between the collection of the Mate dataset (1994-2007) and our tracking study (2013-2014), though this is inconsistent with the coincident late-winter acoustic presence of blue whales in the Cascadia Basin observed in 1994-2000 by Burtenshaw (2004). Several studies have observed recent changes in large baleen whale migration and theorized that they may be due to populations returning to abandoned pre-whaling foraging grounds or may be a response to changing oceanographic conditions (Abrahms et al., 2019; Calambokidis et al., 2009; Szesciorka et al., 2020).

Variations in movement of tracked NEP blue whales within the study region may delineate regions of differing habitat use. The aggregation of most non-transiting tracks in the eastern Cascadia Basin throughout the fall and early winter contrasts with the consistent dominance of north-south transiting tracks in the Gorda Basin (Fig. 4.1, Fig. 4.4). The eastern Cascadia Basin may be an overwintering foraging ground, and the Gorda Basin a migration corridor. Possible reasons for the varying distributions of these behaviors are discussed in the following sections.

B. Links between song and behavior

i. Diel calling behavior identifies regions of foraging and migration

Nighttime dominance of NEP blue whale song has long been observed (Stafford et al., 2005; Wiggins et al., 2005) and is attributed to daytime dominance of foraging on krill swarms during which behavior whales do not sing (Lewis et al., 2018; Oleson et al., 2007). For this reason, nighttime singing dominance is used as a metric of foraging, while uniformly distributed or daytime dominant singing is considered a metric of migration (Oestreich et al., 2020, 2022).

The locations of OBSs with dominantly nighttime singing (Fig. 4.10(a)) in the Cascadia Basin closely matches the distributions of non-transiting whales within the effective localization area (Fig. 4.3(c)). Nighttime singing, and by inference foraging, generally increases in the eastern Cascadia Basin throughout the fall, peaking in early winter before subsiding (Fig. 4.10(a&d), Fig. S4.8). We observe the highest mean and peak call index, and thus the strongest indicators of daytime foraging on OBSs outside the effective localization area along the northern Cascadia slope (Fig. 4.10(a&b)).

The northeastern Cascadia region, especially near the continental slope, may be a popular overwintering foraging ground for NEP blue whales due to prey availability. The highest density

of whale localizations in our study are offshore of the Colombia river estuary (Fig. 4.3), at the southward limit of an extensive complex of submarine canyons off the coast of Washington. These submarine canyons influence local oceanographic conditions that drive aggregations of krill swarms in productive summer months (Santora et al. 2018). Unfortunately, little research has been done to measure krill distributions in late fall or winter. However, if canyon-enhanced krill swarms persist past summer they may support blue whale foraging (Cade et al., 2021; Murase et al., 2002). Future work characterizing distributions of fall and winter krill populations in the northeast Pacific is necessary for better understanding these winter habitats for NEP blue whale foraging.

ii. Trends in song metrics may be driven by energetic costs

Metrics of NEP blue whale song calculated in this study (Fig. 4.8(b)) report the first observation of A-B internote intervals exceeding B-B internote intervals. We found that internote intervals between A-B notes are consistent between singers, and do not vary between AB phrases and ABB phrases. Internote intervals between B-B notes only occur in ABB phrases, are shorter than A-B internote intervals, and are also stereotypical regardless of singers. Stereotypical internote intervals have been well described in previous studies of NEP blue whales, but all have reported A-B internote intervals as shorter than B-B internote intervals (Lewis and Širović, 2018; Stafford et al., 2001). A compilation of previous studies shows that A-B internote intervals have steadily increased since 1990 by ~10 s (Fig. 4.11). This contrasts with patterns in B-B internote intervals, which seem to either be constant or increasing more slowly, although they have not been measured as frequently.

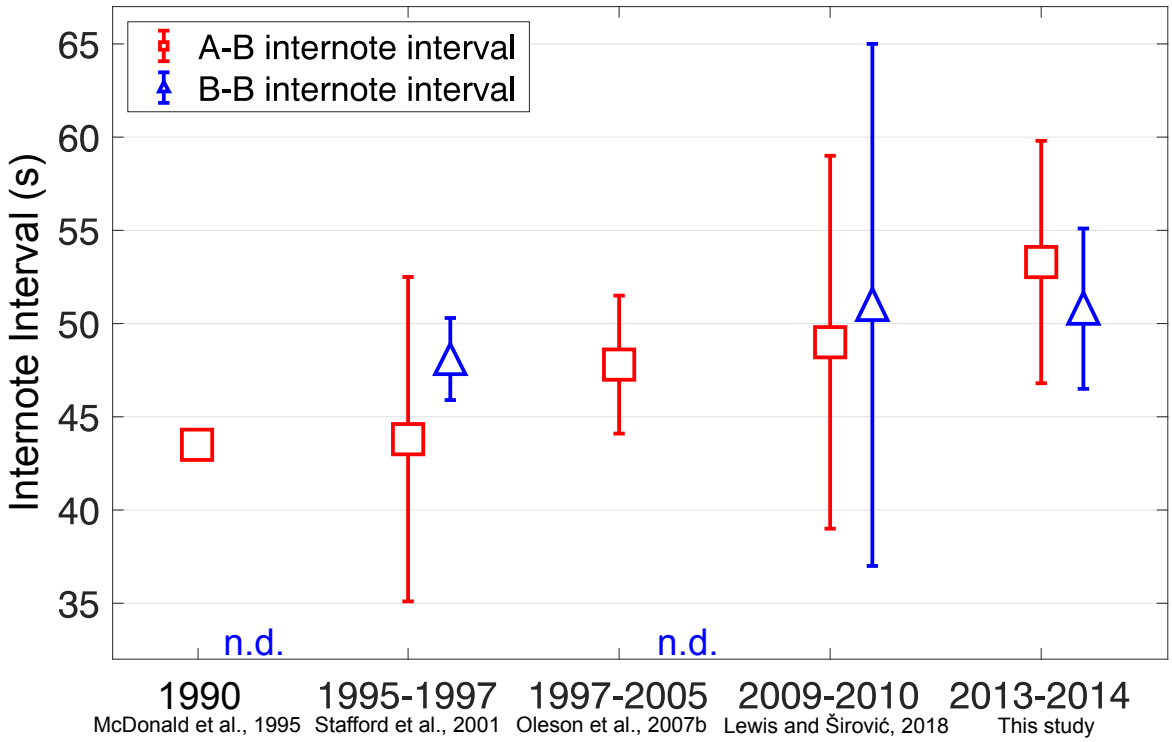

FIG. 4.11: Mean and standard deviation of internote intervals of NEP blue whale song measured in acoustic monitoring studies from 1990-2014. Internote intervals are calculated as the time difference from the start of the first call to the start of the following call. Stafford et al., 2001 and McDonald et al., 1995 reported internote intervals from the end of the first call to the start for the following call, so their reported average note length of the leading call was added to their reported internote intervals to standardize comparisons. McDonald et al., 1995 did not report A-B internote interval standard deviation. Both McDonald et al., 1995 and Oleson et al., 2007b did not report B-B internote intervals (indicated by n.d. (no data) on the plot).

The increase in A-B internote intervals has occurred alongside a well-studied decline in NEP blue whale song frequency. Since their first description in 1963, fundamental song frequencies have decreased from ~21.9 Hz to ~14.5 Hz as measured in 2019 (Mcdonald et al., 2009; Rice et al., 2022b). A-notes are slightly lower in frequency than B-notes, and are amplitude modulated which can make them more energetically expensive. Many reasons have been proposed for this frequency decline, including avoidance of the frequency band of anthropogenic noise, whale response to rising ocean temperatures, and population density increases due to post-whaling recovery. Since more energy is required to producing lower frequency sounds, one hypothesized

trade-off of this frequency decrease was a decline in source level over time (Mcdonald et al., 2009). However, this proposed source level decline has not manifested in acoustic observations of NEP blue whale populations (Rice et al., 2022b). Instead, we speculate that NEP blue whales may be lengthening their A-B internote intervals to extend recovery time as energy requirements for calls increase with declining frequencies. The greater increase in A-B internote interval compared to B-B internote interval provides more evidence that A-notes are more energetically expensive. These energetic tradeoffs contribute to our investigation of behavioral contexts for AB and ABB song in the following section.

Interphrase intervals observed in our study have much greater variability than internote intervals (Fig. 4.8(d)). Previous studies also report variable interphrase intervals, but they are difficult to compare directly to each other since they are characterized using different parameters (Lewis and Širović, 2018; McDonald et al., 1995b; Oleson et al., 2007b; Stafford et al., 2001). Our study is unique in comparing interphrase interval with types of the leading and following phrases. We find significant differences in interphrase interval lengths that are determined by the type of the leading phrase. On average, ABB phrases precede ~30s longer interphrase intervals than AB phrases, regardless of whether the following phrase type is ABB or AB (Table 4.3).

Extended interphrase intervals following ABB phrase types may be driven by a higher energetic cost relative to AB phrase types. ABB phrases are much longer than AB phrases and can contain more than a dozen consecutive B-notes with shorter relative internote intervals. The resulting higher call rates likely make ABB phrases more energetically expensive than AB phrases. As a reproductive display, longer and more frequent song would likely be indicative of higher fitness, which implies that extended rests following ABB phrases are likely driven by

physiological limitations. We suggest that longer interphrase intervals following ABB phrases may be necessary for whales to recover before producing more song.

iii. AB and ABB song phrases may be used in different behavioral contexts

Our dataset is unique in being able to link NEP blue whale AB and ABB song patterns to movement, geographical distribution, and seasonality for dozens of singing individuals. Distinct differences in AB and ABB song phrase associations with location, season, and movement indicate that different phrase types may be used in different behavioral contexts.

Increased ABB song is associated with metrics of migration in our dataset, while AB song is associated with metrics of overwintering. Though AB and ABB song are equally distributed between transiting and non-transiting tracks (Fig. 4.6(g)), it is important to recognize that not all transiting behavior is representative of migration. Our investigation into transiting tracks and their associated song phrases provides several metrics that identify migratory behavior and strongly associates them with ABB phrases. First, ABB phrases are more prevalent in the Gorda Basin migration corridor, while AB phrases are more prevalent in the Cascadia Basin overwintering ground (Fig. 4.6(a&b), Table 4.2, Table 4.3). Second, ABB phrases are strongly associated with north-south transiting azimuths that likely represent migrating whales because of the direction and time of year when these occur, while AB phrases are distributed more equally with respect to azimuth (Fig. 4.6(d), Table 4.2). Third, whales singing ABB phrases swim faster on average than whales singing AB phrases (Fig. 4.6(e), Table 4.2, Table 4.3). Finally, proportions of whales singing ABB phrases decrease throughout the fall as non-transiting track counts and diel foraging metrics approach their peak (Fig. 4.6(f), Fig. 4.10(b)), but increase throughout the winter as a whales increasingly transition to southward migration (Fig. 4.4, Fig. 4.5, Fig. 4.6(f), Table 4.2).

Our interpretation of AB and ABB song phrase preference in different contexts builds upon observations of spatial distributions of AB and ABB phrases produced by NEP blue whales on summer California feeding grounds (Lewis and Širović, 2018). Acoustic recorders in the Southern California Bight recorded higher proportions of AB phrases at nearshore sites, but higher proportions of ABB phrases at offshore sites. Separate visual surveys of Southern California Bight blue whales have observed differing nearshore and offshore behavior. Nearshore whales tended to swim in larger group sizes while feeding and milling, while offshore whales tended to be solitary and transiting (Lomac-MacNair and Smultea, 2016). These patterns correspond to shorter estimated sound propagation distances at nearshore sites and further estimated propagation distances at offshore sites (Širovic et al., 2015), indicating that preferred phrase type may be also informed by environmental factors (Lewis and Širović, 2018). These matching spatial patterns in visual observations of behavior and acoustic observations of AB/ABB phrases imply that phrase type is linked to behavioral state (Lewis and Širović, 2018). Our study provides further evidence of this through explicitly linking ABB phrase type to migration metrics.

We identify two possible motivations for NEP blue whales increasing ABB phrase production when engaging in migration. First, B-calls have high source levels and propagate greater distances than pulsed A-calls, so they may serve as long-distance contact calls for solitary migrating whales (Lewis and Širović, 2018). This may motivate increased B-note production, which manifests as ABB song.

Second, AB and ABB song phrases may display reproductive fitness in different behavioral contexts. A-notes are lower in frequency than B-notes and are amplitude modulated, which requires more power to produce than B-notes. Thus, in closer social proximity when

whales are not migrating, higher rates of A-note production in AB phrases with shorter interphrase intervals may be the most effective display of reproductive fitness. However, B-notes propagate further than A-notes, which makes them more likely to be heard by other whales while populations are more dispersed during migration. This may motivate demonstrations of other behaviors during migration and increased B-note production to signify reproductive fitness. Our observations that transiting ABB singing whales swim faster on average than transiting AB singing whales provides evidence for this interpretation. Similar swimming and song behavior has been described in fin whales (Clark et al., 2019). Fin whale males sing while swimming quickly, which is hypothesized to be a reproductive display of fitness. Bouts of fin whale singing at faster swim speeds are also follower by longer rests, similar to our observed increases in interphrase interval following blue whale ABB song phrases. We suggest that increased B-note production through ABB song at faster swim speeds is an adapted reproductive display exhibited by migrating whales.

iv. Singular A-calls are associated with social interaction

Of the 10 tracks analyzed for song metrics, we found only one track to be composed of two singers travelling together (Fig. 4.9). Song phrases were easily associated with individual whales due to different song phrases and note frequencies (Fig. 4.2). This pair of whales seemed to exhibit two distinct behavioral states. During the first half of the track, individuals interspersed and sometimes overlapped song phrases while swimming at a slightly faster pace (~0.9 km/hr). During the second half of the track, both whales produced many singular A-calls with no following B-call and slowed their swimming speed (~0.5 km/hr). This associates singular A-calls with close social interaction of male whales and a break in transiting.

The spatial distributions of singular A-calls have been observed to differ from spatial distributions of song phrases in several studies (Lewis et al., 2018; Lewis and Širović, 2018; Oleson et al., 2007a), so have been theorized to serve a different function than song. However, only one previous study has managed to link singular A-calls to close social behavior through tagging in summer feeding grounds off of southern California (Oleson et al., 2007a). Singular A-calls of tagged whales were often associated with feeding, resting, and milling in groups. Frequent singular A-call production by males in close proximity were interpreted to function as contact calls used to maintain pair bonds. Our observation of singular A-call production associated with social behavior of two nearby males supports this interpretation and shows that Cascadia overwintering individuals engage in similar social interactions to those on summer feeding grounds.

C. Future applications

Our analysis, though expansive, did not exhaust the potential of OBS datasets for characterizing NEP blue whale behavior or song. One obvious continuation of this research is to apply our tracking method to additional years of the CI (2011-2015) and GDZ (2013-2015) OBS deployments. Other large OBS networks have also been deployed off the US West Coast on the Blanco transform (2014-2015), and off southern California (2010-2011). Compared to our combined 2013-2014 CI and GDZ networks, other deployments had smaller spatial coverage and in some cases were beset by more instrumental failures (Hilmo and Wilcock, 2020). Despite these challenges, they are likely capable of tracking NEP blue whales and would provide valuable data to compare interannual trends in migration and song characteristics. These trends could then be compared to interannual variations in oceanographic parameters such as El Niño, temperature, and productivity.

There is also potential for additional analysis of NEP blue whale song metrics, as we only annotated note timings of 10 selected tracks. Further applications of analyst annotation of tracked whale song could include characterizing additional song metrics including call lengths, amplitude modulation in A-notes, and frequencies of notes. Our speculation on changing internote intervals being driven by energetic requirements of lower frequency calls could be furthered by investigating the length of B-notes and whether that has changed. Though cursory observations describe differences in A-note and B-note frequencies attributed to different whales (Fig. 4.2), we did not systematically include analysis of note frequencies in our investigations of song metrics. Investigating spatial, temporal, and behavioral trends in song frequencies could further our ability to describe population trends with acoustic metrics. Additionally, investigating the shapes of B-notes of tracked whales would allow us to determine whether overwintering NEP blue whales belong exclusively to the California-CRD subpopulation or whether there is some representation from the Gulf of Alaska-Hawaii subpopulation (Carbaugh-Rutland et al., 2021).

4.5 CONCLUCSIONS

In this study we present an extensive dataset of acoustically tracked NEP blue whales that sang offshore of the U.S. West Coast throughout the 2013-2014 Fall-Winter season. Through analysis of whale movement and diel calling patterns we identify two distinct regions of differing habitat use: the Cascadia Basin as a foraging/overwintering ground, and the Gorda Basin as a migration corridor. We demonstrate an instance of overwintering whales engaging in similar social behaviors to those observed on southern California feeding grounds. Additionally, we note different patterns in AB and ABB phrase production, associating ABB phrases with metrics of migration. Our measurements of song metrics compared with historical measurements also indicate song patterns are constrained by energetic costs. Finally, we suggest AB and ABB song

are used as displays of reproductive fitness in different contexts: AB song when not migrating and in closer proximities to other individuals, and ABB song plus increased swimming speeds when migrating and more distant from other individuals. This study expands available research on NEP blue whale behavior and migration and may contribute to future changes in how we characterize their life history and population structure.

4.6 ACKNOWLEGMENTS

We thank Danielle Harris and Dave Mellinger for helpful conversations and Manuel Castellote for reviewing an early version of this manuscript.

Chapter 5: Summary and Future Work

In total, there are thousands of years of publicly available OBS data that have so far been underutilized as a PAM tool to study large baleen whales. Regional OBS networks are generally deployed for a year, but sometimes longer, and are often composed of tens of OBSs spanning thousands of square kilometers. Regional temporary OBS networks have been deployed in critical regions for migratory baleen whales including both temperate and polar summer feeding ranges such as the Gulf of Alaska, Antarctica, the U.S. West and East Coasts, and the Gulf of Cádiz off of Portugal. OBS networks have also been deployed in potential equatorial winter breeding grounds such as Hawaii, off of Madagascar, Marianas, and Puerto Rico. Though they are often only deployed for one song season, these networks provide multi-instrument PAM datasets of unprecedented spatial scale for characterizing large baleen whale population densities and habitat use.

Conversely, PAM datasets from OBSs on cabled ocean instrumentation systems such as Ocean Networks Canada (ONC), Ocean Observatories Initiative (OOI), DONET, and S-net have decadal timescales (Barnes et al., 2013; Cowles et al., 2010; Iwase, 2015; Kawaguchi et al., 2015). Though the OOI and ONC cabled networks in the Northeast Pacific have relatively few OBSs and sparse distributions covering smaller areas than temporary networks, they could be leveraged to describe long-term trends in large baleen whale presence in certain regions. Decadal OBS datasets could monitor long-term interannual calling changes related to whale population recovery, climate change, or El Niño oscillations. PAM potential of some large-scale offshore monitoring systems is even greater. For example, the large cabled DONET and S-net OBS arrays off of Japan include dozens of instruments which inform early earthquake and tsunami warning

systems (Iwase, 2015; Kawaguchi et al., 2015). These observatories may be an ideal combination of long-term and large-scale PAM instrumentation.

This dissertation expands the methodology for exploiting opportunistic OBS instrumentation to monitor blue and fin whale populations. In chapter 2, I expanded a method for ranging to fin whales from OBSs using the timings of multipath arrivals of their calls that reflect off the seafloor and sea surface. I demonstrated the applicability of the method at multiple deep ocean locations and discussed how to account for various site properties. In chapter 3, I demonstrated fin whale call density estimation using OBSs deployed near the Marianas trench by applying multipath ranging and point-transect distance sampling methods. In chapter 4, I applied an acoustic tracking algorithm to characterize NEP blue whale behavior off the coast of the Pacific Northwest. The chapter provided new insight into an understudied subpopulation of NEP blue whales that skips migration to the Eastern Tropical Pacific and instead overwinters in temperate waters. In summary, these chapters exemplify the PAM potential of OBS networks for studying large baleen whales.

Looking forward, multipath ranging can contribute to a growing body of research focused on single station density estimation of fin whales (Harris et al., 2013; Hilmo and Wilcock, 2024; Matias and Harris, 2015; Weirathmueller et al., 2017b). As discussed in Chapter 2 and 3, multipath ranging works best in regions of lower population density because of its extended monitoring area (up to a 40 km radius) and difficultly in ranging to more than a single whale at a time (Hilmo and Wilcock, 2024). In Chapter 2, I briefly describe another method with contrasting limitations that localizes fin whale calls through measuring particle motion recorded on the three orthogonal sensors of a single OBS (Harris et al., 2013; Matias and Harris, 2015). Though the particle motion method is not stymied by multiple overlapping callers, it only works

out to a little less than the critical distance, the range at which the incoming call is fully reflected by the seafloor. This varies with depth and seafloor properties, but is almost always ≤ 5 km. These contrasting strengths mean that multipath and particle motion methods are complementary and ideal for estimating density in different environments. For example, the particle motion method may be ideal for density estimation in high population areas such as the Gulf of Alaska where chorusing song causes the multipath method to fail (Hilmo and Wilcock, 2024). Conversely, I demonstrate in Chapter 3 that the multipath method is ideal for density estimation in low population areas such as the equatorial oceans (Hamilton et al., 2009; Jackson et al., 2004; Mizroch et al., 2009; Rankin et al., 2018). Future studies should systematically compare multipath and particle motion methods in regions of different depth, bathymetry, and seafloor properties to better compare their effectiveness. Additionally, independent tagging studies to characterize fin whale "cue rates" must be undertaken to fully realize the potential of either method to estimate fin whale animal densities.

The acoustic localization methods (Wilcock and Hilmo, 2021) implemented in Chapter 4 have great potential for characterizing blue whale behavior and habitat use in any region where whale ranges overlap large OBS networks. Several of those regions are listed earlier in this chapter. My first suggested follow-up study would be to apply the analysis of Chapter 4 to networks deployed off the U.S. West Coast at different times including other CI and GDZ experiment years, the Blanco Transform experiment (Nabelek and Braunmiller, 2012), and the Albacore experiment (Lin et al., 2015). This would allow for interannual comparisons of NEP blue whale distributions and behavior in this region. Next, I would apply these methods to a large OBS network deployed in the Gulf of Alaska from 2018-2019, the Alaska Amphibious Community Seismic Experiment (AACSE) (Barcheck et al., 2020), to analyze song and

movement of a newly identified acoustic subpopulation of NEP blue whales that migrates between the Gulf of Alaska and Hawaii (Carbaugh-Rutland et al., 2021). That migration corridor is geographically distinct from our observations of NEP blue whales off the Pacific Northwest coast reported in Chapter 4. Comparing Chapter 4 observations of whale behavior with observations from the AASCE will begin to characterize life history differences between the two NEP blue whale acoustic subpopulations.

Bibliography

Abrahms, B., Hazen, E. L., Aikens, E. O., Savoca, M. S., Goldbogen, J. A., Bograd, S. J., Jacox, M. G., et al. (**2019**). "Memory and resource tracking drive blue whale migrations," PNAS, **116**, 5582–5587. doi:10.1073/pnas.1819031116

Abrams, L. J., Larson, R. L., Shipley, T. H., and Lancelot, Y. (**1992**). "Proceedings of the Ocean Drilling Program, 129 Scientific Results," Proceedings of the Ocean Drilling Program, , doi: 10.2973/odp.proc.sr.129.1992. doi:10.2973/odp.proc.sr.129.1992

Affatati, A., Scaini, C., and Salon, S. (**2022**). "Ocean Sound Propagation in a Changing Climate: Global Sound Speed Changes and Identification of Acoustic Hotspots," Earth's Future, **10**, e2021EF002099. doi:10.1029/2021EF002099

Aguilar, A. (**2009**). "Fin Whale, Balaenoptera physalus," Encyclopedia of Marine Mammals, pp. 433–437. doi:10.1016/B978-0-12-373553-9.00102-4

Archer, F. I., Brownell, R. L., Hancock-Hanser, B. L., Morin, P. A., Robertson, K. M., Sherman, K. K., Calambokidis, J., et al. (**2019**). "Revision of fin whale Balaenoptera physalus (Linnaeus, 1758) subspecies using genetics," (R. Moratelli, Ed.) Journal of Mammalogy, **100**, 1653–1670. doi:10.1093/jmammal/gyz121

Archer, F. I., Morin, P. A., Hancock-Hanser, B. L., Robertson, K. M., Leslie, M. S., Bérubé, M., Panigada, S., et al. (**2013**). "Mitogenomic Phylogenetics of Fin Whales (Balaenoptera physalus spp.): Genetic Evidence for Revision of Subspecies," PLOS ONE, **8**, e63396. doi:10.1371/journal.pone.0063396

Archer, F. I., Rankin, S., Stafford, K. M., Castellote, M., and Delarue, J. (**2020**). "Quantifying spatial and temporal variation of North Pacific fin whale (Balaenoptera physalus) acoustic behavior," Marine Mammal Science, **36**, 224–245. doi:10.1111/mms.12640

Au, W., James, D., and Andrews, K. (**2001**). “High-frequency harmonics and source level of humpback whale songs,” The Journal of the Acoustical Society of America, **110**, 2770. doi:10.1121/1.4777702

Bailey, H., Mate, B., Palacios, D., Irvine, L., Bograd, S., and Costa, D. (**2009**). “Behavioural estimation of blue whale movements in the Northeast Pacific from state-space model analysis of satellite tracks,” Endang. Species. Res., **10**, 93–106. doi:10.3354/esr00239

Barcheck, G., Abers, G. A., Adams, A. N., Bécel, A., Collins, J., Gaherty, J. B., Haeussler, P. J., et al. (**2020**). “The Alaska Amphibious Community Seismic Experiment,” Seismological Research Letters, **91**, 3054–3063. doi:10.1785/0220200189

Barnes, C. R., Best, M. M. R., Johnson, F. R., Pautet, L., and Pirenne, B. (**2013**). “Challenges, Benefits, and Opportunities in Installing and Operating Cabled Ocean Observatories: Perspectives From NEPTUNE Canada,” IEEE J. Ocean. Eng., **38**, 144–157. doi:10.1109/JOE.2012.2212751

Baumgartner, M. F., Van Parijs, S. M., Wenzel, F. W., Tremblay, C. J., Carter Esch, H., and Warde, A. M. (**2008**). “Low frequency vocalizations attributed to sei whales (*Balaenoptera borealis*),” The Journal of the Acoustical Society of America, **124**, 1339–1349. doi:10.1121/1.2945155

Bécel, A., Davis, J. K., Shuck, B. D., Avendonk, H. J. A. V., and Gibson, J. C. (**2020**). “Evidence for a Prolonged Continental Breakup Resulting From Slow Extension Rates at the Eastern North American Volcanic Rifted Margin,” Journal of Geophysical Research: Solid Earth, **125**, e2020JB020093. doi:10.1029/2020JB020093

Bermant, P. C., Bronstein, M. M., Wood, R. J., Gero, S., and Gruber, D. F. (**2019**). "Deep Machine Learning Techniques for the Detection and Classification of Sperm Whale Bioacoustics," Sci Rep, **9**, 12588. doi:10.1038/s41598-019-48909-4

Best, P., Marxer, R., Paris, S., and Glotin, H. (**2022**). "Temporal evolution of the Mediterranean fin whale song," Sci Rep, **12**, 13565. doi:10.1038/s41598-022-15379-0

Beyreuther, M., Barsch, R., Krischer, L., Megies, T., Behr, Y., and Wassermann, J. (**2010**). "ObsPy: A Python Toolbox for Seismology," Seismological Research Letters, **81**, 530–533. doi:10.1785/gssrl.81.3.530

Blackwell, S. B., Thode, A. M., Conrad, A. S., Ferguson, M. C., Berchok, C. L., Stafford, K. M., Marques, T. A., et al. (**2021**). "Estimating acoustic cue rates in bowhead whales, Balaena mysticetus, during their fall migration through the Alaskan Beaufort Sea," The Journal of the Acoustical Society of America, **149**, 3611–3625. doi:10.1121/10.0005043

Blevins, C., Busquets-Vass, G., Pardo, M. A., Gendron, D., Jacobsen, J. K., Gómez-Díaz, F., Pérez-Puig, H., et al. (**2022**). "Sex- and age-specific migratory strategies of blue whales in the northeast Pacific Ocean," Frontiers in Marine Science, Retrieved from https://www.frontiersin.org/articles/10.3389/fmars.2022.944918. Retrieved from https://www.frontiersin.org/articles/10.3389/fmars.2022.944918

Borchers, D., Marques, T., Gunnlaugsson, T., and Jupp, P. (**2010**). "Estimating Distance Sampling Detection Functions When Distances Are Measured With Errors," Journal of Agricultural, Biological, and Environmental Statistics, **15**, 346–361.

Bowles, F. A. (**1997**). "Observations on attenuation and shear-wave velocity in fine-grained, marine sediments," The Journal of the Acoustical Society of America, **101**, 3385–3397. doi:10.1121/1.419374

Boyer, T., Locarnini, R. A., Baranova, O., Garcia, H. E., Mishonov, A. V., Paver, C., Reagan, J. R., et al. (**2018**). "The World Ocean Atlas 2018: Improvements and Uses of Climatological Mean Fields," **2018**, OS13D-1506. Presented at the AGU Fall Meeting Abstracts

ten Brink, U. (**2005**). "Vertical motions of the Puerto Rico Trench and Puerto Rico and their cause," Journal of Geophysical Research: Solid Earth, , doi: 10.1029/2004JB003459. doi:10.1029/2004JB003459

Brodie, D. C., and Dunn, R. A. (**2015**). "Low frequency baleen whale calls detected on ocean-bottom seismometers in the Lau basin, southwest Pacific Ocean," The Journal of the Acoustical Society of America, **137**, 53–62. doi:10.1121/1.4904556

Buckland, S. T., Anderson, D. R., Burnham, K. P., Laake, J. L., Borchers, D. L., and Thomas, and L. (**2001**). *Introduction to Distance Sampling: Estimating Abundance of Biological Populations*, Oxford University Press, Oxford, New York, 448 pages.

Burtenshaw, J., Oleson, E., Hildebrand, J., Mcdonald, M., Andrew, R., Howe, B., and Mercer, J. (**2004**). "Acoustic and satellite remote sensing of blue whale seasonality and habitat in the Northeast Pacific," Deep Sea Research Part II: Topical Studies in Oceanography, **51**, 967–986. doi:10.1016/S0967-0645(04)00095-5

Busquets-Vass, G., Newsome, S. D., Calambokidis, J., Serra-Valente, G., Jacobsen, J. K., Aguíñiga-García, S., and Gendron, D. (**2017**). "Estimating blue whale skin isotopic incorporation rates and baleen growth rates: Implications for assessing diet and movement patterns in mysticetes," (M. S. Boyce, Ed.) PLoS ONE, **12**, e0177880. doi:10.1371/journal.pone.0177880

Busquets-Vass, G., Newsome, S. D., Pardo, M. A., Calambokidis, J., Aguíñiga-García, S., Páez-Rosas, D., Gómez-Gutiérrez, J., et al. (**2021**). "Isotope-based inferences of the seasonal foraging and migratory strategies of blue whales in the eastern Pacific Ocean," Marine Environmental Research, **163**, 105201. doi:10.1016/j.marenvres.2020.105201

Calambokidis, J., Barlow, J., Ford, J. K. B., Chandler, T. E., and Douglas, A. B. (**2009**). "Insights into the population structure of blue whales in the Eastern North Pacific from recent sightings and photographic identification," Marine Mammal Science, **25**, 816–832. doi:10.1111/j.1748-7692.2009.00298.x

Carbaugh-Rutland, A., Have Rasmussen, J., Sterba-Boatwright, B., and Širović, A. (**2021**). "Geographically distinct blue whale song variants in the Northeast Pacific," Endang. Species. Res., **46**, 19–33. doi:10.3354/esr01145

Carretta, J. V., Oleson, E. M., Forney, K. A., Bradford, A. L., Yano, K., Weller, D. W., Lang, A. R., et al. (**2023**). "DRAFT U.S. PACIFIC MARINE MAMMAL STOCK ASSESSMENTS: 2023.,"

Castellote, M., Clark, C., and Lammers, M. (**2012**). "Fin whale (Balaenoptera physalus) population identity in the western Mediterranean Sea," , doi: 10.1111/J.1748-7692.2011.00491.X. doi:10.1111/J.1748-7692.2011.00491.X

Christeson, G. L., Purdy, G. M., and Fryer, G. J. (**1994**). "Seismic constraints on shallow crustal emplacement processes at the fast spreading East Pacific Rise," Journal of Geophysical Research: Solid Earth, **99**, 17957–17973. doi:10.1029/94JB01252

Clark, C. W., Charif, R., Mitchell, S., Colby, J., and Woods, S. (**1996**). "Distribution and Behavior of the Bowhead Whale, Balaena mysticetus, Based on Analysis of Acoustic

Data Collected During the 1993 Spring Migration off Point Barrow, Alaska," Reoprt to the International Whaling Commission,.

Clark, C. W., Gagnon, G. J., and Frankel, A. S. (**2019**). "Fin whale singing decreases with increased swimming speed," R. Soc. open sci., **6**, 180525. doi:10.1098/rsos.180525

Constaratas, A. N., McDonald, M. A., Goetz, K. T., and Giorli, G. (**2021**). "Fin whale acoustic populations present in New Zealand waters: Description of song types, occurrence and seasonality using passive acoustic monitoring," PLOS ONE, **16**, e0253737. doi:10.1371/journal.pone.0253737

Cowles, T., Delaney, J., Orcutt, J., and Weller, R. (**2010**). "The Ocean Observatories Initiative: Sustained Ocean Observing Across a Range of Spatial Scales," Marine Technology Society Journal, **44**, 54–64. doi:10.4031/MTSJ.44.6.21

Croll, D. A., Clark, C. W., Acevedo, A., Tershy, B., Flores, S., Gedamke, J., and Urban, J. (**2002**). "Only male fin whales sing loud songs," Nature, **417**, 809–809. doi:10.1038/417809a

Cubaynes, H. C., and Fretwell, P. T. (**2022**). "Whales from space dataset, an annotated satellite image dataset of whales for training machine learning models," Sci Data, **9**, 245. doi:10.1038/s41597-022-01377-4

Data from: Behavioural estimation of blue whale movements in the Northeast Pacific from state-space model analysis of satellite tracks, (**2019**). Available: https://www.datarepository.movebank.org/handle/10255/move.837. Retrieved from https://www.datarepository.movebank.org/handle/10255/move.837

Davis, G. E., Baumgartner, M. F., Corkeron, P. J., Bell, J., Berchok, C., Bonnell, J. M., Thornton, J. B., et al. (**2020**). "Exploring movement patterns and changing distributions of baleen

whales in the western North Atlantic using a decade of passive acoustic data," Global Change Biology, **26**, 4812–4840. doi:https://doi.org/10.1111/gcb.15191

Delarue, J., and Todd, S. K. (**2009**). "Geographic variation in Northwest Atlantic fin whale (Balaenoptera physalus) song: Implications for stock structure assessment," J. Acoust. Soc. Am., **125**, 10.

Douglas Wiens (**2014**). "Mantle serpentinization and water cycling through the Mariana Trench and Forearc.," doi:10.7914/SN/XF_2012

Dreo, R., Bouffaut, L., Guillon, L., and Barruol, G. (**2017**). "Antarctic Blue Whale localization with Ocean Bottom Seismometers in Southern Indian Ocean.,"

Dréo, R., Bouffaut, L., Leroy, E., Barruol, G., and Samaran, F. (**2019**). "Baleen whale distribution and seasonal occurrence revealed by an ocean bottom seismometer network in the Western Indian Ocean," Deep Sea Research Part II: Topical Studies in Oceanography, The 2nd International Indian Ocean Expedition (IIOE-2): Motivating New Exploration in a Poorly Understood Ocean Basin (Volume 1), **161**, 132–144. doi:10.1016/j.dsr2.2018.04.005

Dunn, R. A., and Hernandez, O. (**2009**). "Tracking blue whales in the eastern tropical Pacific with an ocean-bottom seismometer and hydrophone array," The Journal of the Acoustical Society of America, **126**, 1084–1094. doi:10.1121/1.3158929

Dushaw, B. D., and Colosi, J. A. (**1998**). *Ray Tracing for Ocean Acoustic Tomography* (Technical Memorandum), Applied Physics Laboratory: University of Washington. Retrieved from https://apps.dtic.mil/sti/pdfs/ADA360612.pdf

Edwards, E. F., Hall, C., Moore, T. J., Sheredy, C., and Redfern, J. V. (**2015**). "Global distribution of fin whales Balaenoptera physalus in the post-whaling era (1980–2012)," Mammal Review, **45**, 197–214. doi:10.1111/mam.12048

Fiedler, P. C., Reilly, S. B., Hewitt, R. P., Demer, D., Philbrick, V. A., Smith, S., Armstrong, W., et al. (**1998**). "Blue whale habitat and prey in the California Channel Islands," Deep Sea Research Part II: Topical Studies in Oceanography, **45**, 1781–1801. doi:10.1016/S0967-0645(98)80017-9

Gavrilov, A. N., McCauley, R. D., Salgado-Kent, C., Tripovich, J., and Burton, C. (**2011**). "Vocal characteristics of pygmy blue whales and their change over time," The Journal of the Acoustical Society of America, **130**, 3651–3660. doi:10.1121/1.3651817

Goldbogen, J., Stimpert, A., Deruiter, S., Calambokidis, J., Friedlaender, A., Schorr, G., Moretti, D., et al. (**2014**). "Using accelerometers to determine the calling behavior of tagged baleen whales," The Journal of experimental biology, , doi: 10.1242/jeb.103259. doi:10.1242/jeb.103259

Gregr, E. J., Nichol, L., Ford, J. K. B., Ellis, G., and Trites, A. W. (**2000**). "Migration and Population Structure of Northeastern Pacific Whales Off Coastal British Columbia: An Analysis of Commercial Whaling Records from 1908-1967," Marine Mammal Science, **16**, 699–727. doi:https://doi.org/10.1111/j.1748-7692.2000.tb00967.x

Guazzo, R. A., Durbach, I. N., Helble, T. A., Alongi, G. C., Martin, C. R., Martin, S. W., and Henderson, E. E. (**2021**). "Singing Fin Whale Swimming Behavior in the Central North Pacific," Frontiers in Marine Science, , doi: https://doi.org/10.3389/fmars.2021.696002. doi:https://doi.org/10.3389/fmars.2021.696002

Guirado, E., Tabik, S., Rivas, M. L., Alcaraz-Segura, D., and Herrera, F. (**2019**). "Whale counting in satellite and aerial images with deep learning," Scientific Reports, **9**, 14259. doi:10.1038/s41598-019-50795-9

Hamilton, E. L. (**1976**). "Shear-wave velocity versus depth in marine sediments; a review," Geophysics, **41**, 985–996. doi:10.1190/1.1440676

Hamilton, E. L. (**1978**). "Sound velocity–density relations in sea-floor sediments and rocks," The Journal of the Acoustical Society of America, **63**, 366–377. doi:10.1121/1.381747

Hamilton, T., Redfern, J. V., Barlow, J., Ballance, L. T., Taylor, L., Gerrodette, T., Holt, R. S., et al. (**2009**). "Atlas of cetacean sightings for Southwest Fisheries Science Center cetacean and ecosystem surveys, 1986-2005," NOAA technical memorandum NMFS;NOAA-TM-NMFS-SWFSC ; 440;, Retrieved from https://repository.library.noaa.gov/view/noaa/3736. Retrieved from https://repository.library.noaa.gov/view/noaa/3736

Harding, B. W., Storms, M. A., Deutsch, U. K. W., Fay, J.-B., Fierback, R., Floyd, K., Geiser, L., et al. (**1990**). "Proceedings of the Ocean Drilling Program, Initial Reports," Retrieved from http://hdl.handle.net/10.2973/odp.proc.ir.124E.118.1990. Retrieved from http://hdl.handle.net/10.2973/odp.proc.ir.124E.118.1990

Harris, D., Matias, L., Thomas, L., Harwood, J., and Geissler, W. H. (**2013**). "Applying distance sampling to fin whale calls recorded by single seismic instruments in the northeast Atlantic," The Journal of the Acoustical Society of America, **134**, 3522–3535. doi:10.1121/1.4821207

Harris, D. V., Miksis-Olds, J. L., Vernon, J. A., and Thomas, L. (**2018**). “Fin whale density and distribution estimation using acoustic bearings derived from sparse arrays,” The Journal of the Acoustical Society of America, **143**, 2980–2993. doi:10.1121/1.5031111

Hatch, L. T. (**2004**). *Male genes and male song: Integrating genetic and acoustic data in defining fin whale, Balaenoptera physalus, management units* (Ph.D.), Cornell University, United States -- New York, 277 pages.

Hazen, E. L., Palacios, D. M., Forney, K. A., Howell, E. A., Becker, E., Hoover, A. L., Irvine, L., et al. (**2017**). “WhaleWatch: a dynamic management tool for predicting blue whale density in the California Current,” Journal of Applied Ecology, **54**, 1415–1428. doi:10.1111/1365-2664.12820

Helble, T. A., Guazzo, R. A., Alongi, G. C., Martin, C. R., Martin, S. W., and Henderson, E. E. (**2020**). “Fin Whale Song Patterns Shift Over Time in the Central North Pacific,” Front. Mar. Sci., , doi: 10.3389/fmars.2020.587110. doi:10.3389/fmars.2020.587110

Herr, H., Viquerat, S., Devas, F., Lees, A., Wells, L., Gregory, B., Giffords, T., et al. (**2022**). “Return of large fin whale feeding aggregations to historical whaling grounds in the Southern Ocean,” Sci Rep, **12**, 9458. doi:10.1038/s41598-022-13798-7

Hilmo, R., and Wilcock, W. S. D. (**2020**). “Physical Sources of High-Frequency Seismic Noise on Cascadia Initiative Ocean Bottom Seismometers,” Geochemistry, Geophysics, Geosystems, **21**, e2020GC009085. doi:https://doi.org/10.1029/2020GC009085

Hilmo, R., and Wilcock, W. S. D. (**2024**). “Estimating distances to baleen whales using multipath arrivals recorded by individual seafloor seismometers at full ocean depth,” J Acoust Soc Am, **155**, 930–951. doi:10.1121/10.0024615

van Hinte, J. E., Wise, Jr., Sherwood W., Biart, B. N. M., Covington, J. M., Dunn, D. A., Haggerty, J. A., Johns, M. W., et al. (**1987**). "Site 603," (J. E. van Hinte, Jr. Wise Sherwood W., B. N. M. Biart, J. M. Covington, D. A. Dunn, J. A. Haggerty, M. W. Johns, et al., Eds.) Initial Reports of the Deep Sea Drilling Project, Initial reports of the Deep Sea Drilling Project covering Leg 93 of the cruises of the drilling vessel Glomar Challenger, Norfolk, Virginia, to Norfolk, Virginia, May-June, 1983, **93**, 25.

Holland, C. W., and Dosso, S. E. (**2021**). "On compressional wave attenuation in muddy marine sediments," The Journal of the Acoustical Society of America, **149**, 3674–3687. doi:10.1121/10.0005003

IRIS OBSIP (**2011**). "Cascadia Initiative Community Experiment - OBS Component," , doi: 10.7914/SN/7D_2011. doi:10.7914/SN/7D_2011

Irvine, L. M., Mate, B. R., Winsor, M. H., Palacios, D. M., Bograd, S. J., Costa, D. P., and Bailey, H. (**2014**). "Spatial and Temporal Occurrence of Blue Whales off the U.S. West Coast, with Implications for Management," PLOS ONE, **9**, e102959. doi:10.1371/journal.pone.0102959

Iwase, R. (**2015**). "Fin whale vocalizations observed with ocean bottom seismometers of cabled observatories off east Japan Pacific Ocean," Jpn. J. Appl. Phys., **54**, 07HG03. doi:10.7567/JJAP.54.07HG03

Jackson, A., Gerrodette, T., Chivers, S., Lynn, M., Olson, P., and Rankin, S. (**2004**). "Marine Mammal data collected during a survey in the Eastern Tropical Pacific Ocean aboard the NOAA ships McArthur II and David Starr Jordan, July 29 - December 10, 2003," NOAA Technical Memorandum NMFS,.

Jaeger, J. M., Gulick, S. S., LeVay, L. J., Asahi, H., Bahlburg, H., Belanger, C. L., Benedetti Berbel, G. B., et al. (**2014**). *Proceedings of the Integrated Ocean Drilling Program*, (J. M. Jaeger, S. S. Gulick, L. J. LeVay, A. L. Slagle, L. Drab, H. Asahi, H. Bahlburg, et al., Eds.) Proceedings of the Integrated Ocean Drilling Program; southern Alaska Margin; Expedition 341 of the riserless drilling platform; Victoria, British Columbia (Canada), to Valdez, Alaska (USA); Sites U1417-U1421, 29 May-29 July 2013, Integrated Ocean Drilling Program Management International for the Integrated Drilling Program (IODP), Washington, DC, United States, Vol. 341. Retrieved from http://hdl.handle.net/10.2204/iodp.proc.341.103.2014

Joiris, C., and Dochy, O. (**2013**). "A major autumn feeding ground for fin whales, southern fulmars and grey-headed albatrosses around the South Shetland Islands, Antarctica," Polar Biology, , doi: 10.1007/s00300-013-1383-8. doi:10.1007/s00300-013-1383-8

Kaschner, K., Quick, N. J., Jewell, R., Williams, R., and Harris, C. M. (**2012**). "Global Coverage of Cetacean Line-Transect Surveys: Status Quo, Data Gaps and Future Challenges," PLOS ONE, **7**, e44075. doi:10.1371/journal.pone.0044075

Kawaguchi, K., Kaneko, S., Nishida, T., and Komine, T. (**2015**). "Construction of the DONET real-time seafloor observatory for earthquakes and tsunami monitoring," In P. Favali, L. Beranzoli, and A. De Santis (Eds.), SEAFLOOR OBSERVATORIES: A New Vision of the Earth from the Abyss, Springer Praxis Books, Springer, Berlin, Heidelberg, pp. 211–228. doi:10.1007/978-3-642-11374-1_10

Kennett, B. (**2009**). *Seismic Wave Propagation in Stratified Media*, ANU Press. doi:10.26530/OAPEN_459524

King-Nolan, C. D., Rekdahl, M. L., Murray, A., Strindberg, S., Baumgartner, M. F., and Rosenbaum, H. C. (**2024**). "Fin whale song characteristics and potential subpopulation identity in the New York Bight," Sci Rep, **14**, 2931. doi:10.1038/s41598-024-52228-8

Kowarski, K. A., and Moors-Murphy, H. (**2021**). "A review of big data analysis methods for baleen whale passive acoustic monitoring," Marine Mammal Science, **37**, 652–673. doi:10.1111/mms.12758

Kuna, V. M., and Nábělek, J. L. (**2021**). "Seismic crustal imaging using fin whale songs," Science, **371**, 731–735. doi:10.1126/science.abf3962

Lewis, L. A., Calambokidis, J., Stimpert, A. K., Fahlbusch, J., Friedlaender, A. S., McKenna, M. F., Mesnick, S. L., et al. (**2018**). "Context-dependent variability in blue whale acoustic behaviour," Royal Society Open Science, **5**, 180241. doi:10.1098/rsos.180241

Lewis, L. A., and Širović, A. (**2018**). "Variability in blue whale acoustic behavior off southern California," Marine Mammal Science, **34**, 311–329. doi:10.1111/mms.12458

Lin, F., Kohler, M. D., Lynett, P., Ayca, A., and Weeraratne, D. S. (**2015**). "The 11 March 2011 Tohoku tsunami wavefront mapping across offshore Southern California," JGR Solid Earth, **120**, 3350–3362. doi:10.1002/2014JB011524

Lockyer, C., and Waters, T. (**1986**). "Weights and Anatomical Measurements of Northeastern Atlantic Fin (balaenoptera Physalus, Linnaeus) and Sei (b. Borealis, Lesson) Whales," Marine Mammal Science, **2**, 169–185. doi:10.1111/j.1748-7692.1986.tb00039.x

Lomac-MacNair, K., and Smultea, M. A. (**2016**). "Blue Whale (Balaenoptera musculus) Behavior and Group Dynamics as Observed from an Aircraft off Southern California," AB&C, **3**, 1–21. doi:10.12966/abc.02.01.2016

Lu, T., Han, B., and Yu, F. (**2021**). “Detection and classification of marine mammal sounds using AlexNet with transfer learning,” Ecological Informatics, **62**, 101277. doi:10.1016/j.ecoinf.2021.101277

Marques, T. (**2007**). *Incorporating measurement error and density gradients in Distance Sampling surveys* University of St. Andrews.

Marques, T. A., Thomas, L., Martin, S. W., Mellinger, D. K., Ward, J. A., Moretti, D. J., Harris, D., et al. (**2013**). “Estimating animal population density using passive acoustics,” Biol Rev Camb Philos Soc, **88**, 287–309. doi:10.1111/brv.12001

Marques, T., Munger, L., Thomas, L., Wiggins, S., and Hildebrand, J. (**2011**). “Estimating North Pacific right whale Eubalaena japonica density using passive acoustic cue counting,” Endang. Species. Res., **13**, 163–172. doi:10.3354/esr00325

Mate, B. R., Lagerquist, B. A., and Calambokidis, J. (**1999**). *Movements of North Pacific blue whales during the feeding season off southern California and southern fall migration | Cascadia Research*, Available: https://www.cascadiaresearch.org/publications/movements-north-pacific-blue-whales-during-feeding-season-southern-california-and, (date last viewed: 11-Feb-21). Retrieved February 11, 2021, from https://www.cascadiaresearch.org/publications/movements-north-pacific-blue-whales-during-feeding-season-southern-california-and

Matias, L., and Harris, D. (**2015**). “A single-station method for the detection, classification and location of fin whale calls using ocean-bottom seismic stations,” The Journal of the Acoustical Society of America, **138**, 504–520. doi:10.1121/1.4922706

McDonald, M. A., Calambokidis, J., Teranishi, A. M., and Hildebrand, J. A. (**2001**). "The acoustic calls of blue whales off California with gender data," J Acoust Soc Am, **109**, 1728–1735. doi:10.1121/1.1353593

McDonald, M. A., and Fox, C. G. (**1999a**). "Passive acoustic methods applied to fin whale population density estimation," The Journal of the Acoustical Society of America, **105**, 2643–2651. doi:10.1121/1.426880

McDonald, M. A., Hildebrand, J. A., and Webb, S. C. (**1995**). "Blue and fin whales observed on a seafloor array in the Northeast Pacific," The Journal of the Acoustical Society of America, **98**, 712–721. doi:10.1121/1.413565

Mcdonald, M. A., Mesnick, S. L., and Hildebrand, J. A. (**2006**). "Biogeographic characterisation of blue whale song worldwide: using song to identify populations.,"

Mcdonald, M., Hildebrand, J., and Mesnick, S. (**2009**). "Worldwide decline in tonal frequencies of blue whale songs," Endangered Species Research, **9**, 13–21. doi:10.3354/esr00217

Mcdonald, M., and Moore, S. (**2002**). "Calls recorded from North Pacific right whales (Eubalaena japonica) in the eastern Bering Sea," Journal of Cetacean Research and Management, , doi: DOI:10.47536/jcrm.v4i3.838. doi:DOI:10.47536/jcrm.v4i3.838

Mellinger, D. K., and Clark, C. W. (**1997**). "Methods for automatic detection of mysticete sounds," Marine and Freshwater Behaviour and Physiology, **29**, 163–181. doi:10.1080/10236249709379005

Mellinger, D. K., Stafford, K. M., Moore, S. E., Dziak, R. P., and Matsumoto, H. (**2007**). "An Overview of Fixed Passive Acoustic Observation Methods for Cetaceans," Oceanography, **20**, 36–45.

Miksis-Olds, J. L., Harris, D. V., and Heaney, K. D. (**2019a**). "Comparison of estimated 20-Hz pulse fin whale source levels from the tropical Pacific and Eastern North Atlantic Oceans to other recorded populations," The Journal of the Acoustical Society of America, **146**, 2373–2384. doi:10.1121/1.5126692

Miksis-Olds, J. L., Harris, D. V., and Mouw, C. (**2019b**). "Interpreting Fin Whale (Balaenoptera physalus) Call Behavior in the Context of Environmental Conditions," Aquat Mamm, **45**, 691–705. doi:10.1578/AM.45.6.2019.691

Miller, B. S., Madhusudhana, S., Aulich, M. G., and Kelly, N. (**2023**). "Deep learning algorithm outperforms experienced human observer at detection of blue whale D-calls: a double-observer analysis," Remote Sensing in Ecology and Conservation, **9**, 104–116. doi:10.1002/rse2.297

Mizroch, S., Rice, D. W., and Breiwick, J. M. (**1984**). "The fin whale, Balaenoptera physalus," Marine Fisheries Review, **46**, 20–24.

Mizroch, S., RICE, D., ZWIEFELHOFER, D., Waite, J., and Perryman, W. (**2009**). "Distribution and movements of fin whales in the North Pacific Ocean," Mammal Review, **39**, 193–227. doi:10.1111/j.1365-2907.2009.00147.x

Monnahan, C. C., Branch, T. A., and Punt, A. E. (**2015**). "Do ship strikes threaten the recovery of endangered eastern North Pacific blue whales?," Marine Mammal Science, **31**, 279–297. doi:https://doi.org/10.1111/mms.12157

Monnahan, C. C., Branch, T. A., Stafford, K. M., Ivashchenko, Y. V., and Oleson, E. M. (**2014**). "Estimating Historical Eastern North Pacific Blue Whale Catches Using Spatial Calling Patterns," PLOS ONE, **9**, e98974. doi:10.1371/journal.pone.0098974

Moore, S. E., Stafford, K. M., Mellinger, D. K., and Hildebrand, J. A. (**2006**). "Listening for Large Whales in the Offshore Waters of Alaska," BioScience, **56**, 49–55. doi:10.1641/0006-3568(2006)056[0049:LFLWIT]2.0.CO;2

Morano, J. L., Salisbury, D. P., Rice, A. N., Conklin, K. L., Falk, K. L., and Clark, C. W. (**2012**). "Seasonal and geographical patterns of fin whale song in the western North Atlantic Ocean," J Acoust Soc Am, **132**, 1207–1212. doi:10.1121/1.4730890

Nabelek, J., and Braunmiller, J. (**2012**). "Plate Boundary Evolution and Physics at an Oceanic Transform Fault System.," doi:10.7914/SN/X9_2012

Nieukirk, S. L., Stafford, K. M., Mellinger, D. K., Dziak, R. P., and Fox, C. G. (**2004**). "Low-frequency whale and seismic airgun sounds recorded in the mid-Atlantic Ocean," J Acoust Soc Am, **115**, 1832–1843. doi:10.1121/1.1675816

Nosal, E.-M. (**2013**). "Methods for tracking multiple marine mammals with wide-baseline passive acoustic arrays," J Acoust Soc Am, **134**, 2383–2392. doi:10.1121/1.4816549

Oakley, A. J., Taylor, B., and Moore, G. F. (**2008**). "Pacific Plate subduction beneath the central Mariana and Izu-Bonin fore arcs: New insights from an old margin," Geochemistry, Geophysics, Geosystems, , doi: 10.1029/2007GC001820. doi:10.1029/2007GC001820

Oestreich, W. K., Abrahms, B., McKenna, M. F., Goldbogen, J. A., Crowder, L. B., and Ryan, J. P. (**2022**). "Acoustic signature reveals blue whales tune life-history transitions to oceanographic conditions," Functional Ecology, **36**, 882–895. doi:10.1111/1365-2435.14013

Oestreich, W. K., Fahlbusch, J. A., Cade, D. E., Calambokidis, J., Margolina, T., Joseph, J., Friedlaender, A. S., et al. (**2020**). "Animal-Borne Metrics Enable Acoustic Detection of

Blue Whale Migration," Current Biology, **30**, 4773-4779.e3. doi:10.1016/j.cub.2020.08.105

Oleson, E., Calambokidis, J., Burgess, W., Mcdonald, M., LeDuc, C., and Hildebrand, J. (**2007**). "Behavioral context of Northeast Pacific blue whale call production," Marine Ecology-progress Series - MAR ECOL-PROGR SER, **330**, 269–284. doi:10.3354/meps330269

Oleson, E. M., Širović, A., Bayless, A. R., and Hildebrand, J. A. (**2014**). "Synchronous Seasonal Change in Fin Whale Song in the North Pacific," PLoS One, **9**, e115678. doi:10.1371/journal.pone.0115678

Oleson, E. M., Wiggins, S. M., and Hildebrand, J. A. (**2007b**). "Temporal separation of blue whale call types on a southern California feeding ground," Animal Behaviour, **74**, 881–894. doi:10.1016/j.anbehav.2007.01.022

Palacios, D. M., Bailey, H., Becker, E. A., Bograd, S. J., DeAngelis, M. L., Forney, K. A., Hazen, E. L., et al. (**2019**). "Ecological correlates of blue whale movement behavior and its predictability in the California Current Ecosystem during the summer-fall feeding season," Movement Ecology, **7**, 26. doi:10.1186/s40462-019-0164-6

Pearson, E. J., Oestreich, W. K., Ryan, J. P., Haver, S. M., Gedamke, J., Dziak, R. P., and Wall, C. C. (**2023**). "Widespread passive acoustic monitoring reveals spatio-temporal patterns of blue and fin whale song vocalizations in the Northeast Pacific Ocean," Frontiers in Remote Sensing, , doi: doi.org/10.3389/frsen.2023.994518. doi:doi.org/10.3389/frsen.2023.994518

Pereira, A., Harris, D., Tyack, P., and Matias, L. (**2020**). "On the use of the Lloyd's Mirror effect to infer the depth of vocalizing fin whales," The Journal of the Acoustical Society of America, **148**, 3086–3101. doi:10.1121/10.0002426

Pérez-Jorge, S., Tobeña, M., Prieto, R., Vandeperre, F., Calmettes, B., Lehodey, P., and Silva, M. A. (**2020**). "Environmental drivers of large-scale movements of baleen whales in the mid-North Atlantic Ocean," Diversity and Distributions, **26**, 683–698. doi:10.1111/ddi.13038

Pierce, A. D., Carey, W. M., and Zampolli, M. (**2005**). "Low-frequency attenuation of sound in marine sediments," Europe Oceans 2005, 1270-1275 Vol. 2. Presented at the Europe Oceans 2005. doi:10.1109/OCEANSE.2005.1513242

Porter, M. B., and Bucker, H. P. (**1987**). "Gaussian beam tracing for computing ocean acoustic fields," The Journal of the Acoustical Society of America, **82**, 1349–1359. doi:10.1121/1.395269

Rankin, S., Barlow, J., Archer, F., and Jones, B. (**2011**). "Acoustics as a tool in sub-species and population identification for endangered fin whales, Balaenoptera physalus," The Journal of the Acoustical Society of America, **130**, 2421. doi:10.1121/1.3654699

Rankin, S., Castellote, M., Delarue, J., Stafford, K., Archer, F., Koot, B., Richlen, M., et al. (**2018**). "Methods for characterizing fin whale song notes for comparative studies of geographic variation in song.," , doi: 10.7289/V5/TM-SWFSC-592. doi:10.7289/V5/TM-SWFSC-592

Rankin, S., Norris, T. F., Smultea, M. A., Oedekoven, C., Zoidis, A. M., Silva, E., and Rivers, J. (**2007**). "A Visual Sighting and Acoustic Detections of Minke Whales, Balaenoptera acutorostrata (Cetacea: Balaenopteridae), in Nearshore Hawaiian Waters," pasc, **61**, 395–398. doi:10.2984/1534-6188(2007)61[395:AVSAAD]2.0.CO;2

Rice, A., Širović, A., Hildebrand, J. A., Wood, M., Carbaugh-Rutland, A., and Baumann-Pickering, S. (**2022a**). "Update on frequency decline of Northeast Pacific blue whale

(Balaenoptera musculus) calls," PLOS ONE, **17**, e0266469. doi:10.1371/journal.pone.0266469

Rice, A., Širović, A., Trickey, J. S., Debich, A. J., Gottlieb, R. S., Wiggins, S. M., Hildebrand, J. A., et al. (**2021**). "Cetacean occurrence in the Gulf of Alaska from long-term passive acoustic monitoring," Mar Biol, **168**, 72. doi:10.1007/s00227-021-03884-1

Risch, D., Castellote, M., Clark, C. W., Davis, G. E., Dugan, P. J., Hodge, L. E., Kumar, A., et al. (**2014**). "Seasonal migrations of North Atlantic minke whales: novel insights from large-scale passive acoustic monitoring networks," Movement Ecology, **2**, 24. doi:10.1186/s40462-014-0024-3

Roberts, J. J., Best, B. D., Mannocci, L., Fujioka, E., Halpin, P. N., Palka, D. L., Garrison, L. P., et al. (**2016**). "Habitat-based cetacean density models for the U.S. Atlantic and Gulf of Mexico," Sci Rep, **6**, 1–12. doi:10.1038/srep22615

Rocha, J., Clapham, P., and Ivashchenko, Y. (**2015**). "Emptying the Oceans: A Summary of Industrial Whaling Catches in the 20th Century," Marine Fisheries Review, **76**, 37–48. doi:10.7755/MFR.76.4.3

Romagosa, M., Nieukirk, S., Cascão, I., Marques, T. A., Dziak, R., Royer, J.-Y., O'Brien, J., et al. (**2024**). "Fin whale song evolution in the North Atlantic," (L. Rendell, C. Rutz, and C. W. Clark, Eds.) eLife, **13**, e83750. doi:10.7554/eLife.83750

Ryan, T. P. (**2007**). "Confidence Intervals and Hypothesis Tests—Two Samples," Modern Engineering Statistics, John Wiley & Sons, Ltd, pp. 189–213. doi:10.1002/9780470128442.ch6

Samaran, F., Adam, O., and Guinet, C. (**2010**). "Detection range modeling of blue whale calls in Southwestern Indian Ocean," Applied Acoustics, Proceedings of the 4th International

Workshop on Detection, Classification and Localization of Marine Mammals Using Passive Acoustics and 1st International Workshop on Density Estimation of Marine Mammals Using Passive Acoustics, **71**, 1099–1106. doi:10.1016/j.apacoust.2010.05.014

Shabangu, F. W., Findlay, K. P., Yemane, D., Stafford, K. M., van den Berg, M., Blows, B., and Andrew, R. K. (**2019**). "Seasonal occurrence and diel calling behaviour of Antarctic blue whales and fin whales in relation to environmental conditions off the west coast of South Africa," Journal of Marine Systems, **190**, 25–39. doi:10.1016/j.jmarsys.2018.11.002

Shillington, D. J., Bécel, A., Nedimović, M. R., Kuehn, H., Webb, S. C., Abers, G. A., Keranen, K. M., et al. (**2015**). "Link between plate fabric, hydration and subduction zone seismicity in Alaska," Nature Geosci, **8**, 961–964. doi:10.1038/ngeo2586

Širović, A., Hildebrand, J. A., and Wiggins, S. M. (**2007**). "Blue and fin whale call source levels and propagation range in the Southern Ocean," The Journal of the Acoustical Society of America, **122**, te1208-1215. doi:10.1121/1.2749452

Širovic, A., Rice, A., Chou, E., Hildebrand, J., Wiggins, S., and Roch, M. (**2015**). "Seven years of blue and fin whale call abundance in the Southern California Bight," Endang. Species. Res., **28**, 61–76. doi:10.3354/esr00676

Sirovic, A., Williams, L. N., Kerosky, S. M., Wiggins, S. M., and Hildebrand, J. A. (**2013**). "Temporal separation of two fin whale call types across the eastern North Pacific," Mar. Biol., **160**, 47–57. doi:10.1007/s00227-012-2061-z

Smith, L., Barth, J., Kelley, D., Plueddemann, A., Rodero, I., Ulses, G., Vardaro, M., et al. (**2018**). "The Ocean Observatories Initiative," Oceanog, **31**, 16–35. doi:10.5670/oceanog.2018.105

Soule, D. C., and Wilcock, W. S. D. (**2013**). "Fin whale tracks recorded by a seismic network on the Juan de Fuca Ridge, Northeast Pacific Ocean," The Journal of the Acoustical Society of America, **133**, 1751–1761. doi:10.1121/1.4774275

Stafford, K., Citta, J., Moore, S., Daher, M., and George, J. (**2009**). "Environmental correlates of blue and fin whale call detections in the North Pacific Ocean from 1997 to 2002," Marine Ecology-progress Series - MAR ECOL-PROGR SER, **395**, 37–53. doi:10.3354/meps08362

Stafford, K., Fox, C., and Clark, D. (**1999a**). "Long-range acoustic detection and localization of blue whale calls in the Northeast Pacific Ocean," The Journal of the Acoustical Society of America, **104**, 3616–25. doi:10.1121/1.423944

Stafford, K. M., Fox, C. G., and Clark, D. S. (**1998**). "Long-range acoustic detection and localization of blue whale calls in the northeast Pacific Ocean," J Acoust Soc Am, **104**, 3616–3625. doi:10.1121/1.423944

Stafford, K. M., Moore, S. E., and Fox, C. G. (**2005**). "Diel variation in blue whale calls recorded in the eastern tropical Pacific," Animal Behaviour, **69**, 951–958. doi:10.1016/j.anbehav.2004.06.025

Stafford, K. M., Nieukirk, S. L., and Cox, C. G. (**2001**). "Geographic and seasonal variation of blue whale calls in the North Pacific," J. Cetacean Res. Manage., **3**, 65–76. doi:10.47536/jcrm.v3i1.902

Stafford, K. M., Nieukirk, S. L., and Fox, C. G. (**1999b**). "An acoustic link between blue whales in the eastern tropical Pacific and the northeast Pacific," Mar. Mamm. Sci., **15**, 1258–1268. doi:10.1111/j.1748-7692.1999.tb00889.x

Stimpert, A. K., DeRuiter, S. L., Falcone, E. A., Joseph, J., Douglas, A. B., Moretti, D. J., Friedlaender, A. S., et al. (**2015**). "Sound production and associated behavior of tagged fin whales (Balaenoptera physalus) in the Southern California Bight," Animal Biotelemetry, **3**, 23. doi:10.1186/s40317-015-0058-3

Szesciorka, A. R., Ballance, L. T., Širović, A., Rice, A., Ohman, M. D., Hildebrand, J. A., and Franks, P. J. S. (**2020**). "Timing is everything: Drivers of interannual variability in blue whale migration," Scientific Reports, **10**, 7710. doi:10.1038/s41598-020-64855-y

Szesciorka, A. R., Calambokidis, J., and Harvey, J. T. (**2016**). "Testing tag attachments to increase the attachment duration of archival tags on baleen whales," Animal Biotelemetry, **4**, 18. doi:10.1186/s40317-016-0110-y

Thode, A. M., D'Spain, G. L., and Kuperman, W. A. (**2000**). "Matched-field processing, geoacoustic inversion, and source signature recovery of blue whale vocalizations," The Journal of the Acoustical Society of America, **107**, 1286–1300. doi:10.1121/1.428417

Thomas, L., Buckland, S. T., Rexstad, E. A., Laake, J. L., Strindberg, S., Hedley, S. L., Bishop, J. R., et al. (**2010**). "Distance software: design and analysis of distance sampling surveys for estimating population size," J Appl Ecol, **47**, 5–14. doi:10.1111/j.1365-2664.2009.01737.x

Thomas, L., and Marques, T. (**2012**). "Passive Acoustic Monitoring for Estimating Animal Density," Acoustics Today, **8**, 35. doi:10.1121/1.4753915

Thomas, P. O., Reeves, R. R., and Brownell, R. L. (**2016**). "Status of the world's baleen whales," Marine Mammal Science, **32**, 682–734. doi:https://doi.org/10.1111/mms.12281

Tiemann, C. O., Thode, A. M., Straley, J., O'Connell, V., and Folkert, K. (**2006**). "Three-dimensional localization of sperm whales using a single hydrophone," The Journal of the Acoustical Society of America, **120**, 2355–2365. doi:10.1121/1.2335577

Varga, L., Wiggins, S., and Hildebrand, J. (**2018**). "Behavior of singing fin whales Balaenoptera physalus tracked acoustically offshore of Southern California," Endang. Species. Res., **35**, 113–124. doi:10.3354/esr00881

Virgili, A., Authier, M., Boisseau, O., Cañadas, A., Claridge, D., Cole, T., Corkeron, P., et al. (**2019**). "Combining multiple visual surveys to model the habitat of deep-diving cetaceans at the basin scale," Global Ecology and Biogeography, **28**, 300–314. doi:https://doi.org/10.1111/geb.12850

Wang, Z., Duan, P., Chen, M., Mei, Z., Sun, X., Nong, Z., Liu, M., et al. (**2022**). "Vocalization of Bryde's whales (*Balaenoptera edeni*) in the Beibu Gulf, China," Marine Mammal Science, doi: 10.1111/mms.12917. doi:10.1111/mms.12917

Wang, Z., and Wang, R. (**2015**). "Pore pressure prediction using geophysical methods in carbonate reservoirs: Current status, challenges and way ahead," Journal of Natural Gas Science and Engineering, **27**, 986–993. doi:10.1016/j.jngse.2015.09.032

Warner, G. A., Dosso, S. E., and Hannay, D. E. (**2017**). "Bowhead whale localization using time-difference-of-arrival data from asynchronous recorders," The Journal of the Acoustical Society of America, **141**, 1921–1935. doi:10.1121/1.4978438

Watkins, W. A. (**1981**). "ACTIVITIES AND UNDERWATER SOUNDS OF FIN WHALES.,"

Watkins, W. A., Tyack, P., Moore, K. E., and Bird, J. E. (**1987**). "The 20-Hz signals of finback whales (Balaenoptera physalus)," The Journal of the Acoustical Society of America, **82**, 1901–1912. doi:10.1121/1.395685

Weirathmueller, M. J., Stafford, K. M., Wilcock, W. S., Hilmo, R. S., Dziak, R. P., and Tréhu, A. M. (**2017a**). "Spatial and temporal trends in fin whale vocalizations recorded in the NE Pacific Ocean between 2003-2013," PloS one, **12**, e0186127.

Weirathmueller, M. J., Wilcock, W. S. D., and Hilmo, R. S. (**2017b**). "Estimating range to a vocalizing fin whale using the timing and amplitude of multipath arrivals," The Journal of the Acoustical Society of America, **142**, 2101–2120. doi:10.1121/1.5005494

Wiggins, S., Mcdonald, M., Munger, L., Moore, S., and Hildebrand, J. (**2004**). "Waveguide propagation allows range estimates for North Pacific right whales in the Bering Sea," Canadian Acoustics / Acoustique canadienne,.

Wiggins, S., Oleson, E., Mcdonald, M., and Hildebrand, J. (**2005**). "Blue Whale (Balaenoptera musculus) Diel Call Patterns Offshore of Southern California," Aquatic Mammals, **31**, 161–168. doi:10.1578/AM.31.2.2005.161

Wilcock, W. S. D. (**2012**). "Tracking fin whales in the northeast Pacific Ocean with a seafloor seismic network," J Acoust Soc Am, **132**, 2408–2419. doi:10.1121/1.4747017

Wilcock, W. S. D., and Hilmo, R. S. (**2021**). "A method for tracking blue whales (Balaenoptera musculus) with a widely spaced network of ocean bottom seismometers," PLOS ONE, **16**, e0260273. doi:10.1371/journal.pone.0260273

Appendix 1: Supplementary Materials for Chapter 2

OBS and Borehole Site Descriptions

We constrained local sediment properties using seismic velocity and density profiles from the nearest scientific drilling boreholes at Marianas, Alaska, and US East Coast (Table S2.I), and overhead multi-channel seismic (MCS) data at Alaska (Shillington et al., 2015) and US East Coast (Bécel et al., 2020) (Table S2.1). Cross-trench MCS profiles were available >30 km south of the Marianas site and unavailable at the Puerto Rico site. Boreholes near the Puerto Rico site are on the subducting North American plate and thus are not representative of the overriding plate.

The five sites have distinct characteristics. Marianas is the deepest, at 5949 m depth and lies ~80 km east of the Marianas Trench (Table 2.1, Fig. 2.1, Fig. 2.4(a)). The site is thickly sedimented but highly reflective due to a regional shallow lithified cherty claystone/porcellanite layer (Harding et al., 1990). At a borehole that is 50 km to the south-southeast of our site the reflector depth varies between 30 to 75 meters beneath the seafloor (mbsf) over ~2 km. The velocities of samples collected in ODP borehole 777B increased from 1.5 km/s to 2.9 km/s across the reflector. This chert layer is identified in several cross-trench MCS profiles 30-400 km south of our site (Oakley et al., 2008). MCS profiles show that layer depth varies unevenly both along-trench and across-trench from 30-500 m depth due a trenchward increase in sediment thickness, the undulation of the chert layer, and normal faulting due to subducting plate flexure. Because the OBS site is ~20 km trenchward of the borehole, we infer that the reflector is likely deeper than measured near the borehole. The seafloor around the OBS is also slightly sloped, shallowing by ~10 m km^{-1} from west to east, with a few sharp bathymetrical offsets that may be attributed to normal faulting due to subducting plate flexure (Oakley et al., 2008).

The Hawaii site has a basalt seafloor and is at 4410 m depth, ~10 km southeast of the Loihi Seamount off Big Island of Hawaii (Table 2.1, Fig. 2.1, Fig. 2.4(b)). The basalt is reflective, with an estimated seafloor V_P of ~3.6 km/s (Hamilton, 1978). The bathymetry is complex due to the seamount (Fig. 2.2b). Immediately around the site and to the east, the bathymetry unevenly deepens to the southeast by ~50 m km^{-1} but to the west it is complicated by the steep slopes associated with a shallow ridge that extends from Loihi Seamount.

The Puerto Rico OBS site is located at 5426 m depth, ~150 km northeast of the island on the landward side of the Puerto Rico Trench (Table 2.1, Fig. 2.1, Fig. 2.4(c)). The seafloor is rough on the kilometer scale due to trench tectonics and shallows on average from north to south by ~60 m km^{-1} moving up the continental rise. Near our site, the seafloor is composed of Late Oligocene carbonate layers (ten Brink, 2005). Carbonate P-wave velocities and densities vary depending on porosity and fracturing but typically have a high enough impedance contrast at the seafloor to provide clear seafloor reflections (Wang and Wang, 2015).

The Alaska site is located at 4626 m depth, ~400 km south of Kodiak Island in the Gulf of Alaska (Table 2.1, Fig. 2.1, Fig. 2.4(d)). The seafloor is relatively flat with depths varying by <100 m within a 20 km radius of the instrument. At a distant borehole (>750 km away), sediment P-wave velocities gradually increase with depth with no major reflectors besides the basaltic basement ~780 m below the seafloor. An MCS profile over the sites shows a thinner sediment layer with a two-way travel time of ~0.35s (Shillington et al., 2015), equivalent to ~300 m of sediment.

The US East Coast site is located at 5154 m depth, ~400 km east of North Carolina (Table 2.1, Fig. 2.1, Fig. 2.4(e)). The bathymetry is flat, shallowing by ~100 m over 20 km to the northwest. MCS and borehole data show that the sediments are ~2400 m thick and strongly

layered (Table S2.1) (Bécel et al., 2020). The seafloor sediment is weakly reflective, and there are three strong regional reflectors within the sediments (Bécel et al., 2020; van Hinte et al., 1987). We modeled subsurface arrivals at this site with a full-waveform seismic reflectivity algorithm (Kennett, 2009). The seismic model was based on P-wave velocity and density profiles from a nearby borehole (van Hinte et al., 1987) that were adjusted to match the layer travel times observed in the MCS reflection profile at the site (Bécel et al., 2020). We obtained S-wave velocities (V_S) from P-wave velocity values using an empirical relationship for sediments (Hamilton, 1976) and constant P- and S-wave attenuation quality factors appropriate for clay/silt mixtures, Q_p=450 and Q_s=136 (Bowles, 1997). We assumed a call depth of 50 m (Watkins et al., 1987) and used a synthetic fin whale call approximated as a 1-s-long chirp downswept from 26-16 Hz weighted by a Gaussian function with a standard deviation of 0.17 s. We developed our relative arrival time model by measuring the timing difference between the direct and highest amplitude predicted MP1 subsurface arrivals (Fig. S2.3).

1
2 **Supplementary Table**

TABLE S2.1. Summary of sediment characteristics at drilling sites near three of the OBS sites.

Site	Program	Site	Latitude	Longitude	Distance from OBS	Depth	Sediment Thickness	Depth of Major Reflector	Average Velocity	Average Velocity Above Reflector	Velocity at Seafloor	Citation
Marianas	ODP	777	17.7033	148.6967	48 km	5860 m	~300 m	~50 m	2200 m/s	1550 m/s	1430 m/s	Harding et al., (1990) p. 111-135
Gulf of Alaska	IODP	U1417	56.9600	-147.1100	761 km	4188 m	~780 m	None	1730 m/s	1730 m/s	1500 m/s	Jaeger et al., (2014) p. 99
US East Coast	DSDP	603	35.4943	-70.0283	403 km	4643 m	~1600 m	~366 m	2000 m/s	1600 m/s	1550 m/s	van Hinte et al., (1987) p. 603

Supplementary Figures

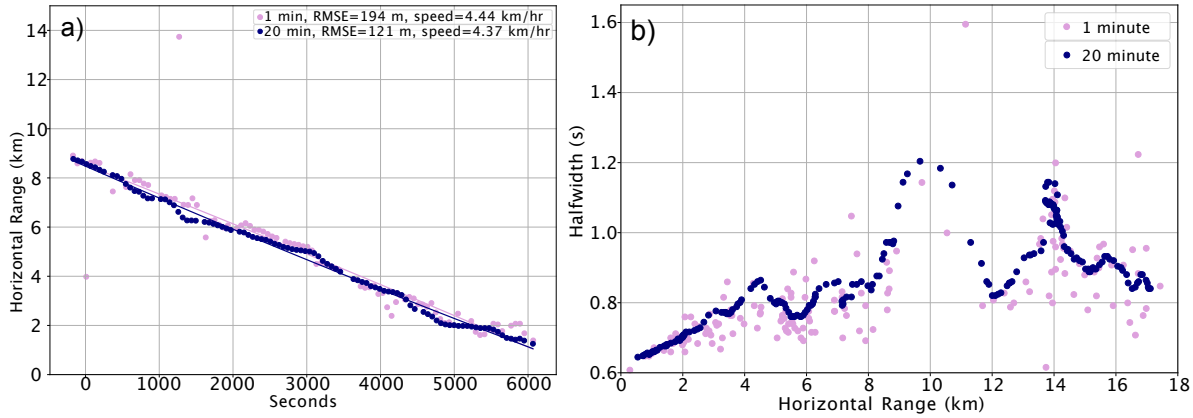

FIG. S2.1. (a) Ranges at Marianas site from 0330-0515 on January 18, 2012, when a fin whale was approaching the OBS site at a near constant rate in Figure 2.4b. Whale swim speed and location root-mean-squared error (RMSE) from a linear path are calculated for autocorrelation ranges for windows of 1 minute (pink) and 20 minutes (blue). (b) Comparison of autocorrelated multipath detection score peak widths calculated at 50% prominence when the fin whale was approaching from 0115-0530.

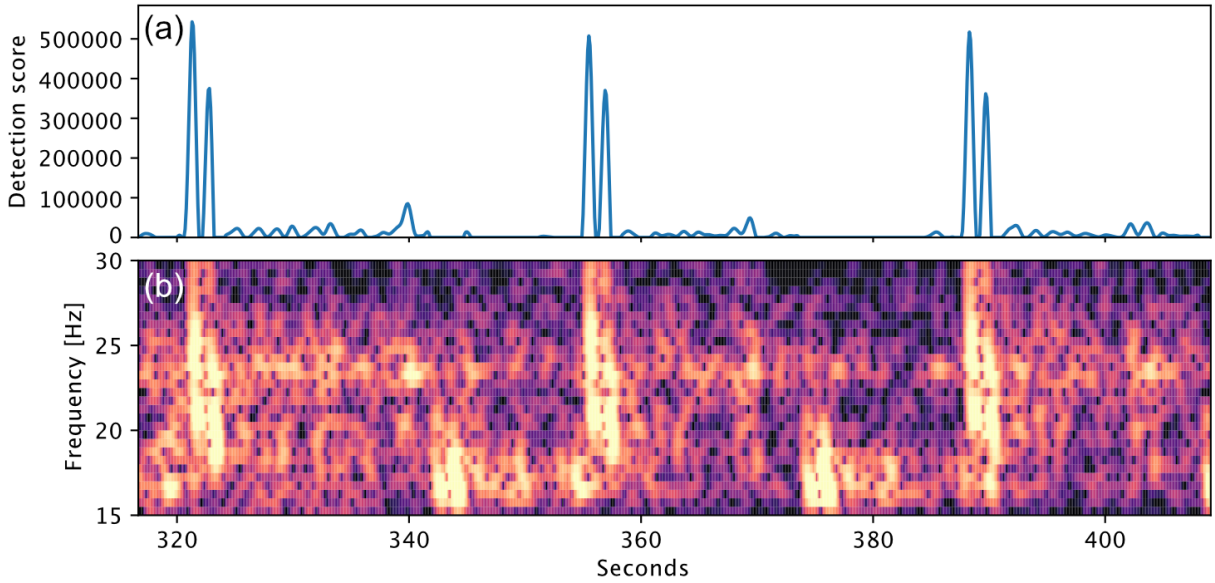

FIG. S2.2. (a) Detection score and (b) spectrogram for the Alaska site at 0945 on February 9, 2019, showing an example of doubled call arrivals separated by ~1 s where the first arrival is stronger than the second.

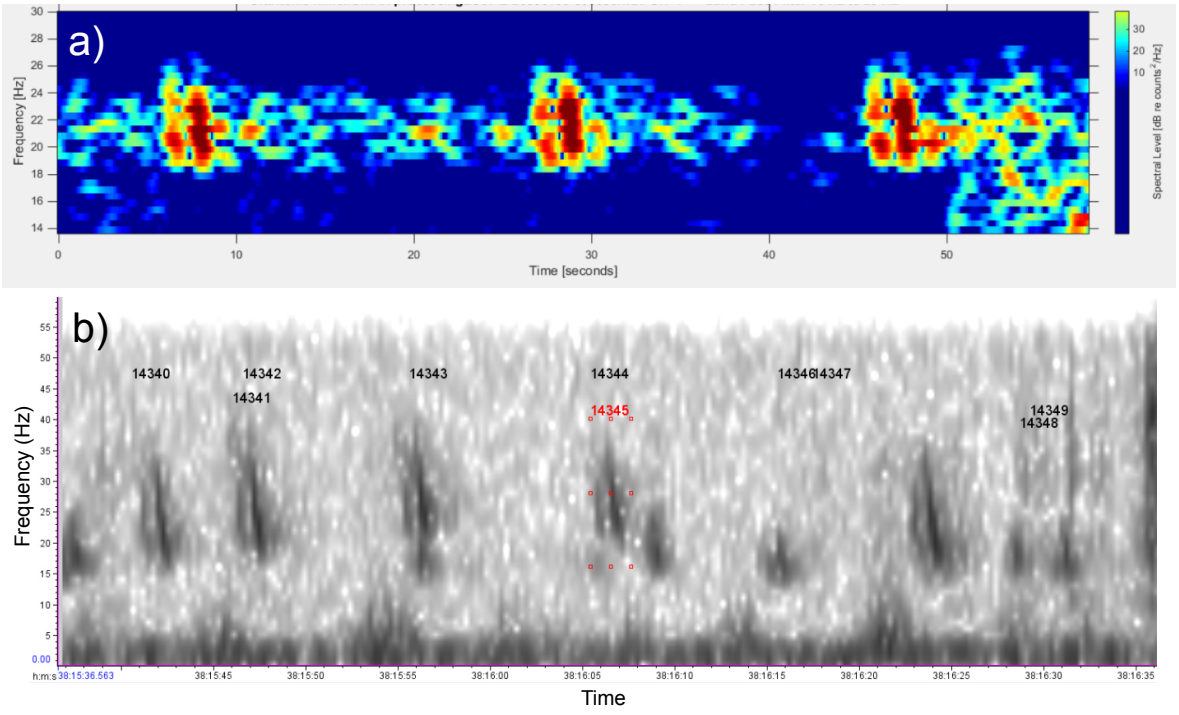

FIG. S2.3. Examples of ~1 s doubling fin whale calls observed (a) on MoMAR (monitoring the Mid-Atlantic Ridge) project OBS LSo7 on January 9, 2008, at 0115 (courtesy of Andreia Pereira) and (b) on hydrophone KZ1 on September 27, 2015, at 2050 in the Bering Strait near Alaska (courtesy of by Daniel Woodrich).

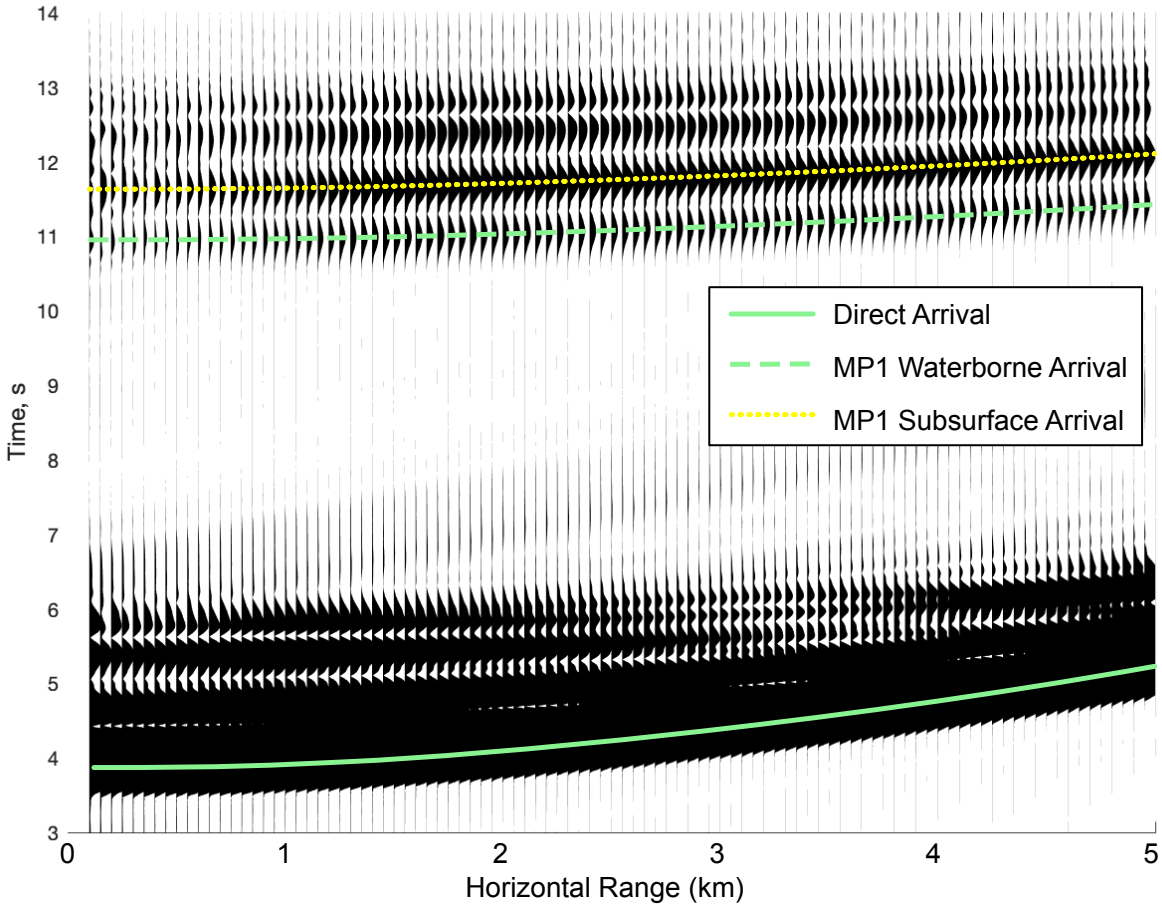

FIG. S2.4. Envelopes of direct and MP1 arrival at 0 to 5 km range modeled at the US East Coast site using a full waveform seismic reflectivity algorithm (Kennett, 2009). Smoothed picked waterborne arrival peaks for the direct and MP1 arrivals (green) and the highest amplitude modeled MP1 subsurface arrivals (yellow).

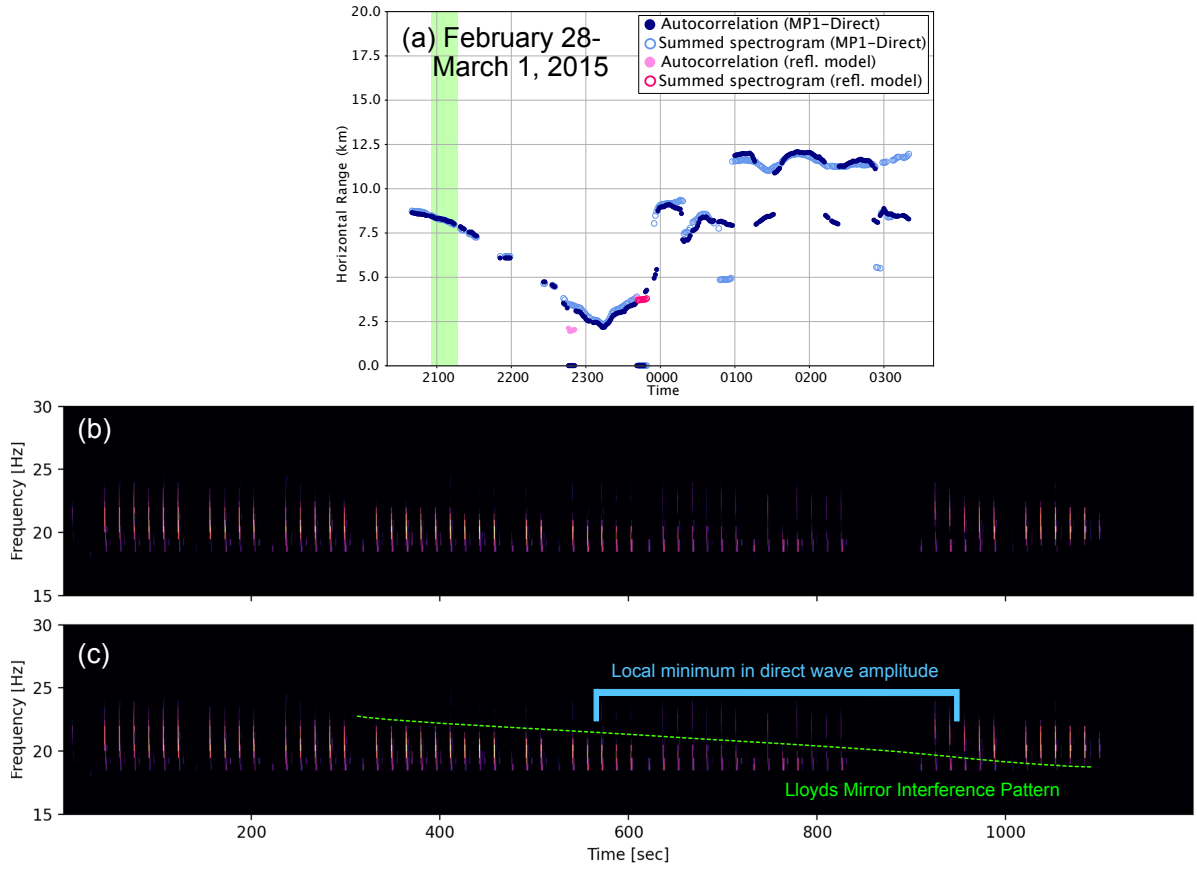

FIG. S2.5. (a) US East Coast track showing 20-minute window from 2055-2115 (green box) where a Lloyd's mirror interference effect is observed in calls as a fin whale approaches the OBS. (b) Spectrogram and (c) annotated spectrogram showing that the frequency of interference decreases as the whale approaches (green line), which is consistent with previous Lloyd's mirror observations (Pereira et al., 2020). The Lloyd's mirror interference coincides with a local minimum in direct wave amplitudes (cyan bracket) that impacts ranging later in the track from 0000-0315 on March 1, 2015 when the fin whale stays at a near constant range.

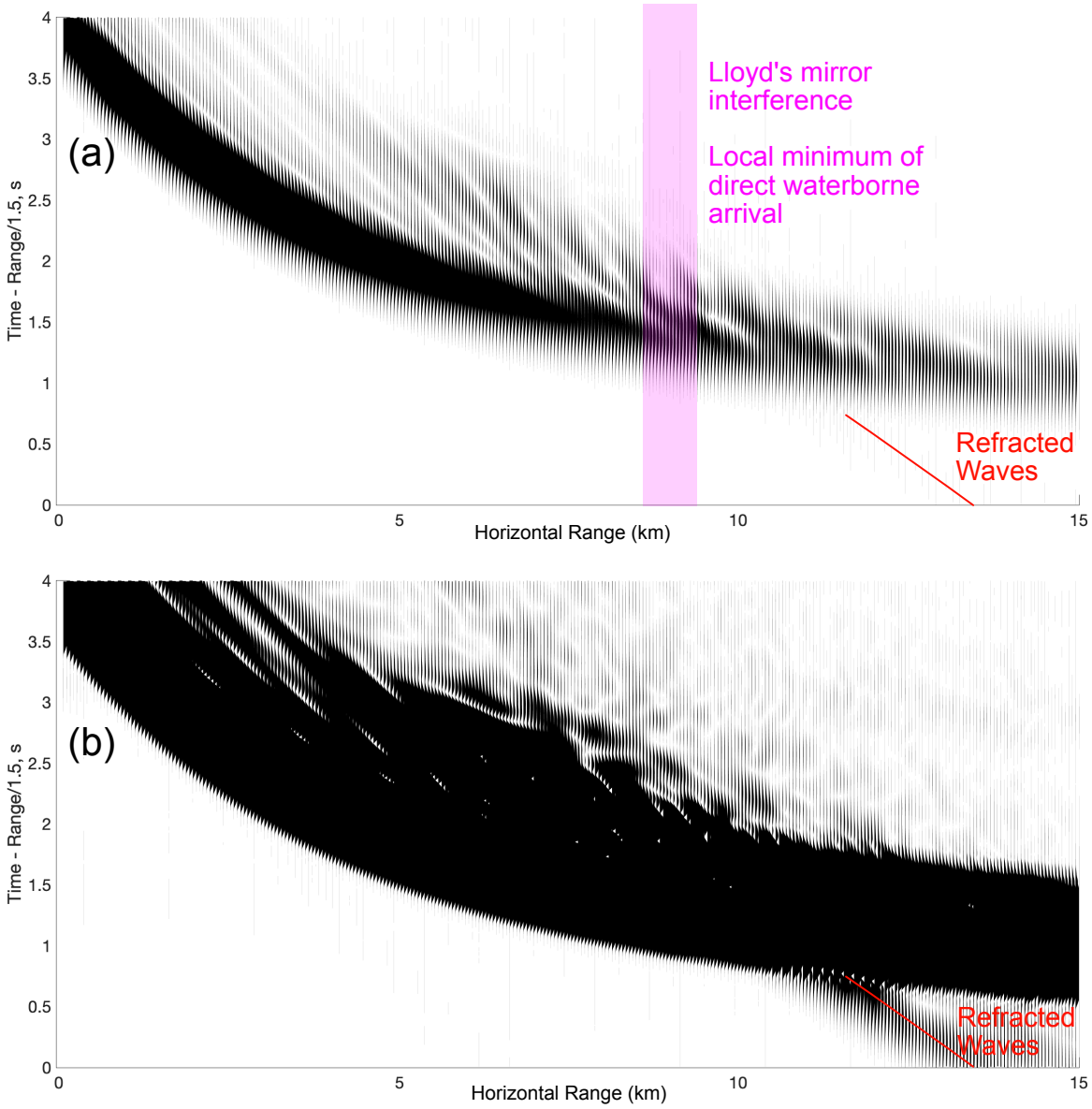

FIG. S2.6. Reflectivity model envelopes with a reduction velocity of 1.5 km/s showing direct arrival patterns with amplitudes scaled to highlight (a) waterborne and subsurface arrival amplitudes and show that a local minimum in waterborne amplitudes at ranges from 8.5 km coincides with our observations of the Lloyd's mirror effect and spurious ranges from 0000-0315 on March 1, 2015, and (b) the emergence of low amplitude refracted waves (red).

Appendix 2: Supplemental Materials for Chapter 3

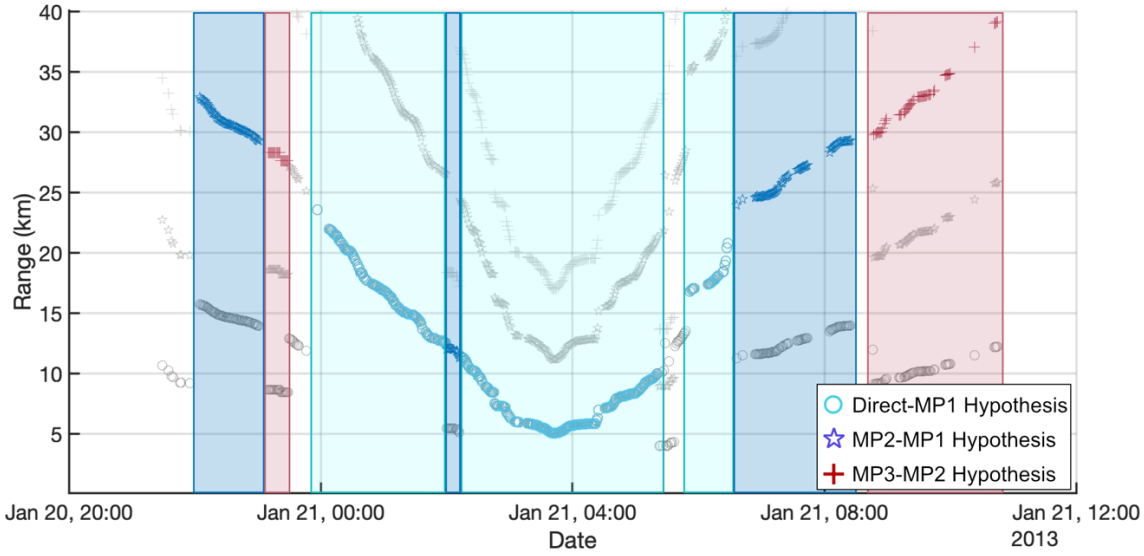

FIG. S3.1: Scatter plot showing results of the automated hypothesis selection algorithm for a single whale track recorded on OBS B19. Grey markers show ranges calculated using each hypothesis (Fig. 3.2(b)). Boxes show same-hypothesis ranges linked into groups due to their closeness in space and time. Colors show the algorithm-selected hypothesis for each group that produced the smoothest overall track. Small (<12 ranges), unassigned groups (not in boxes) are shown at the start of the track, just before 0000, and at ~0530 on January 21. These were later manually assigned (see Fig. 3.4).

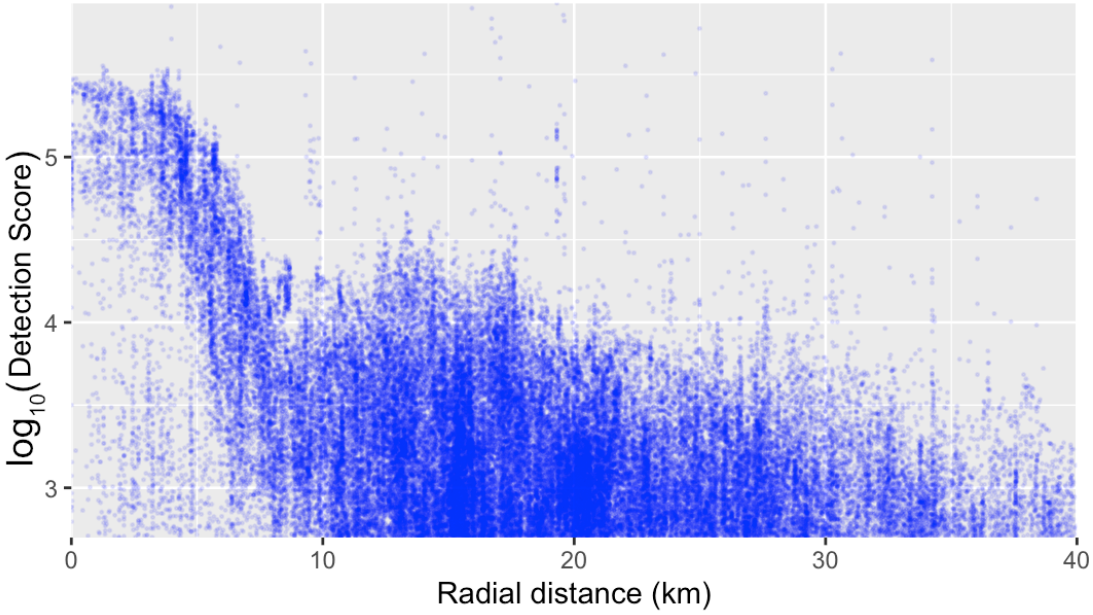

FIG. S3.2: Scatter plot of estimated fin whale call ranges versus their detection score. Note the detection score minimum between 8-12 km that corresponds to a decrease in ranging success (Fig. 3.4, Fig. 3.6).

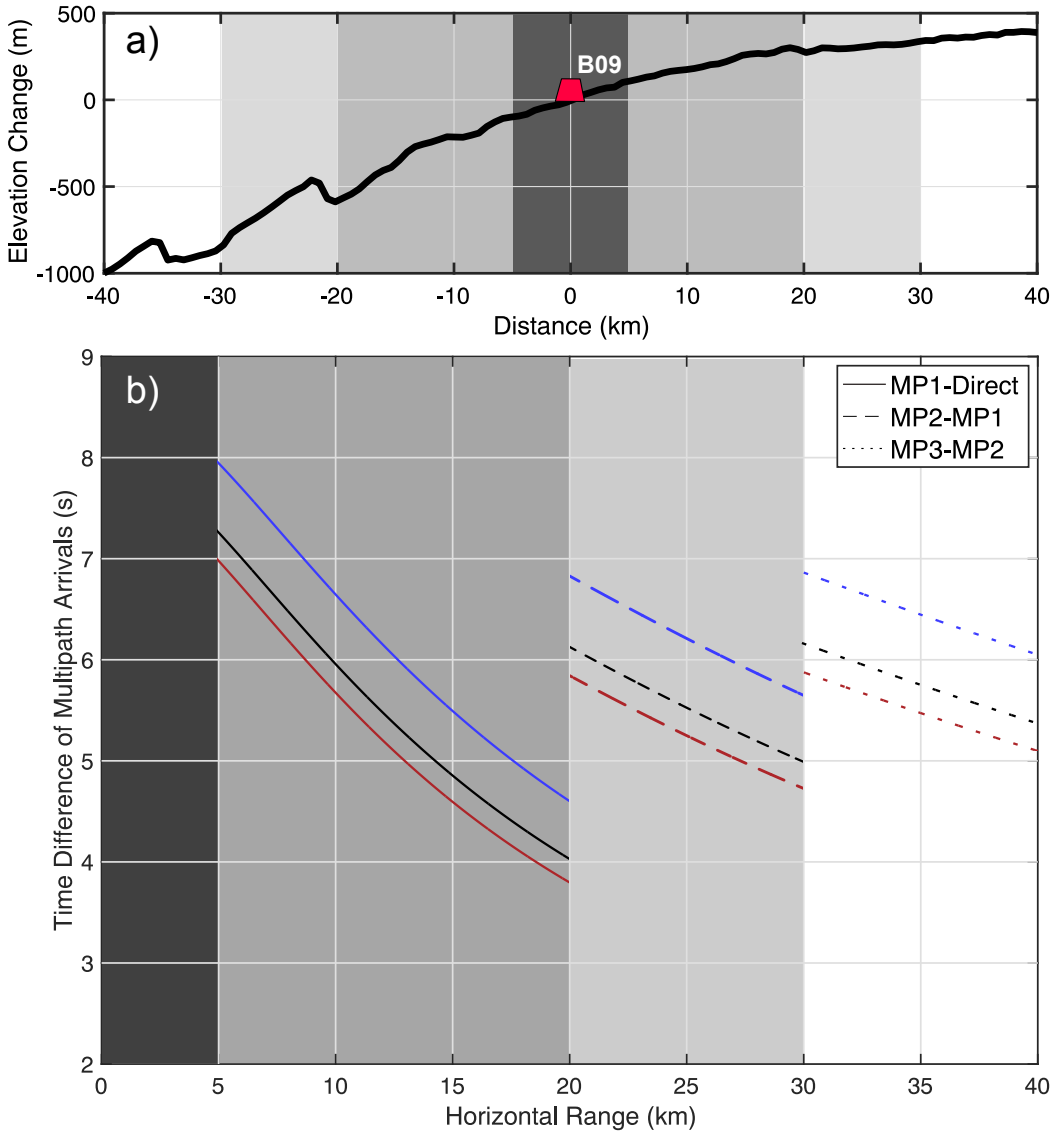

FIG. S3.3: (a) Bathymetrical transect extending 40km east and 40km west of OBS site B09 showing changes in depth due to subducting plate flexure. (b) Time difference of arrival multipath curves calculated assuming a flat seafloor at the site depth (black), 200 m shallower (red), and 500 m deeper (blue). The dominant multipath arrival hypotheses used to calculate ranges are shown for each range bin, MP1-Direct for 5-20 km, MP2-MP1 for 20-30 km, and MP3-MP2 30-40 km.

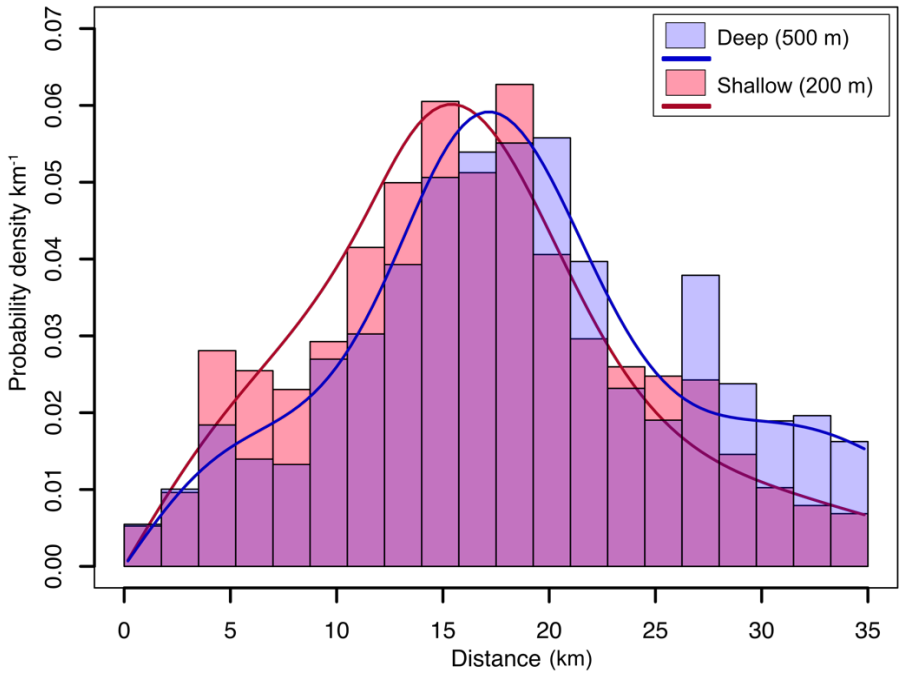

FIG. S3.4: Histograms of range distributions and associated detection functions plotted as probability density functions adjusted as described in Section 3 for the deeper (blue) and shallower (red) bathymetry assumptions (Fig. S3.3). Detection functions are fit with the site as a covariate and 4 cosine adjustments as for our preferred model (Fig. 3.7). $\hat{P}_{det}$ is 37.2% and $\hat{P}_{det}$ is 43.5%, for the shallower and deeper bathymetry assumption models, respectively.

Month	**Call Density (per km2)**	$SE(\hat{D})$	$CV(\hat{D})$	**LCL**	**UCL**	**DF**
Dec	1.44	0.53	0.37	0.71	2.91	6.0
Jan	2.15	0.47	0.22	1.40	3.29	6.0
Mar	2.35	0.63	0.27	1.40	3.95	6.0
Apr	0.52	0.35	0.67	0.16	1.72	6.0

TABLE S3.1: Monthly call densities calculated for the shallower bathymetry assumption using the detection function shown in Fig. S3.4. The columns are the same as Table 3.3.

Month	**Call Density (per km2)**	$SE(\hat{D})$	$CV(\hat{D})$	**LCL**	**UCL**	**DF**
Dec	1.23	0.46	0.37	0.61	2.48	6.0
Jan	1.84	0.40	0.22	1.20	2.82	6.0
Mar	2.01	0.54	0.27	1.19	3.38	6.0
Apr	0.45	0.30	0.67	0.14	1.48	6.0

TABLE S3.2: Monthly call densities calculated for the deeper bathymetry assumption using the detection function shown in Fig. S3.4. The columns are the same as Table 3.3.

Appendix 3: Supplementary Materials for Chapter 4

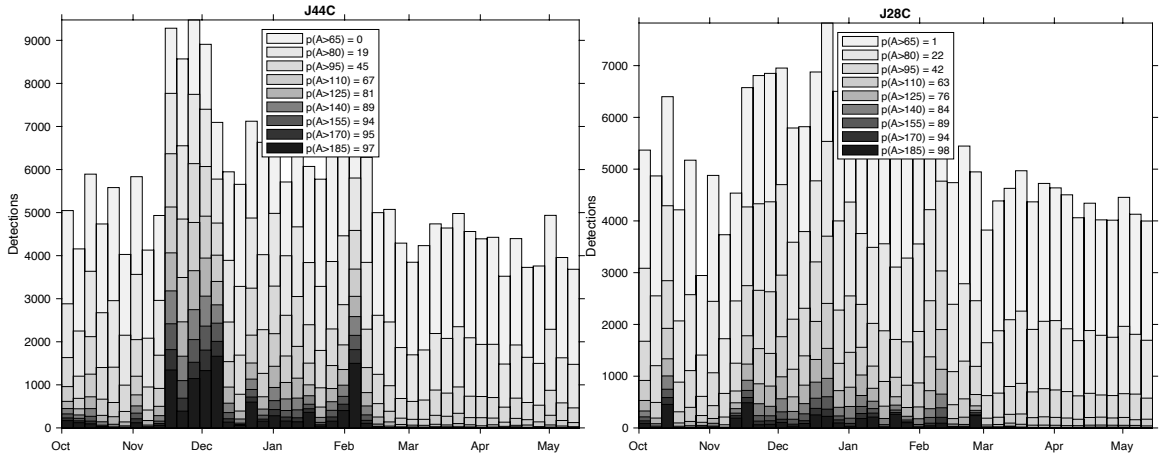

FIG. S4.1: Histograms showing counts of automated detections in 5-day bins from October 2013-May 2014 for stations (a) J44C and (b) J28C. Comparisons of detection counts from October-March with counts from May 1-15 are used to estimate the probability (p) that different detection scores (A) are true assuming uniform rates of false detections in both intervals and no true detections from May 1-15.

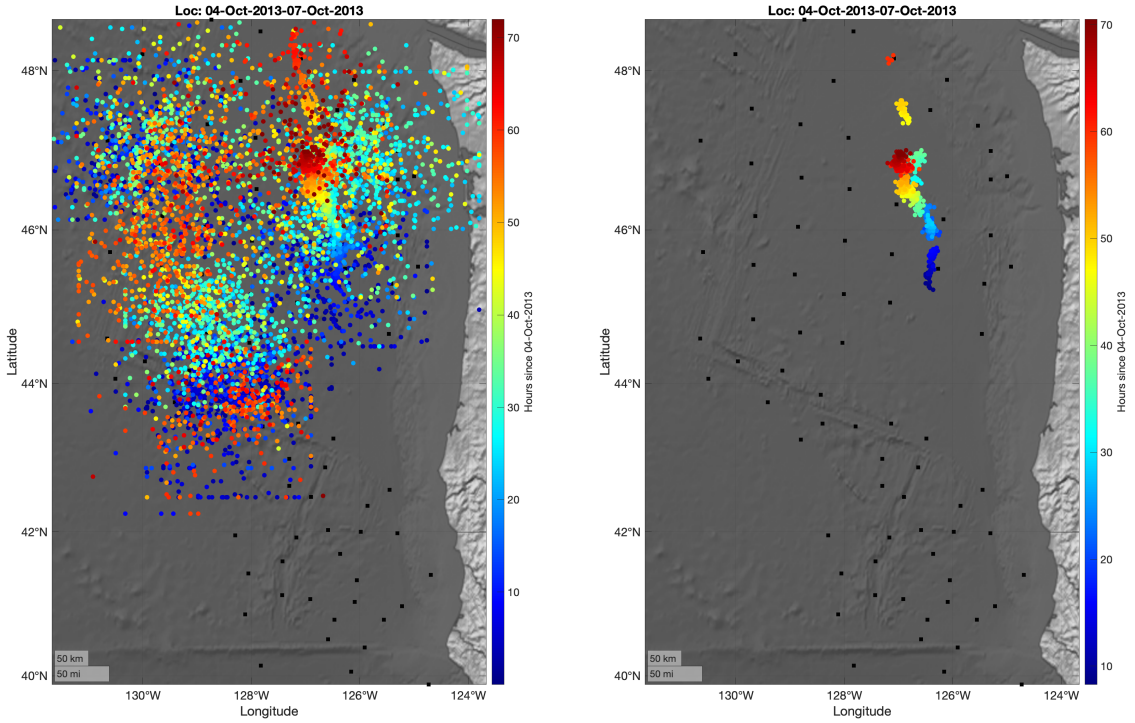

FIG. S4.2: Maps showing localizations in the Cascadia Initiative network from October 4-7, 2013, with color indicating hours after 0000 UT on October 4, for all locations produced by the Bayesian algorithm (left) and locations extracted by the spatio-temporal filter (right).

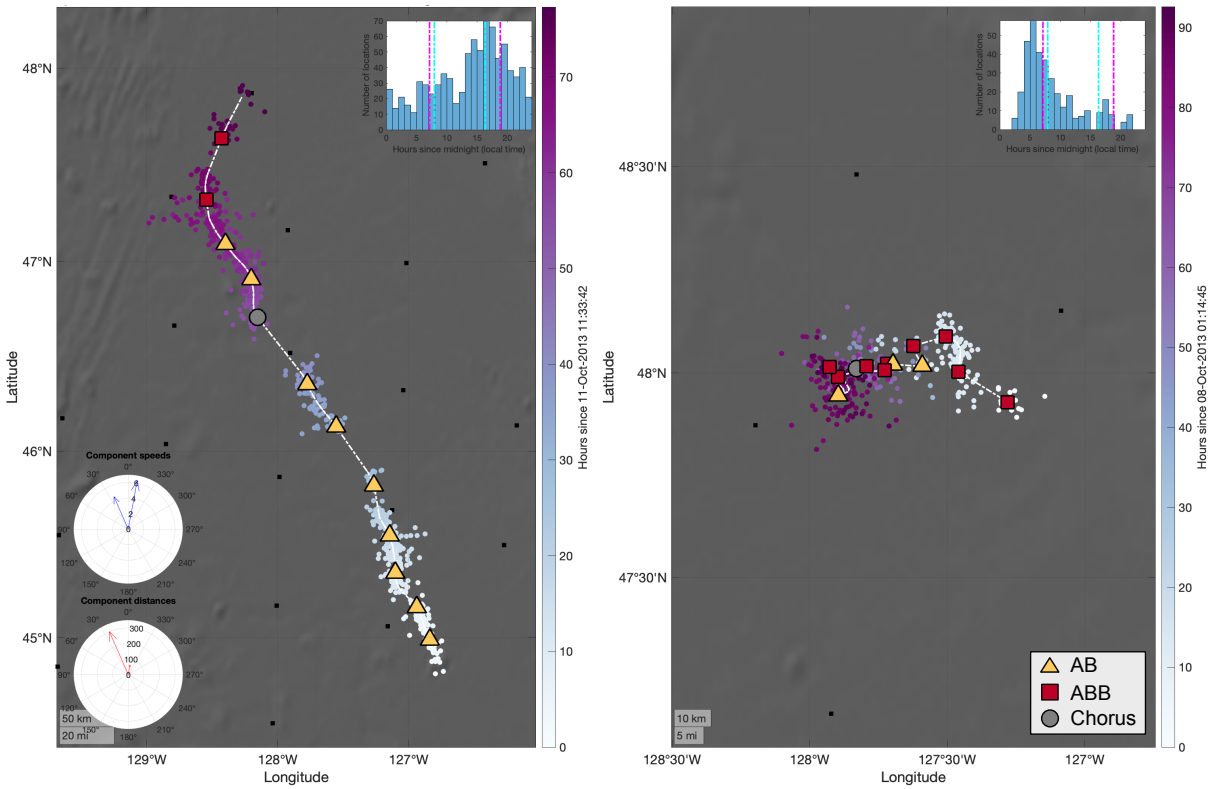

FIG. S4.3: Examples of tracks calculated by the localization algorithm, spatiotemporally filtered into track segments, then compiled manually by an analyst into full tracks for (a) a transiting whale and (b) a non-transiting whale. Localizations are shown by filled circles with color indicating hours since the start of the track. White dotted lines show the smoothed whale path. Markers on the dotted lines show song type categorization for every fifth hour. The top right windows show hourly diel histograms of track localizations, with dotted lines showing sunrise and sunset for the equinox (pink) and solstice (cyan). Bottom left plots for the transiting whale show the azimuth scaled by (upper) average speed in km/hr and (bottom) distance travelled in km for the two segments with distinct directions obtained by k-means clustering.

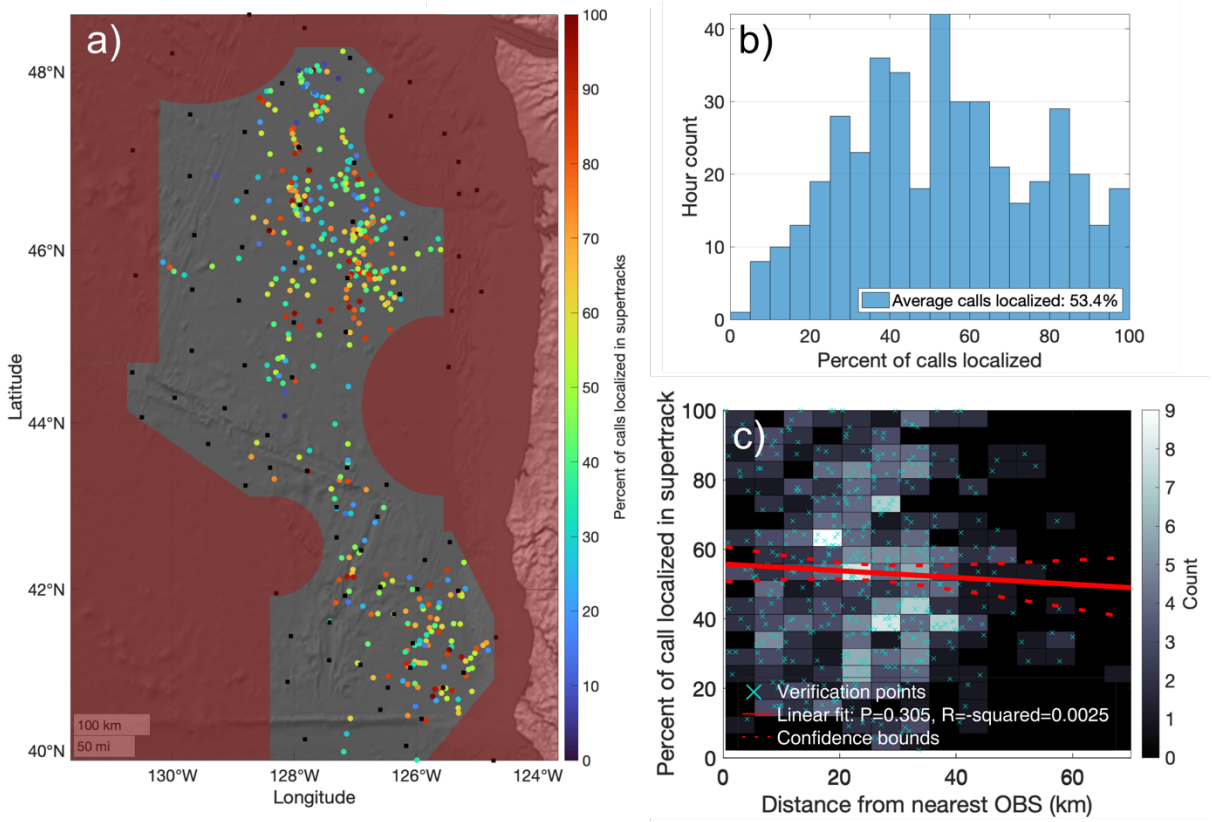

FIG. S4.4: (a) Map showing the success rate of B-call localizations in the tracks for every 5th hour plotted using a color scale with filled circles at the average position of the track for the hour. OBSs used in the localizations are shown as black squares. Map coloring delineates the effective localization area (gray) where the network is able to localize calls from other regions (red). (b) Histogram of the percent of B-calls successfully localized for all hours verified. (c) Two-dimensional histogram of the number of verified hours versus the average distance to the nearest OBS and percent of calls localized. A red line shows a linear fit to the percent of B-calls verified versus distance from nearest OBS averaged over the hour with 95% confidence bounds shown as dotted lines. The model shows there is not a significant relationship between whale distance from the nearest OBS and the success rate of our localization algorithm.

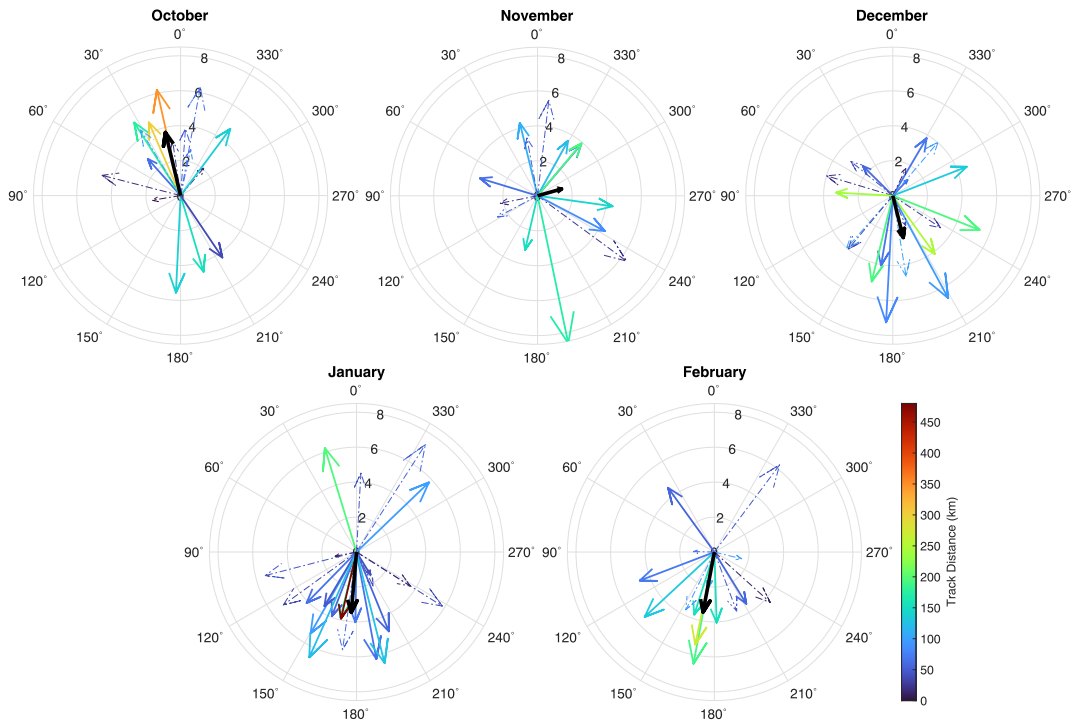

FIG. S4.5: Monthly polar plots showing the direction and net speed of the transiting smoothed blue whale tracks. Vectors represent velocity (km/hr) and color represents distance along smoothed track (km). One vector is plotted for each k-means cluster section of each track. The cluster with the largest directional component is plotted with a solid line, and smaller components are plotted with dotted lines. Black arrows show the average whale velocity from all cluster segments.

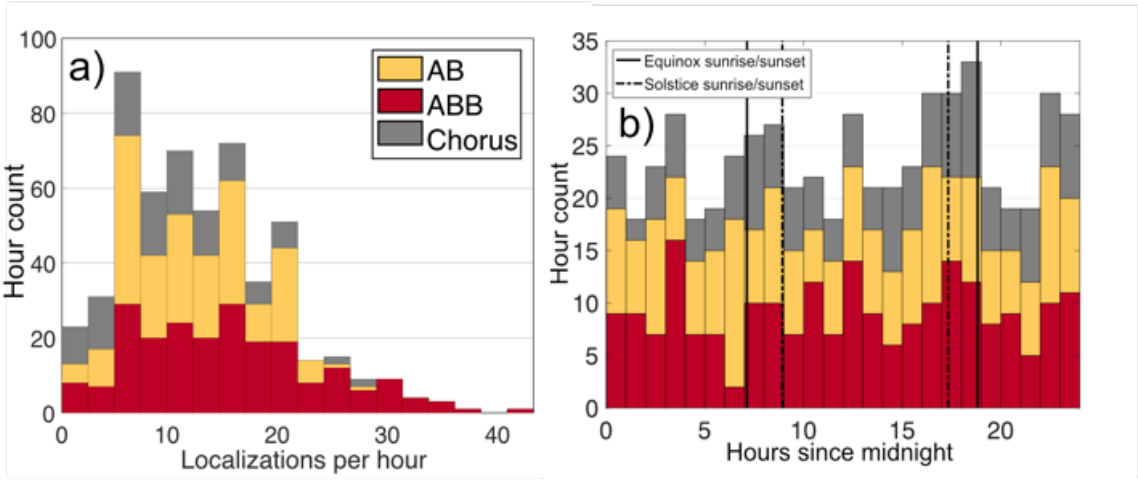

FIG. S4.6: Summative histograms showing song type distributions with (a) localizations of B-calls per hour and (b) hour of day. Red represents ABB song, yellow AB song, and gray chorus.

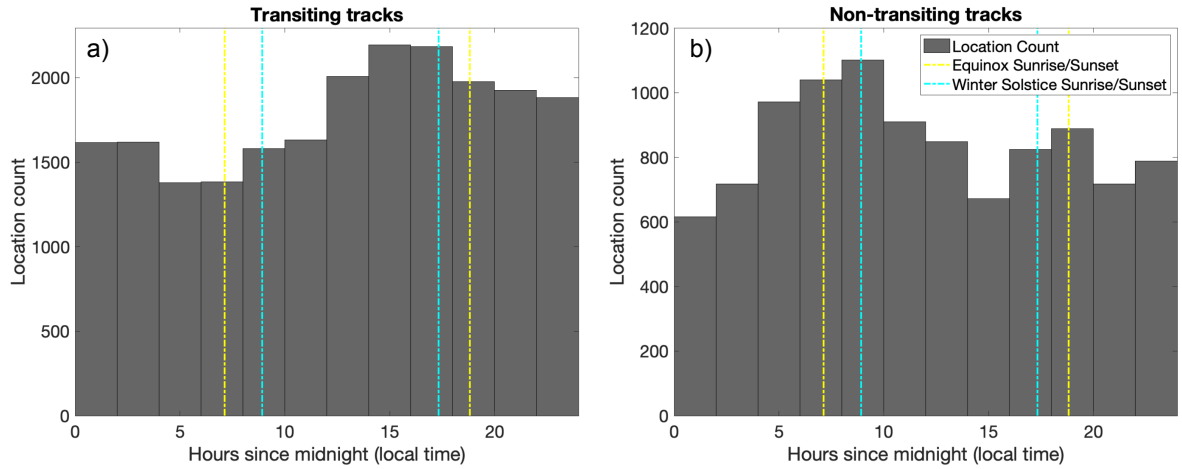

FIG. S4.7: Histogram of diel localization counts in (a) transiting tracks and (b) non-transiting tracks.

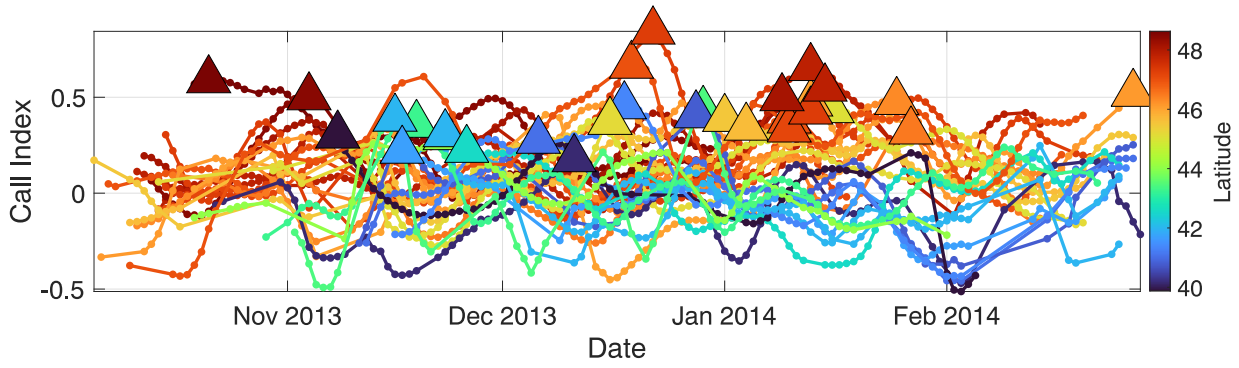

FIG. S4.8: Timeseries of call index values for each OBS with at least 20 high-probability detections (P > 0.8) on at least %50 of deployment days. Lines show 15-day smoothed timeseries, while dots show days with B-call detections with P>0.8. Large triangles show time and value of call index maximums for each OBS. Color shows OBS latitude.